

REPORT NO.  
UCB/EERC-91/11  
NOVEMBER 1991

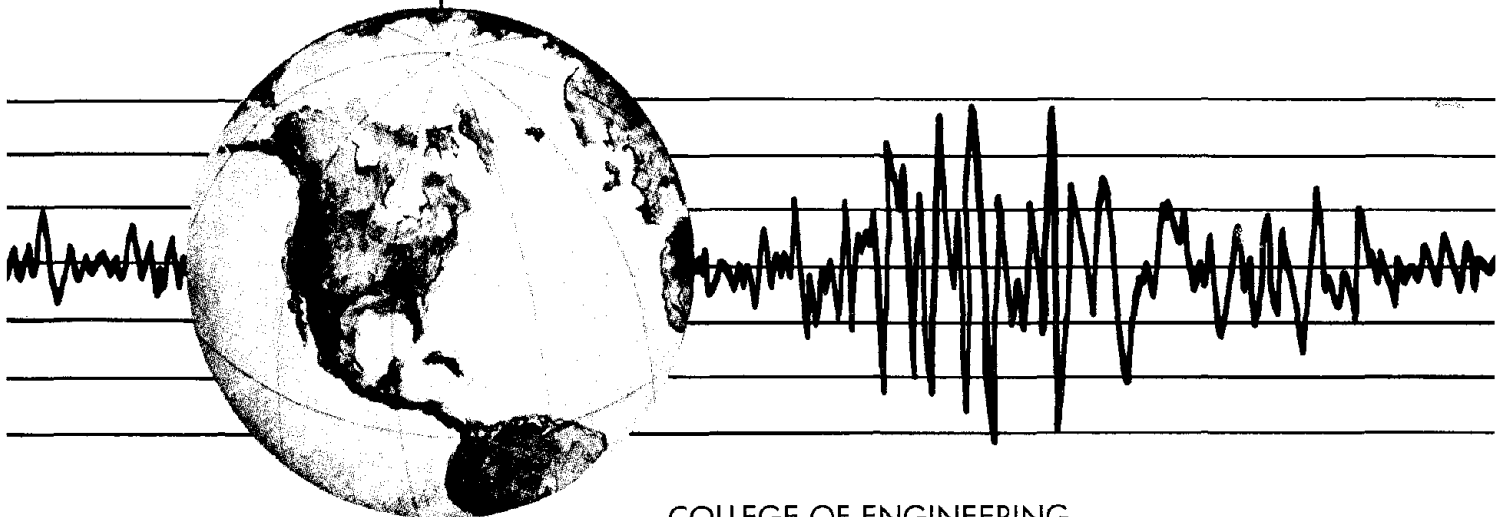
EARTHQUAKE ENGINEERING RESEARCH CENTER

# SEISMIC PERFORMANCE OF AN INSTRUMENTED SIX-STORY STEEL BUILDING

by

JAMES C. ANDERSON  
VITELMO V. BERTERO

Report to the National Science Foundation



COLLEGE OF ENGINEERING

UNIVERSITY OF CALIFORNIA AT BERKELEY

REPRODUCED BY  
U.S. DEPARTMENT OF COMMERCE  
NATIONAL TECHNICAL INFORMATION SERVICE  
SPRINGFIELD, VA. 22161

For sale by the National Technical Information Service, U.S. Department of Commerce, Springfield, Virginia 22161

See back of report for up to date listing of EERC reports.

**DISCLAIMER**

Any opinions, findings, and conclusions or recommendations expressed in this publication are those of the authors and do not necessarily reflect the views of the National Science Foundation or the Earthquake Engineering Research Center, University of California at Berkeley.

REPORT DOCUMENTATION PAGE	1. REPORT NO. NSF/ENG - 91012	2.	3. PB93-114809
4. Title and Subtitle "Seismic Performance of an Instrumented Six-Story Steel Building"		5. Report Date November 1991	
7. Author(s) James C. Anderson and Vitelmo V. Bertrero		8. Performing Organization Rept. No. UCB/EERC - 91/11	
9. Performing Organization Name and Address Earthquake Engineering Research Center University of California, Berkeley 1301 So. 46th Street Richmond, Calif. 94804		10. Project/Task/Work Unit No.	
12. Sponsoring Organization Name and Address National Science Foundation 1800 G. Street, N.W. Washington, D.C. 20550		11. Contract(C) or Grant(G) No. (C) (G) CES - 8804305	
15. Supplementary Notes		13. Type of Report & Period Covered	
16. Abstract (Limit: 200 words)		14.	
<p>This study investigates the seismic performance of a six-story steel building instrumented with thirteen accelerometers at the time of the Whittier Narrows earthquake (October, 1987). The lateral force system is a moment-resistant perimeter frame. The building was not severely tested by the motions recorded at its base during this earthquake. The dynamic seismic response was entirely linear elastic. System identification techniques are used to identify the periods of vibration from the recorded response. Recorded data are also used to evaluate the contribution of gravity, framing and nonstructural components to the dynamic properties. A detailed stress check of all members is performed for the design loading. Using a three-dimensional elastic model of the structure, the directional effects are shown to increase the stress in the critical members by 9%.</p> <p>Static nonlinear analyses are used to identify the potential failure mechanism and regions of increased ductility demand, and show that the structure has an overstrength which resulted in an ultimate lateral resistance more than 20% over the code required strength. Nonlinear dynamic analyses are used to evaluate the behavior of the building under stronger motions which have recently been recorded on similar sites. The value of <math>R_w</math> for this moment-resistant frame is shown to vary between 5.6 and 7.4, well below the value of 12 specified in the 1985 UBC.</p>			
17. Document Analysis a. Descriptors			
b. Identifiers/Open-Ended Terms			
c. COSATI Field/Group			
18. Availability Statement Release Unlimited		19. Security Class (This Report) unclassified	21. No. of Pages 147
		20. Security Class (This Page) unclassified	22. Price



**SEISMIC PERFORMANCE OF AN INSTRUMENTED  
SIX-STORY STEEL BUILDING**

by

**James C. Anderson**

and

**Vitelmo V. Bertero**

**Report to the National Science Foundation**

**Report No. UCB/EERC-91/11  
Earthquake Engineering Research Center  
College of Engineering  
University of California at Berkeley**

**November 1991**



**ABSTRACT**

This study investigates the seismic performance of a six-story steel building which was instrumented with thirteen accelerometers at the time of the Whittier Narrows earthquake (October, 1987). The lateral force system is a moment-resistant perimeter frame. The building was not severely tested by the motions recorded at its base during the Whittier narrows earthquake. The dynamic seismic response was entirely linear elastic. System identification techniques are used to identify the periods of vibration from the recorded response. Recorded data are also used to evaluate the finite element model of the structure and to evaluate the contribution of gravity, framing and nonstructural components to the dynamic properties. A detailed stress check of all members is performed for the design loading. Using a three-dimensional elastic model of the structure, the effect of the direction of the earthquake input is evaluated by considering the developed stress ratios. The directional effects are shown to increase the stress in the critical members by 9%.

Static nonlinear analyses are used to identify the potential failure mechanism and regions of increased ductility demand. Relationships between global and local ductility are investigated along with the distribution of inelastic behavior throughout the frame. The static nonlinear analysis shows that the structure has an overstrength which resulted in an ultimate lateral resistance of more than 20% over the code required

strength. Nonlinear dynamic analyses are used to evaluate the behavior of the building under stronger motions which have been recorded on similar sites during recent earthquakes. Using these results, the structural system coefficient,  $R_w$ , is evaluated.

The value of  $R_w$  for this moment-resistant frame is shown to vary between 5.6 and 7.4, well below the value of 12 specified in the 1985 UBC.

**ACKNOWLEDGEMENTS**

The research reported herein is part of a research project on "Response of Engineered Buildings to the Whittier Narrows Earthquake," supported by National Science Foundation (NSF) Grant No. CES-8804305. The support provided by NSF is gratefully acknowledged. The authors also acknowledge the continuing support of NSF Program Manager Dr. S.C. Liu. The opinions, discussions, findings and conclusions expressed in this report are solely those of the authors, and do not necessarily reflect those of the sponsor.



**TABLE OF CONTENTS**

<b>ABSTRACT</b> . . . . .	i
<b>ACKNOWLEDGEMENTS</b> . . . . .	iii
<b>TABLE OF CONTENTS</b> . . . . .	v
<b>LIST OF TABLES</b> . . . . .	vi
<b>LIST OF FIGURES</b> . . . . .	vii
<b>1. INTRODUCTION</b> . . . . .	1
<b>2. BUILDING DETAILS</b> . . . . .	2
<b>3. INSTRUMENTATION AND RECORDED DATA</b> . . . . .	4
<b>4. SYSTEM IDENTIFICATION STUDIES</b> . . . . .	6
4.1 Linear Elastic Response Spectra (LERS) . . . . .	7
4.2 Fourier Analyses . . . . .	8
4.3 Inelastic Response Spectra . . . . .	12
<b>5. MATHEMATICAL MODELS FOR ELASTIC RESPONSE</b> . . . . .	13
5.1 Two and Three-dimensional Models . . . . .	13
5.2 Weight (Mass) Determination . . . . .	15
<b>6. CODE ANALYSIS AND STRESS CHECK</b> . . . . .	15
6.1 1973 Code Seismic Design Requirement . . . . .	16
6.2 1973 Code Wind Design Requirement . . . . .	17
6.3 Initial Stress Check . . . . .	17
6.4 1988 Code Seismic Design Requirement . . . . .	19
6.5 1988 Code Wind Design Requirement . . . . .	20
<b>7. ELASTIC RESPONSE ANALYSES</b> . . . . .	21
7.1 Modal Analyses . . . . .	21
7.2 Dynamic Response Analyses . . . . .	24
7.3 Directional Input Analyses . . . . .	25
<b>8. NONLINEAR STATIC ANALYSES</b> . . . . .	26
<b>9. ANALYSIS OF STRUCTURAL OVERSTRENGTH</b> . . . . .	35
<b>10. NONLINEAR RESPONSE ANALYSIS</b> . . . . .	39
10.1 Inelastic Response Spectra . . . . .	41
10.2 Multiple Degree of Freedom Response Analyses . . . . .	42
10.3 Linear Dynamic Analyses . . . . .	43
10.4 Nonlinear Dynamic Analyses . . . . .	43
10.5 Effect of Increased Ground Accelerations . . . . .	48
<b>11. SUMMARY AND CONCLUSIONS</b> . . . . .	50
<b>FIGURES</b> . . . . .	55
<b>REFERENCES</b> . . . . .	127

## LIST OF TABLES

TABLE 1. BUILDING RECORDS, WHITTIER NARROWS EARTHQUAKE . . . .	3
TABLE 2. PEAK RECORDED RESPONSES . . . . .	5
TABLE 3. IDENTIFICATION OF TRANSLATIONAL MODAL PERIODS . . . .	9
TABLE 4. PERIODS OF VIBRATION, 3D MODELS . . . . .	21
TABLE 5. PERIODS OF VIBRATION, 2D MODEL . . . . .	22

## LIST OF FIGURES

- Figure 1 CSMIP Strong Motion Stations near Whittier
- Figure 2 Plan View of the Building
- Figure 3 Elevation View of the Building
- Figure 4 Location of Building Instrumentation
- Figure 5 Recorded Acceleration at Ground Level
- (a) Channel 1, Up, NW Corner
  - (b) Channel 13, N-S, NW Corner
- Figure 6 Recorded Acceleration at Ground Level
- (a) Channel 8, E-W, NW Corner
  - (b) Channel 9, E-W, SW Corner
- Figure 7 Recorded Acceleration at Second Floor Level
- (a) Channel 6, E-W, NW Corner
  - (b) Channel 7, E-W, SW Corner
  - (c) Channel 12, N-S, NW Corner
- Figure 8 Recorded Acceleration at Third Floor Level
- (a) Channel 4, E-W, NW Corner
  - (b) Channel 5, E-W, SW Corner
  - (c) Channel 11, N-S, NW Corner
- Figure 9 Recorded Acceleration at Roof Level
- (a) Channel 2, E-W, NW Corner
  - (b) Channel 3, E-W, SW Corner
  - (c) Channel 10, N-S, NW Corner
- Figure 10 Spectra Comparison, Torsional Effects
- (a) Base
  - (b) Roof
- Figure 11 Spectra Comparison, Amplification Effects
- (a) E-W Motions
  - (b) N-S Motions
- Figure 12 Fourier Amplitude Spectra for Base Motions
- (a) North-South, Channel 13
  - (b) East-West, Channel 9
- Figure 13 Fourier Amplitude Spectra, E-W, NW Corner
- (a) Roof Level
  - (b) Third Floor
  - (c) Second Floor

Figure 14 Fourier Amplitude Spectra, E-W, SW Corner

- (a) Roof Level
- (b) Third Floor
- (c) Second Floor

Figure 15 Fourier Amplitude Spectra, N-S, NW Corner

- (a) Roof Level
- (b) Third Floor
- (c) Second Floor

Figure 16 Transfer Functions, E-W, SW Corner

- (a) Roof Level
- (b) Third Floor
- (c) Second Floor

Figure 17 Transfer Functions, E-W, NW Corner

- (a) Roof Level
- (b) Third Floor
- (c) Second Floor

Figure 18 Transfer Functions, N-S, NW Corner

- (a) Roof Level
- (b) Third Floor
- (c) Second Floor

Figure 19 Moving Window Fourier Analyses, Base, Vertical

Figure 20 Moving Window Fourier Analyses, Base, E-W

Figure 21 Moving Window Fourier Analyses, Base, N-S

Figure 22 Moving Window Fourier Analyses, E-W, Roof Level

Figure 23 Moving Window Fourier Analyses, E-W, Third Floor

Figure 24 Moving Window Fourier Analyses, E-W, Second Floor

Figure 25 Moving Window Fourier Analyses, N-S, Roof Level

Figure 26 Moving Window Fourier Analyses, N-S, Third Floor

Figure 27 Moving Window Fourier Analyses, N-S, Second Floor

Figure 28 Fourier Amplitude Spectra, Torsional Effects

- (a) Base Level
- (b) Second Floor
- (c) Third Floor
- (d) Roof Level

Figure 29 Inelastic Response Spectra

- (a) Recorded Base Motion, N-S
- (b) Recorded Base Motion, E-W

- Figure 30 Elastic Finite Element Building Models  
(a) Two Dimensional  
(b) Three Dimensional
- Figure 31 Code Loading and Resulting Deformations  
(a) Gravity Loading  
(b) Deformed Shape, Gravity Load  
(c) Lateral Seismic Loading  
(d) Deformed Shape, Lateral Seismic Load
- Figure 32 Interstory Drift Index, Code Lateral Loads
- Figure 33 Stress Ratios for Code Loads  
(a) Gravity Load  
(b) Gravity Load plus Lateral Seismic Load
- Figure 34 Three Dimensional ETABS Building Model
- Figure 35 Mode Shapes, 3D Building Model  
(a) First Mode  
(b) Second Mode  
(c) Third Mode
- Figure 36 Mode Shapes, 2D Building Model  
(a) First Mode  
(b) Second Mode  
(c) Third Mode
- Figure 37 Building Model Including Interior Gravity Frame
- Figure 38 Roof Response Spectra  
(a) Damping Ratios = 5%, 5%, 5%, 5%  
(b) Damping Ratios = 7%, 10%, 13%, 15%
- Figure 39 Acceleration Time Histories, Roof Level  
(a) Channel 2, E-W  
(b) Channel 3, E-W  
(c) Channel 10, N-S
- Figure 40 Third Floor Response Comparisons  
(a) Floor Response Spectra  
(b) Channel 4, E-W  
(c) Channel 5, E-W  
(d) Channel 11, N-S
- Figure 41 Stress Ratios, Input Angle =  $0^{\circ}$
- Figure 42 Stress Ratios, Input Angle =  $15^{\circ}$
- Figure 43 Stress Ratios, Input Angle =  $30^{\circ}$
- Figure 44 Stress Ratios, Input Angle =  $45^{\circ}$
- Figure 45 Stress Ratios, Input Angle =  $60^{\circ}$

- Figure 46 Stress Ratios, Input Angle =  $75^{\circ}$
- Figure 47 Stress Ratios, Input Angle =  $90^{\circ}$
- Figure 48 Roof Displacement vs. Base Shear, Uniform Lateral
- Figure 49 Uniform vs. Triangular Lateral Loading
- Figure 50 Lateral Load Distribution and Lateral Resistance
- Figure 51 Resistance, Nominal vs. Actual Steel Strength
- Figure 52 Steel Strength and Lateral Resistance
- Figure 53 Strain Hardening and Lateral Resistance
- Figure 54 Interstory Shear vs. Displacement, Triangular Load
- Figure 55 Ductility Requirements vs. Story Level
- Figure 56 Rotation Requirements vs. Story Level
- Figure 57 Sequence of Plastic Hinge Formation
- Figure 58 Idealized Elastic-Plastic Shear vs. Displacement
- Figure 59 Stresses in an Idealized Member
- Figure 60 LERS for Recent Earthquakes
- Figure 61 Motion Recorded at Obregon Park, Whittier Narrows  
(a) Acceleration Time History  
(b) Response Spectra Comparison
- Figure 62 Acceleration Time Histories of Recent Earthquakes  
(a) Bucharest, 1977  
(b) Hollister, 1989  
(c) James Road, 1979  
(d) SCT, Mexico City, 1985
- Figure 63 Inelastic Response Spectra  
(a) Bucharest, 1977  
(b) Hollister, 1989  
(c) James Road, 1979  
(d) SCT, Mexico City, 1985
- Figure 64 Acceleration Comparisons, Nonlinear Model  
(a) Roof Level  
(b) Third Floor
- Figure 65 Base Shear Time Histories, Whittier Narrows  
(a) Building Base  
(b) Obregon Park

- Figure 66 Base Shear Time Histories, Recent Earthquakes  
(a) Bucharest, 1977  
(b) Hollister, 1989  
(c) James Road, 1979  
(d) SCT, Mexico City, 1985
- Figure 67 Maximum Displacement Response  
(a) Lateral Displacement  
(b) Interstory Drift Index
- Figure 68 Curvature Ductility Demand  
(a) Girders  
(b) Columns
- Figure 69 Maximum Rotation Demand  
(a) Girders  
(b) Columns
- Figure 70 Maximum Story Shear Envelopes
- Figure 71 Story Shear vs. Interstory Displacement, Bucharest  
(a) Sixth Story  
(b) Fifth Story  
(c) Fourth Story  
(d) Third Story  
(e) Second Story  
(f) First Story
- Figure 72 Story Shear vs. Interstory Displacement, Hollister  
(a) Sixth Story  
(b) Fifth Story  
(c) Fourth Story  
(d) Third Story  
(e) Second Story  
(f) First Story
- Figure 73 Input Energy From Recent Earthquakes
- Figure 74 Maximum Displacement Response, Increased PGA  
(a) Lateral Displacement  
(b) Interstory Drift Index
- Figure 75 Curvature Ductility Demand, Increased PGA  
(a) Girders  
(b) Columns
- Figure 76 Maximum Rotation Demand, Increased PGA  
(a) Girders  
(b) Columns
- Figure 77 Base Shear vs. Interstory Disp., Increased PGA  
(a) Bucharest  
(b) Hollister



## 1. INTRODUCTION

The Whittier Narrows Earthquake occurred at 7:42 am on the morning of October 1, 1987 and was assigned a local Richter Magnitude of 5.9 ( $M_L$ ). The epicenter was north of Whittier, California, approximately nine miles (15 km) east of downtown Los Angeles. Following the earthquake, the California Strong Motion Instrumentation Program (CSMIP) obtained records from 27 extensively instrumented building structures [1]. In addition, the U.S. Geological Survey (USGS) collected data in approximately ten instrumented buildings [2] and the University of Southern California collected data in four. Other data may have been obtained but is not readily available in the public domain. It is estimated that over 200 buildings in Los Angeles have been instrumented by the building owners in compliance with the local building code. However, a recent code change in the city of Los Angeles has reduced the seismic instrumentation requirement to only a single instrument at the roof level. As a result of this change, many structures which had recorders at three levels at the time of the San Fernando Earthquake (1979) now have only a single recorder at the roof, rendering them unusable for analytical studies. Unfortunately, this is a step backward in the continuing efforts to improve understanding and prediction of the seismic behavior of buildings.

In order to perform detailed studies of structural response during an earthquake, it is necessary to use a copy of both the structural plans and the architectural plans. A partial list of

the major structures from the above database of instrumented buildings for which the structural plans are available is given in Table 1. Here it can be seen that most of the available data is for low to mid-rise structures and that only limited data is available for high-rise buildings over 25 stories. The one exception is the 33-story structure at 1100 Wilshire Boulevard, instrumented by USGS. From this list, the six-story steel building in Burbank, instrumented by CSMIP [1] was selected for detailed study. The structure uses a steel perimeter moment frame for resistance to lateral loads. A map of the CSMIP strong motion stations is shown in Fig. 1. The building is station number 370, which is located approximately 16 miles (26 km) from the epicenter.

## 2. BUILDING DETAILS

The building in Burbank was designed in 1976 to the requirements of the 1973 Uniform Building Code [3] as amended by the city of Burbank. The primary structural system for carrying lateral load is a steel moment-resisting frame around the perimeter of the building, which is shown in the plan view of the structure in Fig. 2a. Note that the moment continuity of the peripheral frame is broken at the corners where a connection is required to the weak axis of a wide flange column. At these four locations a simple, shear connection is used instead of a moment connection. This pin connection is represented by a circle in Figs. 2 and 3. Gravity loads are carried by an interior framing system consisting of much

TABLE 1. BUILDING RECORDS, WHITTIER NARROWS EARTHQUAKE

Building	Height (Stories)	Framing System	Recorded Accelerations
1. Office Building	8	Shear Wall/ Frame	Base 0.39 2nd 0.41 Roof 0.48
2. Apartment Building	10	Shear Wall	Base 0.63 Fifth 0.63 Roof 0.61
3. Financial Building	6	Steel Perimeter Moment Frame	Base 0.22 2nd 0.21 3rd 0.24 Roof 0.30
4. Commercial Storage	14	Shear Wall	Base 0.12 8th 0.19 12th 0.14 Roof 0.21
5. Apartment Building	10	Precast Shear Wall	Base 0.22 4th 0.31 8th 0.28 Roof 0.54
6. Office Building	12	Steel Perimeter Moment Frame	Base 0.30 6th 0.47 Roof 0.28
7. Hotel	20	RC Moment Frame	Base 0.11 3rd 0.19 9th 0.12 16th 0.13 Roof 0.17
8. Dormitory	11	Shear Wall	Base 0.10 6th 0.18 Roof 0.29
9. Classroom Building	10	Steel Perimeter Moment Frame	Base 0.14 6th 0.08 Roof 0.07
10. Financial Building	13	RC Moment Frame	Base 0.26 2nd 0.18 8th 0.13 Roof 0.14

connected by simple, shear connections. Soil conditions at the site consist of silty sands extending to a depth of 25 feet having a blow count of 1-2. Below 25 feet the sands become well graded and the blow count increases to 14-15. Because of these soil conditions, the exterior columns of the lateral force system are supported on two 30-inch diameter reinforced concrete piles which are 32 feet long. Interior columns are supported on spread footings. An elevation of a typical moment frame is shown in Fig. 3. In the initial stage of this study, the structure is assumed to be fixed at the base. The validity of this assumption will be checked by comparing the calculated response with the recorded response. At the second floor level and at the roof, the floor deck extends a distance of 6 1/2 feet beyond the perimeter moment frame, giving it a plan dimension of 132 feet by 132 feet. No damage was reported in the structure.

### 3. INSTRUMENTATION AND RECORDED DATA

The building was instrumented with 13 strong motion recorders at the time of the Whittier Narrows Earthquake. The location and orientation of these instruments is shown in Fig. 4, which is taken from reference [1]. Peak recorded responses are summarized in Table 2. The vertical acceleration recorded at the base of the structure is given by channel 1, which is shown in Fig. 5a. Here it can be seen that the peak vertical acceleration was about 0.09g and that there is not an apparent long period motion which would indicate rocking motions of the building. The horizontal acceleration in the north-south

direction at the base is given by channel 13 which is shown in Fig. 5b. Here the relatively short duration and high frequency of the base motion become readily apparent. The peak acceleration is approximately 0.22g, but this is due to a high frequency acceleration spike, and the duration of strong motion is only about five seconds.

TABLE 2. PEAK RECORDED RESPONSES

Ident.	Location	Component	Accel. (cm/s <sup>2</sup> )	Velocity (cm/s)	Disp. (cm)
Chan. 1	Ground	Up	84.98	3.61	0.38
Chan. 2	Roof N.W.	090	183.58	21.29	4.03
Chan. 3	Roof S.W.	090	156.73	18.48	3.66
Chan. 4	3RD N.W.	090	176.65	12.32	2.12
Chan. 5	3RD S.W.	090	146.75	10.90	1.96
Chan. 6	2ND N.W.	090	146.27	10.37	1.70
Chan. 7	2ND S.W.	090	143.86	9.99	1.50
Chan. 8	Ground N.W.	090	165.77	9.74	1.20
Chan. 9	Ground S.W.	090	162.23	9.56	1.19
Chan. 10	Roof N.W.	180	283.72	31.98	6.30
Chan. 11	3RD N.W.	180	233.16	18.44	2.49
Chan. 12	2ND N.W.	180	194.64	15.94	1.68
Chan. 13	Ground N.W.	180	221.74	12.51	1.27

Horizontal motions at the base in the east-west direction are given by channels 8 and 9, which are shown in Fig. 6a and 6b respectively. Here it can be seen that the peak acceleration in

this direction is also due to a high frequency acceleration spike having an amplitude of 0.17g, and that the duration of strong motion shaking is even shorter than in the north-south direction. Horizontal accelerations at the second floor level are given by channels 6, 7 and 12 which are shown in Fig. 7. Similar data for the third floor level are given by channels 4, 5 and 11 which are shown in Fig. 8. Roof accelerations in the horizontal direction are given by channels 2, 3 and 10 which are shown in Fig. 9. From a comparison of the three acceleration plots, it would appear that the period of vibration in both directions is approximately the same, having a value of about 1.2 to 1.3 seconds. The peak roof acceleration was recorded in the north-south direction by channel 10 and has a value of 0.29g.

A cursory examination of the time history plots at the roof level indicates that there is no appreciable increase in the period of vibration over the entire time history. This indicates that the response is linear elastic.

#### **4. SYSTEM IDENTIFICATION STUDIES**

In order to understand the recorded dynamic response of the building better and to evaluate the dynamic characteristics of the building prior to performing the detailed response analyses, the recorded response data was processed using Fourier amplitude spectra, transfer functions, moving window Fourier analyses, linear elastic response spectra and inelastic response spectra.

The results of these studies are discussed in the following sections.

#### 4.1 Linear Elastic Response Spectra (LERS)

In order to obtain a better evaluation of the recorded response, LERS for 5% damping were generated and plotted for selected recorded building motions. Rotation of the structure was evaluated using the spectra shown in Fig. 10. LERS for the base are compared in Fig 10a using motions recorded on channels 8 and 9. These channels recorded base accelerations on the north and south sides of the structure in the E-W direction. Comparison of the response spectra shows that the two spectra are identical and therefore there is little or no rotation at the base. Similar data for channels 2 and 3 on the roof are shown in Fig. 10b. There is some variation between the spectra in the period range below 0.7 second which could include the torsional mode of the building but the variation is small.

An LERS for motions in the east-west direction at the roof level are shown in Fig. 11a. Here it can be seen that the fundamental period of the response occurs at approximately 1.3 seconds which agrees with that observed from the zero crossing of the time history data. Amplified response between the base and the roof in this direction can be evaluated by comparing the spectral values for channels 2 and 8. As would be expected, the largest amplification occurs for the fundamental mode and has a value of approximately 6.3 with smaller amplification for the second and higher modes. Similar spectra for the north-south

direction are shown in Fig. 11b. Here a fundamental mode can be identified at a period of 1.3 seconds and the second mode can be seen at a period of 0.44 second. The maximum amplification between base and roof occurs in this direction and has a value of approximately 9.2.

#### 4.2 Fourier Analyses

Fourier amplitude spectra (FAS) of the recorded accelerations at the base of the structure are shown in Fig. 12, for the motion in the north-south direction in Fig. 12a, and for the east-west direction in Fig. 12b. In the north-south direction, the strongest input has a frequency content between 0.5 and 2.0 Hz with a strong peak between 0.75 and 1.0 Hz. In the east-west direction the strongest input is between 0.5 and 1.75 Hz.

Fourier amplitude spectra for motions recorded at other locations in the building are compared with the corresponding base FAS in Figs. 13 and 14 for east-west motions and Fig. 15 for north-south motions. All plots have a similar characteristic shape showing a strong peak at 0.75 Hz (1.33 second) and another at 2.2 Hz (0.45 second).

Transfer functions for the motions recorded in the east-west direction are shown in Figs. 16 and 17. From Fig. 16, it is possible to identify the first three modes in this direction as occurring at the following frequencies: the first mode has a frequency of 1.0 Hz ( $T=1.0$  second), the second mode occurs at a frequency of 2.4 Hz ( $T=0.42$  second), and the third

mode occurs at a frequency of 3.2 Hz ( $T=0.31$  second). Similar results can be seen in Fig. 17 for the other side of the structure. In the north-south direction, the transfer functions shown in Fig. 18, show that the first mode is dominant at all three levels and occurs at a frequency of 0.75 Hz ( $T=1.33$  seconds). In this direction the second mode shows up clearly at the second and third floor levels and has a value of 2.25 Hz ( $T=0.44$  second). A third mode can also be seen in this direction at approximately 3.2 Hz ( $T=0.31$  second). The modal frequencies and periods identified from the Fourier analyses are summarized in Table 3.

**TABLE 3. IDENTIFICATION OF TRANSLATIONAL MODAL PERIODS**

Direction	Mode 1	Mode 2	Mode 3
East-West	1.00	0.42	0.32
North-South	1.33	0.44	0.32

In order to identify changes in the frequency content of the input motions during the earthquake, moving window Fourier analyses are performed using the recorded base motions. In these analyses, the FAS has been calculated for ten second window lengths starting from the beginning of the record and then offsetting the window by five seconds at each step. For each window, the length of the record was extended by adding zeros to obtain good resolution in the spectra.

The result for the vertical component of the base motion is shown in Fig. 19. This figure shows that although the amplitude is small, the frequency content during the first ten seconds is

relatively uniform over a wide band. Two dominant frequencies appear during the second ten second interval. After ten seconds the amplitudes drop to almost zero. Moving window analysis of the base motion in the east-west direction is shown in Fig. 20. Here it can be seen that during the first ten seconds there is a relatively strong input in a frequency band between 0.5 Hz and 1.75 Hz. This diminishes significantly during the next window and reduces to very small amplitudes in succeeding windows. In the north-south direction, Fig. 21, the moving window analysis shows that during the first ten second window the input frequency band extends from 0.7 Hz to 2.5 Hz with a strong peak at 2.0 Hz.

Moving window analyses of motions in the east-west direction are shown in Figs. 22, 23 and 24. The moving window analysis of the motion at the roof level is shown in Fig. 22 where it can be seen that the response is predominantly first mode at a frequency of 0.75 Hz. Corresponding results for the third floor level are shown in Fig. 23. Here it can be seen that there is an increased contribution from the second mode at a frequency of 2.4 Hz. particularly during the first twenty seconds. The moving window FAS at the second floor has characteristics which are similar to the base motion, particularly during the first ten second window. In succeeding windows, the FAS at the second mode diminishes and the first mode becomes dominant.

Moving window analyses of motions in the north-south direction are shown in Figs. 25, 26 and 27. At the roof level, shown in Fig. 25, the response is predominantly first mode although there is some second mode response during the first ten second window. The moving window analyses for the third level which are shown in Fig. 26, indicate that there is a significant second mode response at this level during the first ten second period. This diminishes significantly during the second window and after ten seconds the first mode becomes dominant. A similar result is obtained for the second floor, which is shown in Fig. 27. During the first window, the response is influenced by the base motion and the second mode is dominant. As at the third level, the second mode diminishes during the second window and the first mode becomes dominant after ten seconds.

Torsional effects can be evaluated by comparing the FAS of motions recorded on opposite sides of the building. Results of this analysis are presented in Fig. 28. The spectra shown in Fig. 28a represent the motions at the base of the structure and here it can be seen that there is no difference in the input motions. This result is similar to that obtained from a comparison of LERS. At the second floor level, Fig. 28b, it can be seen that there is a small torsional effect at frequencies of 0.75, 2.3 and 3.2 Hz, which represent the first three modes of vibration. A similar effect can be seen at the third and roof levels shown in Fig. 28c and 28d. In all cases the torsional

effect is very small and can probably be neglected in the structural analyses.

#### 4.3 Inelastic Response Spectra

Inelastic response spectra were generated for the recorded base motions using a modified version of the NONSPEC [4] program. Results from this program are presented in terms of the yielding seismic resistance coefficient of the structure, defined as

$$C_y = R_y / W_e \quad (1)$$

where  $R_y$  = yield resistance of the structure, and

$W_e$  = total seismic dead load which in most cases is taken as the total dead load,  $W$ .

The nonlinear spectra for the motions recorded on base channel 9 in the E-W direction are shown in Fig. 29b. The solid line represents a ductility requirement of one (elastic behavior) and the dashed or broken lines represent ductilities of 2, 3, 4, 5, and 6. Considering the fundamental period of the structure to be 1.2 seconds, this figure indicates that a yielding seismic resistance coefficient of about 0.09 will be required to ensure elastic response of this structure if the response in the fundamental mode is dominant. Considering a similar spectrum for motions recorded on base channel 13 (Fig. 29a) in the N-S direction, it can be seen that at the fundamental period of the structure, a yielding seismic resistance coefficient of 0.1 is required for an equivalent single-degree-of-freedom system to obtain elastic response.

## 5. MATHEMATICAL MODELS FOR ELASTIC RESPONSE

### 5.1 Two and Three-dimensional Models

Both two dimensional and three-dimensional models were developed for the structure. Because of the symmetry of the structure and the framing system, two dimensional models can be used with the resulting savings in coding effort and computational time. Elastic analyses were done using the SAP90 [5] and ETABS [6] computer programs, although it is recognized that several alternative programs could have been used for this phase of the response analysis. The reasons for selecting the SAP90 program included the following:

1. The program has large capacity which permits modeling the structure in detail in either two or three dimensions on a personal computer.
2. The program allows the user to plot the time history response of any node. This feature was crucial for comparison of calculated results with the recorded response.
3. The program permits consideration of a rigid floor diaphragm through the use of a master node. This greatly reduces the time required to perform a dynamic analysis, particularly for a three-dimensional system.
4. The program has a postprocessor [7] which performs a stress check of every member for the provisions of the AISC Specification [8]. This greatly facilitates

an evaluation of the stress level in the structure under both the code design loading and the recorded earthquake loading.

The current version of the ETABS program can not produce time history response plots and therefore does not permit a comparison of recorded response with calculated response. Otherwise, this program could have been used for all response analyses for this structure. Its one significant capability that SAP90 does not have is the ability to calculate the stress ratios in each member for a time history ground motion applied in any direction with respect to the principal axes of the structure. Therefore, this program was used to study the directionality effects of the input motion.

The two-dimensional finite element model of a typical perimeter moment frame is shown in Fig. 30a. Here the joint numbering is shown along with the pinned moment releases at one end of the frame. The three-dimensional model is shown in Fig. 30b. Although not shown in this figure, pinned element releases are incorporated at one end of each frame in a similar manner to the two dimensional model. Nodes 169 through 174 in the middle of the figure are master nodes which connect to all nodes at a particular story level and define the displacement response of the story level.

## 5.2 Weight (Mass) Determination

A set of the architectural drawings for the structure was not available, rendering it necessary to estimate the weights of

some of the finish materials. The weight of the structure was estimated based on the following unit loads:

**ROOF:**

Roof Deck.....	46.0 psf
20 gage metal deck 3" deep with	
3 1/4" lightweight concrete on top	
Roofing .....	6.0 psf
Hung Ceiling .....	8.0 psf
Mechanical Equipment Penthouse .....	43.0 psf

**TYPICAL FLOOR:**

Floor Deck .....	46.0 psf
20 gage metal deck 3" deep with	
3 1/4" lightweight concrete on top	
Hung Ceiling .....	8.0 psf
Floor Finish .....	1.0 psf
Partitions .....	15.0 psf
Steel	
Beams and joists .....	7.1 psf
Columns .....	3.7 psf

**PERIMETER WALL:**

Glass with mullions.....	10.0 psf
--------------------------	----------

The weight of the second floor is higher than that of a typical floor because of the effect of the 6 1/2 foot overhang of the floor deck at that level. The weight of the roof is also higher than that of a typical floor because of the overhang of the roof deck and the addition of a mechanical equipment penthouse. The total weight of the structure is estimated as 7785 kips.

## 6. CODE ANALYSIS AND STRESS CHECK

The structure was designed to the requirements of the 1973 Uniform Building Code. Therefore, the existing strength will be based on this lateral force requirement. The structure will also be checked for the current requirements of the 1988 Uniform

Building Code. Lateral forces specified in building codes are defined in terms of the base shear and have the general form:

$$V = C_s W_e \quad (2)$$

where  $C_s$  is the design seismic resistance coefficient and  $W_e$  is the total seismic dead load.

### 6.1 1973 Code Seismic Design Requirement

The seismic lateral force requirements of the 1973 Uniform Building Code are expressed in terms of a base shear which is given by the formula

$$V = (ZKCIS)W \quad (3)$$

where

$$T = 0.1N = 0.6 \text{ sec.} \quad (4)$$

$$C = 1/(15 \sqrt{T}) = 0.086 \quad (5)$$

$$K = 0.67 \quad (6)$$

If  $Z$ ,  $S$  and  $I$  are taken as unity, the design seismic resistance coefficient becomes

$$C_s = 1.0 * 0.67 * 0.086 * 1.0 * 1.0 = 0.0577 \quad (7)$$

and the base shear  $V$ , can be calculated as

$$V_{\text{code}} = 0.0577 * 7785 = 449 \text{ kips.} \quad (8)$$

It should be noted that the expression used in the 1973 code to estimate the period tends to underestimate the actual building period by more than 50%. As discussed earlier, the recorded data from the building indicates that the fundamental period is approximately 1.3 seconds in each direction. This may be due in part to the fact that the estimate of period given by Eq. 4 is based on experience with moment-resistant space frames and not moment-resistant perimeter frames. In the Commentary to

the 1975 SEAOC Recommendations, it was suggested that the following expression be used to estimate the period,

$$T = 0.45 N^{2/3} \quad (9)$$

which results in a value of  $T=1.48$  seconds for this building.

The underestimation of period tends to increase the seismic design requirement by 41% over what it would be if the period were estimated more accurately.

### 6.2 1973 Code Wind Design Requirement

The lateral forces due to design winds in the 1973 code are based on a wind pressure map given in the code. The basic wind pressure for southern California is 20 psf. The distribution of wind pressure over the height of the building is the following:

Story height	Wind pressure
< 30'	15 psf
30' to 49'	20 psf
50' to 99'	25 psf

Based on these values, the base shear is determined to be 180 kips which is well below the seismic requirement for the structure.

### 6.3 Initial Stress Check

The initial stress check considered the loads for which the structure was originally designed, and was performed on the two-dimensional SAP90 model. Therefore, it was assumed that the total lateral force was equally divided between the two perimeter frames parallel to the direction of the lateral, force and the effects of the exterior end frames and the interior gravity frames were neglected. Because of the square plan of the

structure, the effect of accidental torsion was approximated by increasing the lateral seismic force by 5%. In this manner, the base shear for a single plane frame was calculated as

$$V = 448 * 1.05/2 = 235 \text{ kips} \quad (10)$$

The code loading and resulting deformation of the frame are shown in Fig. 31. Gravity loading is input as a uniformly distributed load as shown in Fig. 31a, and this results in the deformed shape of the frame shown in Fig. 31b. The controlling lateral force is due to earthquake and the equivalent lateral forces are shown in Fig. 31c. These result in deformation of the frame as shown in Fig. 31d where it can be seen that the maximum deformation at the roof level is 2.07 inches. The relative displacements (story drifts) under design wind load and design seismic load are shown in Fig. 32. Here, the seismic deformation is based on the lateral loads multiplied by  $1/k$  as specified in the building code. Normal design procedure usually limits the drift under design wind load to 0.002 to 0.003 to prevent motion of the structure which is discernable to the occupants. It can be seen from the figure that the calculated wind drift is in the middle of this range. The drift under seismic load is 0.0035 which is well within the code limit of 0.005.

The stress ratio (SR) is defined as the ratio of the actual stress in the member to the allowable stress. Therefore, to meet the allowable stress design criteria commonly used for steel structures, the stress ratio of all members must be less than or at most equal to unity. Stress ratios for the members of

the frame are shown in Fig. 33. The stress ratios due to gravity load acting alone are shown in Fig. 33a. In the case of combined gravity load and seismic load, shown in Fig. 33b, the allowable stresses have been increased by 33% as permitted in the code. It can be seen that the larger stress ratios are the result of the combined gravity load and seismic load and that the critical values occur in the columns of the first floor. The maximum value of the stress ratio can be seen to be 0.69 which implies that the structure has a design conservatism for this combined load condition of  $1./0.69$  or 45%.

#### 6.4 1988 Code Seismic Design Requirement

The 1988 Uniform Building Code defines the base shear as

$$V = (ZIC/R_w)W_e = C_s W_e \quad (11)$$

where

$$C = 1.25S/T^{2/3} \quad (12)$$

and the period,  $T$ , may be estimated as either

$$T = 0.035h^{3/4} \quad (13)$$

which results in the following estimate:

$$T = 0.035*(82.5)^{3/4} = 0.96 \text{ sec.} \quad (14)$$

Alternatively, the period can be estimated using a Rayleigh procedure as

$$T \text{ (Rayleigh)} = 1.48 \text{ seconds} \quad (15)$$

Use of these estimates of the period along with  $R_w = 12$ ,  $Z = 0.4$ ,  $S=1.0$  and  $I = 1.0$  results in design seismic resistance coefficients of either

$$C_s(T=0.96) = 0.0428 \quad \text{or} \quad C_s(T=1.48) = 0.0321$$

and corresponding base shears of either

$$V(T=0.96) = 333.1 \text{ kips} \quad \text{or} \quad V(T=1.48) = 249.4 \text{ kips}$$

Since the value of 249.4 kips is 75% of the 333.1 value, the minimum base shear is limited to  $0.8 \times 333.1 = 266.4$  kips which results in a design seismic resistance coefficient of 0.0342. It can be seen that these values are 74% and 59% of the 1973 code value. It can also be noted that the actual recorded building period of 1.3 seconds is between the two estimates of the period,  $T=0.96$  and  $T=1.48$ .

#### 6.5 1988 Code Wind Design Requirement

The lateral forces due to design winds in the 1988 Code are based on a basic wind speed map given in the code. The design wind speed for southern California is given as 70 mph and the design wind pressure as

$$p = C_e C_q q_s I \quad (4)$$

where  $I=1$ ,  $C_q=0.8+0.5=1.3$  and  $C_e$  is determined from

Height	$C_e$
0-20	0.7
20-40	0.8
40-60	1.0
60-100	1.1

Use of these values results in a base shear due to wind of 139.3 kips which is 77% of the 1973 code value. Therefore it can be concluded that the lateral forces used in the original design will still govern the design and that the structure as built will satisfy the current code requirements.

## 7. ELASTIC RESPONSE ANALYSES

### 7.1 Modal Analyses

Using the three-dimensional SAP90 model of the structure and the corresponding ETABS model shown in Fig. 34, the mode shapes and frequencies for the first nine modes were evaluated. The deflected shapes of the first three modes obtained from the SAP90 model are shown in Fig. 35. Here it can be seen that the first two modes are translational modes and that the third mode is a torsional mode. The dynamic properties of the two models are summarized in Table 4.

TABLE 4. PERIODS OF VIBRATION, 3D MODELS

Mode	1	2	3	4	5	6	7	8	9
SAP90	1.42	1.42	0.83	0.51	0.51	0.30	0.29	0.29	0.19
ETABS	1.42	1.42	0.82	0.51	0.51	0.30	0.29	0.29	0.20

It can be seen that, because of symmetry, the translational modes are the same in each orthogonal direction. It should also be noted that the value for the fundamental mode compares well with the estimate of period obtained from the code using the Rayleigh procedure (1.48) and the recorded response (1.33). However, it should be recalled that this represents the period of the bare frame and not the existing frame which will be stiffened by the addition of the gravity load framing and the nonstructural components as indicated by the recorded value. Use of nine modes of vibration represents 98.7% of the participating mass which is well above the 90% requirement in the code. In

this model, the first mode contributed 83% of the participating mass.

The deflected shapes for the first three modes obtained using the two dimensional model are shown in Fig. 36. These modes compare with modes 1, 4 and 7 of the three-dimensional model. The modal periods for the two dimensional model are summarized in Table 5 below.

**TABLE 5. PERIODS OF VIBRATION, 2D MODEL**

Mode	1	2	3	4	5
SAP90	1.447	0.525	0.304	0.209	0.157
ETABS	1.425	0.506	0.291	0.198	0.147

In this case using three modes of vibration represents 99.9% of the participating mass, with the first mode contributing 84.1%, the second mode contributing 11.9%, and the third mode contributing 2.9%.

From the system identification studies described previously, the fundamental period of the building based on the recorded response is approximately 1.3 seconds which is about 9% lower than the calculated bare frame period. This implies that the structure at this level of base excitation is about 21% stiffer than indicated by the bare frame analysis. This additional stiffness is due to several sources including the following: (a) the composite action between the concrete and steel deck and the main girders, (b) the influence of the

internal gravity framing, which is assumed to have pinned connections but which has a certain flexural stiffness, and (c) the influence of the nonstructural components such as the exterior cladding and the interior partitions. Modifying the models developed above, an attempt was made to evaluate the contribution of these sources of additional stiffness.

The three-dimensional model, including the interior gravity frame, is shown in Fig. 37. In this investigation, the simple framing is assumed to be completely rigid to give an upper bound to the increase in stiffness. A modal analysis of this system shows that the fundamental period of vibration is reduced by only 5%. The deck system consists of three components. The metal decking is welded to the steel girders and then filled with 3 inches of normal weight concrete. On top of this is added another 3 1/2 inches of lightweight concrete. If the steel decking with 3 inches of concrete acts in a composite manner with the girder, the fundamental period of the structure is reduced by an additional 4%, resulting in a total reduction of 9.2%. The directional properties of the steel decking may account for the difference in period in the two orthogonal directions noted in the system identification studies. In the elastic response analyses that follow, these effects are lumped together by the use of an effective modulus of elasticity of 42,000 ksi rather than 29,000 ksi. Since the period of the fixed base model agrees reasonably well with the recorded period, additional flexibility at the base was not considered in this

study. Although the base is not completely fixed in the actual structure, at the low acceleration levels experienced by the building during this earthquake it may have acted as though it were fixed.

## 7.2 Dynamic Response Analyses

In these analyses, the three-dimensional SAP90 model was subjected simultaneously to base accelerations recorded in the north-south and east-west directions. The response spectrum for the accelerations calculated at the roof level is compared with that for the recorded accelerations in Fig. 38. In the spectra presented in Fig. 38a, the calculations assume there is 5% of critical damping in all modes, and the spectra are developed for 5% damping. The periods for the first four translational modes for the structure using the higher modulus are 1.2, 0.44, 0.25, 0.17 seconds. These can be seen as the four peaks on the response spectra. The match for the first mode is quite good, while in the higher modes the calculated values exceed the recorded values. This result can be adjusted by increasing the damping in the higher modes. The results shown in Fig. 38b are for damping values of 7, 10, 13, and 15% of critical damping in the first four modes. This produces a good match of the recorded spectra over most of the period range with the possible exception of the fourth mode.

Time history responses at the roof level are compared in Fig. 39 for the three recording channels. In all cases, the comparison is good for the peak values although there are

differences in the lower responses after 20 seconds. In these comparisons, the calculated accelerations are for the master node at the center of the structure. Some differences with the recorded results may be due to torsional effects.

The calculated and recorded responses at the third story level are compared in Fig. 40. A representative floor spectrum at the third level is shown in Fig 40a. Here the match of the spectral values over the period range of the first two modes is good with a small deviation in the higher modes. The time histories of the acceleration at the three recording stations on the third level are compared in Figs. 40b, 40c and 40d and again show a reasonable correlation.

### 7.3 Directional Input Analyses

The three-dimensional ETABS model was used to study the effect of the direction of the input motion on the stresses in the members of the structure. Only one component of recorded base acceleration could be used, and that recorded on Channel 13 in the north-south direction was selected. This input motion was then rotated through a total angle of 90 degrees in increments of 15 degrees and the corresponding stress ratios were calculated. The stress ratios (SR) resulting from the motion acting in the north-south direction are shown in Fig. 41. Here it can be seen that the maximum stresses occur in the frames parallel to the input motion and that the time history values for this input compare well with the code values obtained earlier. This implies that this earthquake was close to the

minimum requirement specified in the building codes. Note that the maximum value of 0.67 in the critical column of the first story compares with 0.69 obtained in the static code analysis. The effect of applying the input motion at an angle of 15 degrees is shown in Fig. 42. Here it can be seen that the SR in the critical column increases to 0.71. Further rotation of the input motion through 30 degrees increases the critical SR to 0.73 as shown in Fig. 43. Note that as the angle of incidence increases the stresses in the east-west frames begin to increase as would be expected. As the angle of incidence reaches 45 degrees (Fig. 44), the stress ratio in the critical column reduces to 0.70. However, the critical column is now in the east-west frame with a SR of 0.71. Further rotations to 60, 75 and 90 degrees are shown in Figs. 45, 46 and 47, respectively. In these figures the stresses in the critical members of the north-south frame are reduced while those in the east-west frames are increased. In both directions, the maximum SR in the columns of the first story reached a value of 0.73, which is 9% larger than the value of 0.67 in the recorded position of zero degrees.

## 8. NONLINEAR STATIC ANALYSES

Nonlinear static analyses were performed on the two dimensional model of the frame in order to obtain estimates of the following: (a) yield strength (resistance) of the frame, (b) ultimate strength (resistance) of the frame, (c) overall displacement ductility, (d) corresponding curvature ductility of

individual elements, (e) total rotation requirements of individual elements, (f) ultimate interstory drift and (g) story displacement ductility. Two computer programs were used to investigate the nonlinear static behavior. Both assume the loading is applied in a proportional manner and that the plasticity is concentrated in plastic hinges.

The ULARC [9] program is event driven, where an event corresponds to either the formation of a new plastic hinge or the unloading of an existing plastic hinge. If the structure is assumed to be piecewise linear between events, the load increment required to produce a new event can be determined by linear scaling. Loads may be applied at the joints and the element resistance is assumed to be elasto-plastic: however, bilinear behavior can be handled by adding an additional element in parallel with the elasto-plastic elements.

The NODYN2 program, developed by one of the investigators, uses a step-by-step procedure to determine the nonlinear behavior. This procedure is used because the program was originally developed and primarily used for the step-by-step determination of nonlinear dynamic response. Therefore, application to nonlinear static response in this manner was a straightforward modification. Using this procedure, the total load is divided into a given number of equal load increments which are then applied sequentially to the structure. Linear behavior is assumed to occur between each load increment. Moment resistance of the individual elements is bilinear and gravity

loads may be applied as equivalent fixed end forces. Elasto-plastic behavior can be approximated using a small percentage of strain hardening in the bilinear element. Analyses using the ULARC program are terminated whenever one of the following conditions occurs: a collapse mechanism is formed, the full specified load is applied or a specified maximum displacement is reached. The NODYN2 program is terminated when the full specified load is applied.

In the analyses that follow, the lateral resistance of the building is evaluated by plotting the lateral roof displacement versus the base shear. A plot of this type comparing the results obtained using SAP90, ULARC and NODYN2 is shown in Fig. 48. Here the resistance in the SAP90 program is linear elastic, the resistance in the ULARC program is elasto-plastic and the resistance in the NODYN2 program is bilinear with the rate of strain hardening equal to 0.5%. In this example, the lateral loading is taken as uniform over the height of the building. In the linear elastic range, all three programs give the same result. In the inelastic range, the results of the ULARC and NODYN2 programs are very similar. Both depart from the linear SAP90 curve at a base shear of approximately 640 kips, reach an ultimate load of 760 kips and attain a maximum displacement of 10.3 inches. Because of the inclusion of strain hardening in the NODYN2 model, it is able to carry load beyond that indicated by the ULARC model. However, at some point, the deformation demands on the individual elements will become excessive and

these in turn will place a bound on the overall displacement. In this case the total load was adjusted to produce the same displacement as that obtained using the ULARC model.

It is also of interest to consider the effect of the vertical distribution of the lateral load on the lateral resistance of this building. Reasonable lateral load distribution functions include

(a)  $\Phi(x) = \text{constant}$  (uniform)

(b)  $\Phi(x) = x/h$  (linear)

(c)  $\Phi(x) = \sin(\pi x/2h)$

(d)  $\Phi(x) = 1 - \cos(\pi x/2h)$

where  $h$  is the height of the structure and  $x$  is the height of the story level above the base.

Differences between the triangular and uniform distributions are shown in Fig. 49. Here it can be seen that since the triangular distribution raises the height of the lateral force resultant, the lateral displacement at the roof level increases substantially. However, the lateral load capacity of the frame does not change. The shear versus displacement curves for the other lateral load distributions are shown in Fig. 50. Here it can be seen that the largest lateral resistance of the structure is obtained when the resultant lateral force is at its lowest position. This condition also results in the least displacement at the roof level. Conversely, the least lateral resistance occurs when the resultant lateral load is at its highest position with the resulting maximum roof

displacement. For this building the ultimate resistance is relatively insensitive to the lateral load distribution. This is a function of the failure mechanism and the distribution of plastic hinges in the building. For other buildings the difference in ultimate resistance as a function of load distribution may be more significant.

Up to this point, the resistance curves have been developed using the nominal yield stress of 36 ksi for the A36 steel used in the building. Coupon tests on the steel used in the building indicate that the true yield stress of the material is approximately 44 ksi. If this value is used in the model with a triangular load distribution, the resistance changes considerably as shown in Fig. 51. For the same total load and the higher yield stress, the building resistance is almost linear and first yielding does not occur until a base shear of 780 kips is reached. In order to determine the maximum lateral resistance of the building with the increased yield strength, it is necessary to increase the total applied load. Results of increasing the lateral load are shown in Fig. 52. The curve for the 36 ksi steel is included for comparison. Also included is a curve for the nominal resistance of the building had Grade 50 steel been used for the columns. It can be seen that the ultimate resistance of the building with 44 ksi steel increases to 910 kips. The use of the 50 ksi columns gives a resistance similar to the 44 ksi steel throughout.

The influence of strain hardening on the lateral resistance of the frame is shown in Fig. 53, where the difference in lateral force capacity for strain hardening rates of 0.5% and 3.0% is also shown.

It is also of interest to consider the lateral story displacement (relative displacement) as a function of the story shear, using the triangular loading results in the resistance curves shown in Fig. 54. Here it can be seen that the 6th story is linear elastic and that the maximum inelastic displacement occurs in the first story. The second story level has the largest lateral stiffness, because the column size is the same as the first story but the story height is less. Using these curves, the displacement ductility requirements of the individual stories can be estimated. For these calculations, the story ductility will be defined as the ratio of maximum relative displacement to relative displacement at first yield. This data will then be compared with the curvature ductility requirements of individual members.

The maximum curvature ductility requirement for the beams and columns of a particular story level is compared with the story displacement ductility requirement in Fig. 55. Here it can be seen that the maximum requirement for the beams is 3.25 at the first level. Although this is not excessive for a compact section, it may cause problems at the connection to the column. On the other hand, the maximum ductility requirement for the columns of the first story is 3.47, which for a column under

combined axial load and flexure is approaching that which can reasonably be obtained. The story ductility, which is based on displacement, compares well with the curvature ductility of the individual members for this system, reaching a maximum value of 3.75 at the first level.

The maximum total rotation for the beams and columns of a particular story level is shown in Fig. 56 along with the interstory drift index (drift angle). The interstory drift index is obtained by dividing the maximum relative (interstory) displacement by the story height. For the beams the maximum total rotation is just over 2% which is close to the capacity of a typical beam-to-column moment connection [10, 11]. For the columns of the bottom floor, the maximum total rotation is close to 3.5% which is excessive and provides the justification for limiting the total lateral load applied to the frame at this point. A similar result can be seen for the interstory drift ratios. In the first story level, the interstory drift is close to 2.6% which is large and along with the column rotation is reason for limiting the applied lateral load.

The nonlinear static behavior of this structure can be further illustrated by considering the sequence of plastic hinge formation shown in Fig. 57. This data was taken from a ULARC analysis using the nominal yield strength and a triangular load distribution. It clearly shows that with the formation of the 30th plastic hinge, a sway mechanism is formed in the first story level which in turn results in the severe ductility and

drift requirements on the columns of this level. This is a limitation of the design which results in a soft story at ultimate load. It can also be seen that at ultimate lateral load, only one plastic hinge has formed in the columns of the second story level. This is due to the design practice of holding the column size constant for at least two story levels. Because of the increased story height of the bottom story, the columns of the second story are considerably larger than required for strength. This tends to concentrate the inelastic deformation in the first story level and leads to the formation of a soft story at ultimate load.

By referring to the base shear versus roof displacement shown in Fig. 58, the overall displacement ductility of the structure can be approximated. Since the shear versus displacement curve has a smooth transition from linear behavior to inelastic behavior, it does not exactly fit the context of displacement ductility which is defined for a perfectly elasto-plastic relationship. The displacement ductility is defined as the ratio of the maximum displacement to the displacement at yield. With a smooth transition, there can be several definitions of displacement at yield. Two of these are the following: (a) the displacement at yield is the displacement when yielding occurs at the first critical section and (b) the displacement at yield is determined by comparison with an idealized elasto-plastic response curve. In the NODYN2 response curve, first yield occurs at a load of 640 kips and a

corresponding displacement of 6.5 inches. Using this value, the displacement ductility of the frame becomes  $13.5/6.5$  or 2.08. If an idealized elasto-plastic curve is constructed (Fig. 58), the yield displacement is 7.5 and the displacement ductility becomes  $13.5/7.5$  or 1.8. Note that both of these values are considerably less than the values of 4 or 5 often quoted in building code commentaries.

The results of this type of analysis also provide a means for evaluating the seismic resistance coefficient for this structure. The yielding seismic resistance coefficient has been defined previously as

$$C_y = R_y/W_e$$

In this equation, the yield resistance,  $R_y$ , is taken as the lateral resistance of an equivalent elasto-plastic system. Considering both frames, the yield seismic resistance coefficient for this structure becomes

$$C_y = 2*750/7785 = 0.19$$

Referring to the elastic response spectra shown in Fig. 11b for the recorded base motion (Channel 13), it can be seen that for this earthquake the demand seismic resistance coefficient,  $C_d$ , is approximately 0.07. It is of interest to recall that this value is above the design seismic resistance coefficient used in the design (0.058). Since lateral forces specified in the building codes are based on working stress, this coefficient must be multiplied by 1.4 to obtain the ultimate seismic resistance design coefficient (0.081). Comparing the ultimate

seismic design coefficient with the yield seismic design coefficient indicates that this structure has an overstrength represented by the overstrength ratio (OSR) of

$$\text{OSR} = C_y/C_d = 0.190/0.081 = 2.35$$

The inherent overstrength of this structure will be investigated in more detail in the following section.

### 9. ANALYSIS OF STRUCTURAL OVERSTRENGTH

Using the results of the previous sections, it is possible to obtain an estimate of the overstrength ratio for this structure. The OSR can be assumed to consist of the following five major components: (a) a factor representing the ratio of the ultimate strength of a member to the allowable strength, (b) a factor representing the ratio between the actual stress in the member and the limiting allowable stress permitted by code, (c) a factor representing the effect of load redistribution, (d) a factor representing the effect of strain hardening and (e) a factor representing the ratio between the nominal yield stress of the material and the actual yield stress. The allowable stress for a generic member including the 33% increase for inclusion of seismic loads can be expressed as

$$F_a = 0.6 * F_y * 1.33 = 0.8 F_y$$

which implies that

$$F_y = 1.25 * F_a$$

The ratio of ultimate moment to yield moment can be expressed as

$$M_p = (Z/S) M_y = 1.14 * F_y * S = 1.14 * 1.25 * M_a$$

$$M_p = 1.425 * M_a$$

and therefore

$$\text{ultimate strength/allowable strength} = 1.425$$

where

$Z$  = plastic section modulus

$S$  = elastic section modulus

$M_a$  = allowable moment

$M_y$  = yield moment

$M_p$  = plastic moment capacity.

The stress in a member is usually expressed in terms of the ratio of the actual stress to the allowable stress (Fig. 33) and the limiting value of this ratio is unity. From Fig. 33b it can be seen that for combined gravity and lateral load, the stress ratio in the critical member is 0.69. In Fig. 33a, the stress ratio for this member due to gravity load acting alone is 0.25. For this value to be used with the gravity plus lateral load above, the allowable stress must be increased by 33% or conversely the stress ratio must be reduced by 0.75 resulting in a value of 0.1875. These values along with those developed in the preceding paragraphs for estimating the ultimate resistance are represented on an idealized force versus displacement curve in Fig. 59.

The capacity of the member to carry additional lateral force up to the allowable value can be obtained by subtracting the maximum stress ratio (SR) for gravity loads acting alone (Fig. 33a) from unity to obtain:

$$\text{Allowable seismic SR supply} = 1.0 - 0.1875 = 0.8125$$

Considering the SR due to combined gravity and seismic forces (Fig. 33b), the SR for the seismic lateral load condition can be obtained as:

$$\text{Code seismic SR demand} = 0.69 - 0.1875 = 0.5025$$

Using these two values the overstrength due to design conservatism can be estimated as

$$\text{Design conservatism} = 0.8125/0.5025 = 1.6169$$

In a similar manner, the overstrength due to the factor of safety incorporated in the allowable stress design procedure on first plastic hinge formation can be obtained as

$$\text{Factor of safety} = \frac{1.425 - 0.1875}{1.0 - 0.1875} = 1.5231$$

Combining these two factors, the overstrength on first yield (plastic hinge formation) can be estimated as

$$\text{OSR}_{(\text{yield})} = 1.617 * 1.523 = 2.463$$

and for this structure the base shear at first yield would be estimated to be

$$V_y' = 2.46 * V_{\text{code}} = 2.46 * 235 = 578.8 \text{ kips}$$

From the base shear versus displacement curve shown in Fig. 48, it was noted that the initial yield actually occurred at a value of 640 kips representing a difference of 9.5%. The seismic resistance coefficient at first yield,  $C_y'$ , can be expressed in terms of the design seismic resistance coefficient,  $C_s$ , as

$$C_y' = 2.46 C_s$$

Beyond first yield, the increase in strength is due to a combination of strain hardening and redistribution of internal

forces as plastic deformation occurs. Considering the ultimate shear to be 750 kips without the effect of strain hardening, the increase due to moment redistribution can be determined as

$$\text{redistribution} = 750/579 = 1.30$$

The amount of increase due to redistribution of moment is limited by the formation of a sway mechanism in the first story level with only a limited amount of inelastic behavior being distributed to the upper stories. Referring to Fig. 53, the ultimate shear can be estimated at 800 kips when including strain hardening, and the increase due to this effect is

$$\text{strain hardening} = 800/750 = 1.06$$

Summarizing the above results, the OSR for this structure can be expressed in terms of the four parameters as

$$\text{OSR} = 1.52 \text{ (factor of safety)}$$

$$* 1.62 \text{ (design conservatism)}$$

$$* 1.30 \text{ (redistribution)}$$

$$* 1.06 \text{ (strain hardening)} = 3.39$$

The yield seismic resistance coefficient,  $C_y$ , can then be expressed in terms of the design seismic resistance coefficient for this building as

$$C_y = 3.39 C_s$$

The resistance  $R_y$  can now be estimated as

$$R_y = 3.39 * V_{\text{code}} = 3.39 * 235 = 797 \text{ kips.}$$

This overstrength which is inherent in the current design process is undoubtedly a significant factor in reducing or

preventing earthquake damage, particularly for low to moderate earthquake motions.

The above discussion of overstrength has been based on the nominal yield strength of the steel. For most rolled steel shapes, the actual yield stress can be considerably higher than the minimum specification. In the case of this building, coupon tests indicated a yield stress of 44 ksi as compared with the nominal 36 ksi. From Fig. 52, it can be seen that this increase in yield stress results in an increase of  $910/750=1.21$  or 21% in the structure resistance. If this factor is combined with those discussed above, the OSR for this structure becomes 4.11.

#### 10. NONLINEAR RESPONSE ANALYSIS

In order to evaluate the inelastic dynamic response of the structure, it is necessary to select an ensemble of possible strong motion earthquakes. The design earthquake should then be the selected ground motion that will drive the structure to its critical response. Linear elastic response spectra (LERS) for acceleration records obtained during major earthquakes over the past 13 years are shown in Fig. 60. Also included in the figure is a plot of the LERS specified by the 1988 Uniform Building Code. Of particular interest to this study is the spectrum from Obregon Park which was obtained from the 1987 Whittier Narrows Earthquake. This motion, which is shown in Fig 61a, is representative of the strongest motion to be recorded during this earthquake. The response spectrum of this motion is compared with that of the motion recorded at the base of the

building in Fig. 61b. Here it can be seen that the Obregon Park motion is considerably stronger over the entire period range. It should also be noted that the UBC spectrum, shown in Fig. 60, is exceeded by a considerable margin in the period range from 0.0 to 3.0 seconds by several of these ground motions.

Acceleration time histories for these strong motion earthquakes are shown in Fig. 62. The acceleration recorded at Bucharest, Romania in 1977 is shown in Fig. 62a. The peak ground acceleration is a modest 0.2g but the motion is characterized by two long duration acceleration pulses which can have a significant effect on the dynamic response. The motion recorded at Hollister during the Loma Prieta Earthquake of 1989 is shown in Fig. 62b. This motion has a peak acceleration of 0.35g and a duration of strong shaking of about 7 seconds. The ground motion recorded at James Road during the 1979 Imperial Valley Earthquake is shown in Fig. 62c. This motion is also characterized by two large acceleration pulses. Previous studies [12] have indicated that this ground motion can create a strong response in a flexible frame. The final ground motion considered in this study is the motion recorded in Mexico City at SCT during the Michoacan Earthquake of 1985 which is shown in Fig. 62d. This motion has a modest peak acceleration of 0.17g but the duration of strong motion is in excess of 30 seconds. Note that the peak acceleration does not occur until almost 60 seconds into the recording.

### 10.1 Inelastic Response Spectra

Nonlinear response analyses of single-degree-of-freedom systems were performed using the NONSPEC program. Results of these analyses were used to obtain values of the required yield seismic resistance coefficient as a function of building period and displacement ductility for each of the ground motions just discussed. This data is presented in Fig. 63. These curves are very useful and can be used in either an analysis or a design context. From an analysis standpoint,  $C_y$  is known and the figures can be used to estimate the average displacement ductility requirement. Using the yield seismic resistance coefficient determined for this structure neglecting the effect of strain hardening ( $C_y = 0.19$ ), the average displacement ductility requirement under the above ground motions can be estimated as follows: Bucharest = 1.8, Hollister = 3.5, James Road = 3.0 and Mexico City SCT = 2.0. Plots of  $C_y$  versus building period have been developed by Uang and Bertero [13] for other earthquake ground motions. From a design standpoint, one can enter these graphs with the estimated period and the design ductility and obtain an estimate of the required seismic yield resistance coefficient.

### 10.2 Multiple Degree of Freedom Response Analyses

The nonlinear dynamic analyses are based on the two dimensional model of a typical perimeter frame. The analyses are done using the NODYN2 computer program which was also used for the static nonlinear analyses. Before considering the inelastic

response, the computer model to be used for the nonlinear response calculations was used to calculate the elastic response and to compare it with that recorded in the building. In order to include the effect of viscous damping in the nonlinear response calculation, it is convenient to represent the damping matrix as a linear combination of the mass and stiffness matrices. This results in two constants which can be selected to specify a given percentage of damping in two modes of vibration. Once these are selected, the damping in the other modes is defined. Based on the results of the elastic analyses, the constants were chosen to give 5% of critical damping in the first mode and 8% of critical in the 4th mode. This resulted in 4.4% of critical in the second mode and 6% in the third mode.

### 10.3 Linear Dynamic Analyses

Using these values and a two dimensional model similar to that used for the elastic analyses, the elastic response of the frame was calculated. The acceleration calculated at the roof level is compared with the recorded acceleration in Fig. 64a. A similar comparison of accelerations at the third story level is shown in Fig. 64b. In both cases, the comparisons are quite good.

The time history of the calculated base shear due to the recorded base acceleration is shown in Fig. 65a. Here it can be seen that the peak value of the base shear is about 270 kips which is well below the initial yield value of 640 kips obtained from the nonlinear static analysis. The time history for the

base shear under the Obregon Park motion is shown in Fig. 65b. The peak value in this case is 490 kips which is still considerably less than the 640 kips required to cause initial yield.

#### 10.4 Nonlinear Dynamic Analyses

The base shear under the Bucharest motion, shown in Fig. 66a has a peak value of 925 kips which is 44% above initial yield and 22% above the ultimate shear as determined by the static analysis. This increased base shear in the dynamic case above that obtained from a static analysis has been discussed by Bertero [14]. It is considered reasonable because of the following factors: (a) the opening and closing of plastic hinges with time and their migration through the structure, (b) the time variation of inertia forces and (c) the effect of higher modes of vibration. The base shear for the Hollister ground motion, shown in Fig. 66b, has a peak value of 850 kips which is also above the initial yield and the ultimate values. A similar result is shown for the base shear due to the James Road motion which is shown in Fig. 66c and has a peak value of 850 kips. The base shear for the SCT record is shown in Fig. 66d and has a peak value of 900 kips which is 18% above the ultimate static value. These studies indicate that the motion recorded at Bucharest generates the largest base shear and the only records which are insignificant for considering inelastic response are those obtained from the Whittier Narrows earthquake.

The base shear for a single frame based on the 1988 UBC is either 124.7 kips or 166.5 kips, depending on how the fundamental period of the building is estimated (see Section 6.4). Dividing the ultimate base shear of 925 kips by these values results in structural system factors of 7.4 and 5.6, respectively. Note that both of these values for  $R_w$  are well below those specified in the building code.

The inelastic displacement response is shown in Fig. 67. The envelope of maximum lateral displacement for the five ground motions is shown in Fig. 67a. Also included on this figure is the displacement required by the building code. It can be seen that as in the case of the base shear, the Bucharest motion results in the greatest displacement demand. The displacement requirement for Obregon Park is considerably less than the others and much closer to the code requirement. For the Bucharest, James Road and Mexico City records, most of the lateral displacement occurs in the first story level, whereas for the Hollister record there is also a major displacement increment between the 4th and 5th levels. The former records are characterized by some significant acceleration pulses which tend to concentrate the deformation in the first story, particularly if the first story tends to be a soft story as indicated from the static analysis. The later record is more sinusoidal in character, and this allows the inertia forces to build up in the upper stories. A similar condition can be seen in the plot of interstory drift shown in Fig. 67b. The Bucharest record has an

interstory drift of 2.9% in the first story. This value is relatively large but it is still less than the almost 4% indicated in the static analysis. Note the large interstory drift requirement of the Hollister record at the 5th story level

The curvature ductility requirements are shown in Fig. 68. The ductility requirements for the girders are shown in Fig. 68a. Here it can be seen that all values are less than 2.3 which can readily be developed in a standard moment connection of two compact members. As noted previously for the displacement response, the ductility requirements for the Obregon Park record are the least and, in fact, are considerably less than unity indicating elastic behavior. It can also be seen that the ductility required by the static analysis is about 2.5. The ductility requirements for the column elements are shown in Fig. 68b. The largest ductility requirement occurs in the first story columns for the Bucharest motion and has a value of 5.2 which is quite large for a column. Other column ductilities are 3.1 or less and should be sustainable.

The element rotation requirements are shown in Fig. 69. The girder rotations shown in Fig. 69a are all less than 1.4% and should be readily developed with a standard moment connection of two compact sections. The column rotation requirements are shown in Fig. 69b. Here it can be seen that the rotation requirements for the columns of the first floor under all ground motions except Obregon Park are quite large. It will be difficult to develop the large rotations required for the Bucharest and

Mexico motions. The rotation requirement obtained from the static analysis gives a good estimate of that which will be required in the most severe case.

The envelopes of maximum story shear are shown in Fig. 70. The values given in this figure are based on the sum of the maximum column shears at a given story level. As such, they represent an upper bound on the story shear since all of the maximum column values may not occur at the same time. This effect can be seen by comparing the base shear to the time history values given previously in Fig. 66. In addition, the code loads have been increased by 40% to represent the ultimate condition. It can be seen that the adjusted code values clearly represent the minimum shear. The story shears resulting from the four recent earthquakes are considerably larger than the adjusted code values and those obtained from the Obregon Park record. This is further evidence that the Whittier Narrows earthquake was not a very severe event.

Hysteresis curves of the story shear versus the interstory displacement are shown in Fig. 71 for the Bucharest ground motion. At the sixth story, shown in Fig. 71a the behavior is entirely linear. There is some limited ductility in the fifth story as shown in Fig. 71b. The fourth story also has only a limited amount of inelastic deformation, Fig. 71c. At the third story there is an increase in inelastic deformation followed by a decrease in the second story, Figs. 71d and 71e. As indicated previously, the primary inelastic deformation for this ground

motion occurs in the first (base) story as can be seen in Fig. 71f.

Similar hysteresis data for the Hollister ground motion is shown in Fig. 72. Here it can be seen that the sixth and second floors are elastic, Figs. 72a and 72e. From Figs. 72c and 72d it can be seen that the fourth and third floors have a limited amount of inelastic deformation. The main regions of inelastic deformation for this ground motion are on the fifth and first (base) floors as shown in Figs. 71b and 71f.

A plot of input energy for four of the ground motions used in this study are presented in Fig. 73. As in the previous cases, the Bucharest ground motion results in the largest amount of input energy indicating that it has the largest damage potential for this particular structure. It can also be seen that the energy from the Whittier Narrows earthquake is very low indicating that this is not a very severe earthquake. The Hollister record also has a significant amount of input energy for this structure and as shown previously controls some of the response parameters, particularly in the upper stories. The James Road energy input, while being substantial, is not the controlling one for this structure.

#### 10.5 Effect of Increased Ground Accelerations

The effect of a larger earthquake on the building is evaluated by increasing the accelerations recorded at Bucharest and Hollister by 30%. The effect of this increase on the maximum displacement envelope is shown in Fig. 74a. From this figure, it

can be seen that the effect of the increased acceleration on the displacement is greatest for the Bucharest motion where the roof displacement increases from 10.5 inches to 15 inches. The effect on the interstory drift index is shown in Fig. 74b. For both records the effect of the increase is greatest in the first story level. For the Hollister motion, the IDI in the first story increases to 2.1% and for Bucharest it increases to a very high 3.9%.

The girder ductility, shown in Fig. 75a, is affected in a similar manner. The largest increase is due to the Bucharest motion and the largest increase in girder ductility demand occurs in the bottom three floors. In the case of the column ductility demand, shown in Fig. 75b, the largest increase is again due to the Bucharest motion and occurs in the bottom two floors.

The maximum rotation demand is shown in Fig. 76. For the girders, shown in Fig. 76a, the maximum increase in the rotation requirement occurs in the lower three floors and is due to the Bucharest motion. At the first and third story levels, the rotation is above 1.5% which is close to that which can be developed in a moment connection. Considering the columns, shown in Fig. 76b, the maximum increase in rotation occurs in the first floor level. For all cases, the amount of rotation required in the first floor level is above 2%. For the Bucharest motion the rotation was 3.7% and it in turn increased to almost

5%. It is very doubtful that rotations of this magnitude could be developed in standard beam-to-column moment connections.

The effect of increased acceleration amplitude on the hysteresis curves of base shear versus interstory displacement of the first story is shown in Fig. 77. The hysteresis for the Bucharest motion is shown in Fig. 77a. Comparing this curve with that of Fig. 71f indicates that the interstory displacement has increased from 5.0 inches to 7.0 inches, an increase of 40%. However, the base shear increases only from 900 kips to 950 kips, an increase of 5.5%. This clearly indicates that in the inelastic range, the base shear becomes relatively insensitive to changes in seismic demand and that large changes can occur in the displacement response which are not reflected in the changes in the base shear. In the case of the Hollister motion, shown in Fig. 77b, the base shear increases from 860 kips to 890 kips, an increase of 3.5%. However, the maximum interstory displacement increases from 3.0 to 3.9 inches, an increase of 30%. Obviously, the maximum base shear is not going to be a very accurate parameter for evaluating damage potential.

## 11. SUMMARY AND CONCLUSIONS

This study has investigated the seismic behavior of a six-story steel building which was instrumented with thirteen strong motion accelerometers at the time of the Whittier Narrows earthquake. The building has a square plan with lateral resistance provided by a perimeter moment-resistant frame. Recorded peak accelerations were in the north-south direction

and ranged from 0.226g at the base to 0.289g at the roof. No damage was reported as a result of this motion.

System identification techniques were applied to the recorded data to identify the predominant periods of vibration. Moving window Fourier analyses were performed to investigate changes in the period of vibration during the earthquake. The effect of torsion was also evaluated using Fourier amplitude spectra and linear elastic response spectra. Linear elastic two dimensional and three-dimensional models of the building were developed to study the behavior of the building under code lateral forces and the recorded base motion. Two dimensional nonlinear models of the building were developed and used to evaluate the ultimate strength of the building under monotonically applied static lateral forces. Using these results, the overstrength of the structure was estimated. The two dimensional nonlinear models were also used to evaluate the behavior of the building when subjected to the ground motions of selected strong motion earthquakes which have been recorded previously.

On the basis of these extensive studies, the following general conclusions are presented:

1. This building was not severely tested by the ground motion recorded at the base during the Whittier Narrows Earthquake. The base accelerations were short duration acceleration spikes which did not result in a significant energy input to the structure. Furthermore, the duration of strong motion shaking was a

relatively short three seconds. Results show that the dynamic response was completely linear elastic.

2. Using commercially available computer programs, two dimensional and three-dimensional mathematical models can be developed which accurately predict the linear elastic dynamic response as represented by recorded accelerations at various locations in the building.

3. The design seismic resistance coefficient specified by current building codes has been reduced substantially for a building of this type when compared with the value used in the original design in 1973. It is not clear to the investigators how this significant reduction can be justified.

4. The directional effects of the input ground motion are shown to increase the stress in the critical members of this structure by 9%. With current computer programs, this effect can easily be incorporated into the design analysis.

5. Nonlinear static analyses can be very useful in estimating the following mechanical characteristics of the structure which can be used as an indication of inelastic dynamic response behavior:

- (a) The ultimate resistance of the structure as represented by the base shear versus roof displacement relationship.
- (b) The maximum rotation requirements and ductility

requirements of critical members.

- (c) The distribution of inelastic behavior (plastic hinges) at ultimate load.
- (d) Determination of the yield seismic resistance coefficient for the building.

6. The concept of the yield seismic resistance coefficient can be very useful in estimating the seismic behavior of a structure for purposes of design. Using a nonlinear static analysis of the building, the yield seismic resistance coefficient,  $C_y$ , can be determined. Using  $C_y$ , the fundamental period of the building and inelastic response spectra for single-degree-of-freedom systems, the average ductility requirements for various strong motions earthquakes can be estimated.

7. The structure considered in this study has an inherent overstrength which resulted in an ultimate lateral resistance which was more than 200% above the code requirement. This has undoubtedly had a significant effect on the favorable seismic response of this structure, particularly under the relatively low seismic input of this earthquake.

8. Using the nominal values for the material yield stress, the perimeter frame formed a sway mechanism in the first story level at ultimate load. This behavior is undesirable since it limits the redistribution of plastic hinges (inelastic deformation) into the upper floors and results in a reduced resistance at

ultimate lateral load. It also causes the resistance curve to have a relatively flat post yield characteristic which results in large lateral displacements for small increases in the lateral force.

9. The displacement ductility requirement of the individual story levels shows a relatively good correlation with the curvature ductility of individual members in the story. However, the overall displacement ductility is considerably less than either the story displacement ductility or the member curvature ductility.

10. The design practice of keeping a column size constant for at least two story levels causes the inelastic deformation at ultimate load to be concentrated in a limited number of story levels rather than being distributed over the height of the frame in a more uniform manner. This becomes readily apparent from the results of a nonlinear static analysis.

11. Input motions characterized by strong acceleration pulses (Bucharest and James Road) tend to affect the lower floors of buildings. If these floors become soft stories at ultimate load, the combination of pulse load and soft story can lead to poor seismic performance. Motions characterized by numerous zero crossings and longer duration (Hollister, SCT) tend to have more effect on the upper floors of the structure.

12. The structural system factor,  $R_w$ , evaluated for this moment-resistant steel frame is shown to vary between 5.6 and 7.4. Both values are well below the value of 12 specified in the 1988 UBC.

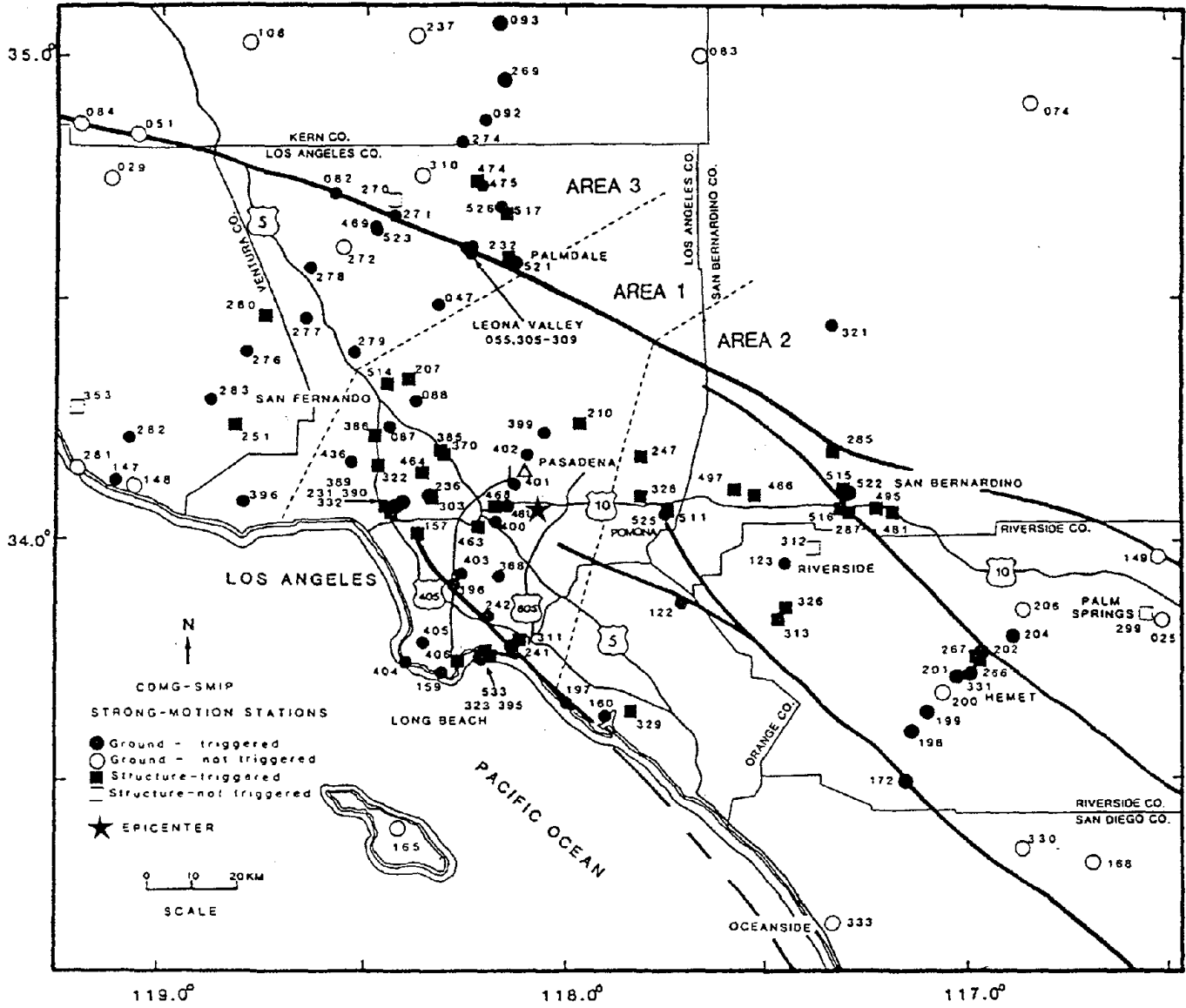


Fig. 1 CSMIP Strong Motion Stations near Whittier

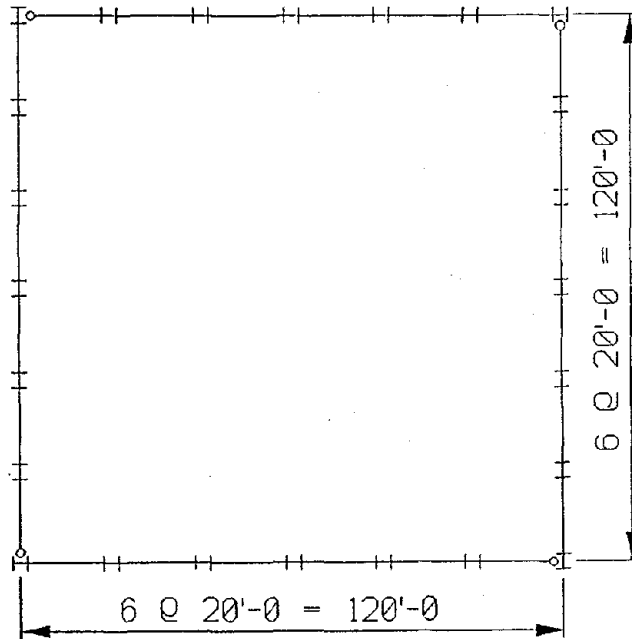


Fig. 2 Plan View of the Building

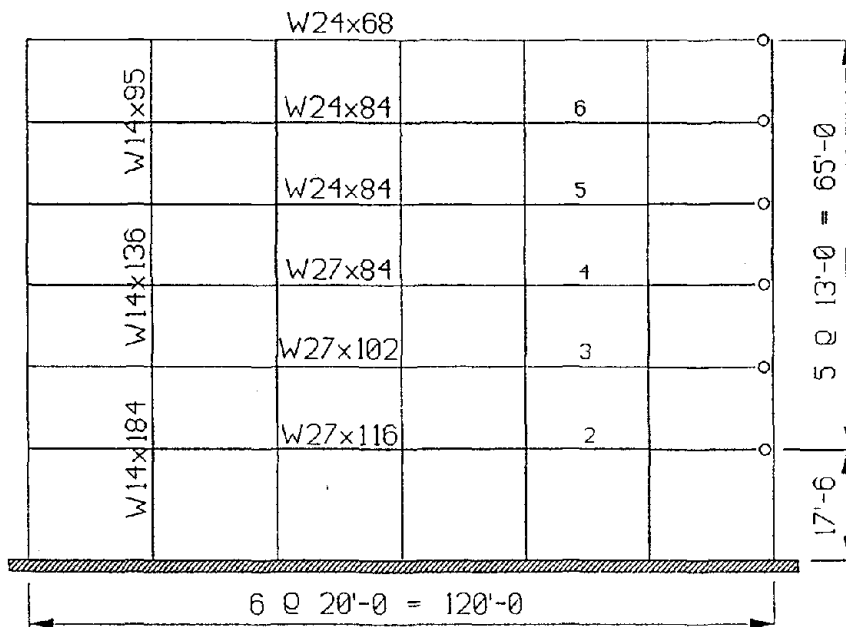


Fig. 3 Elevation View of the Building

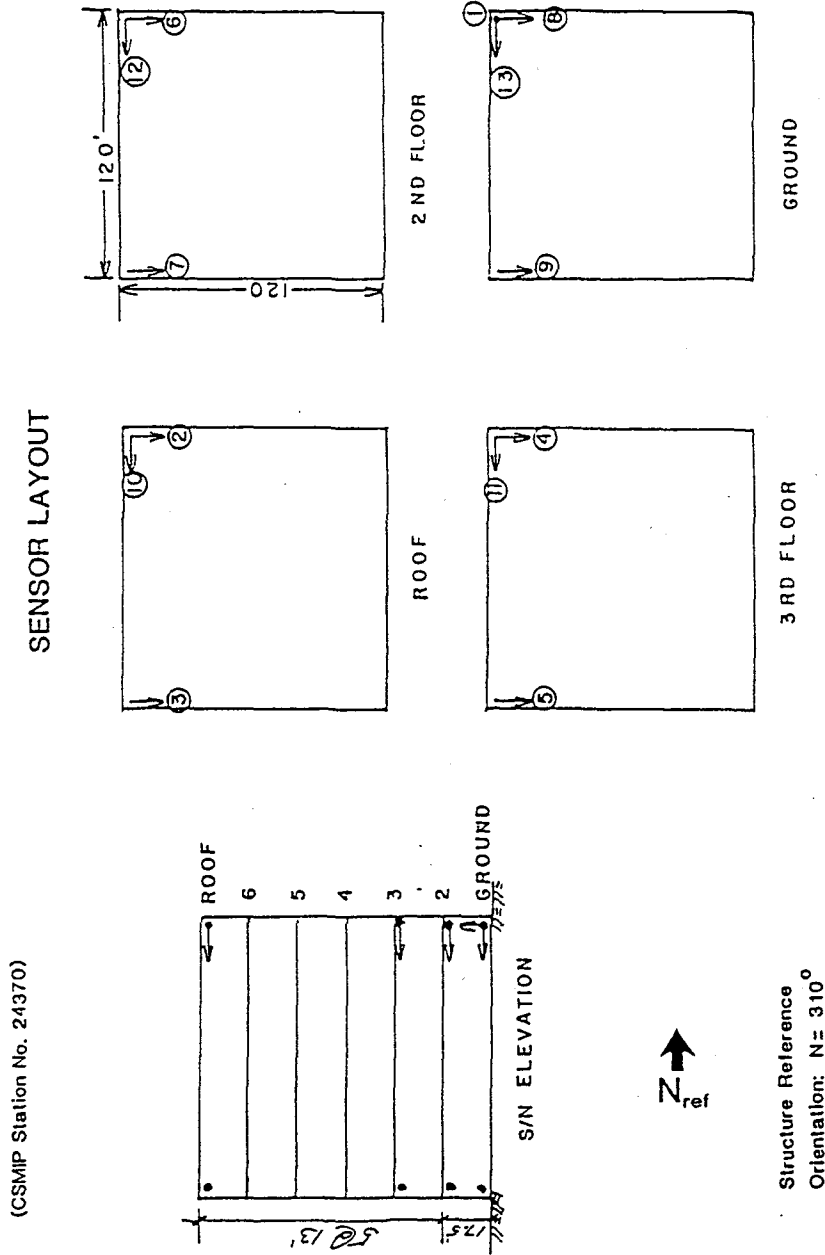
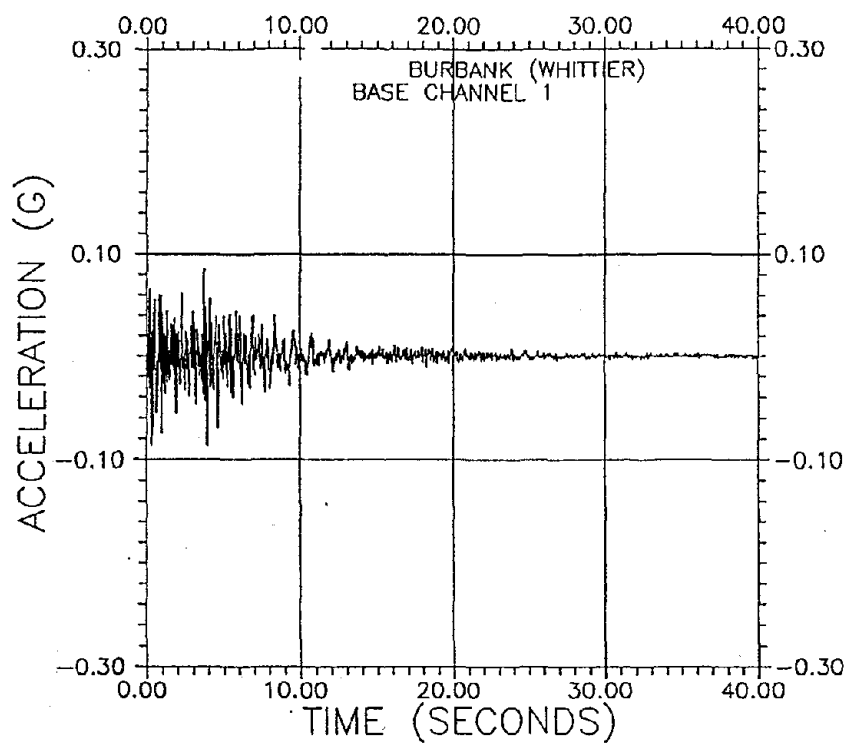
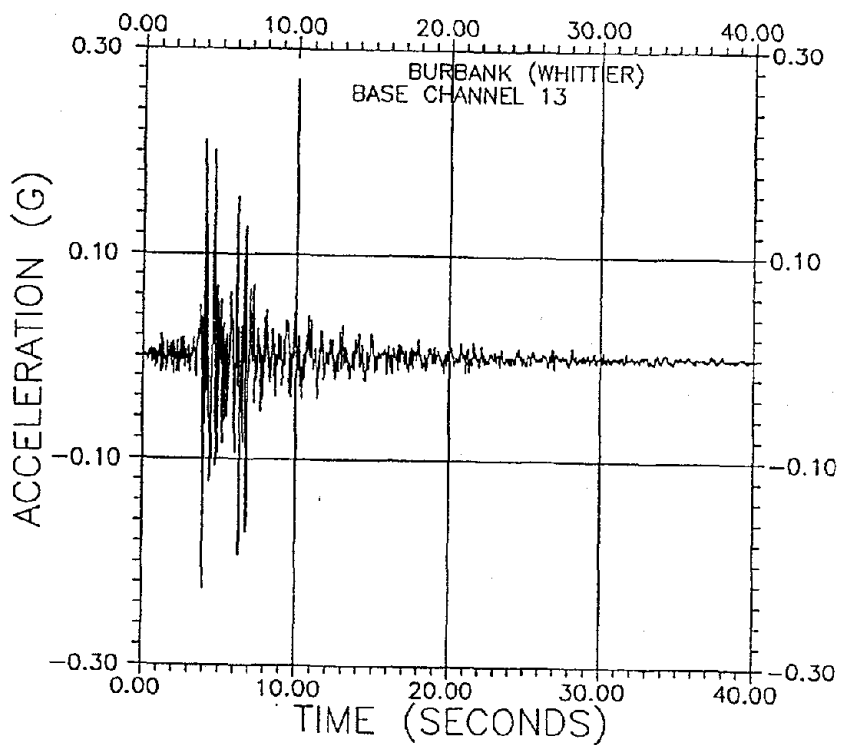


Fig. 4 Location of Building Instrumentation

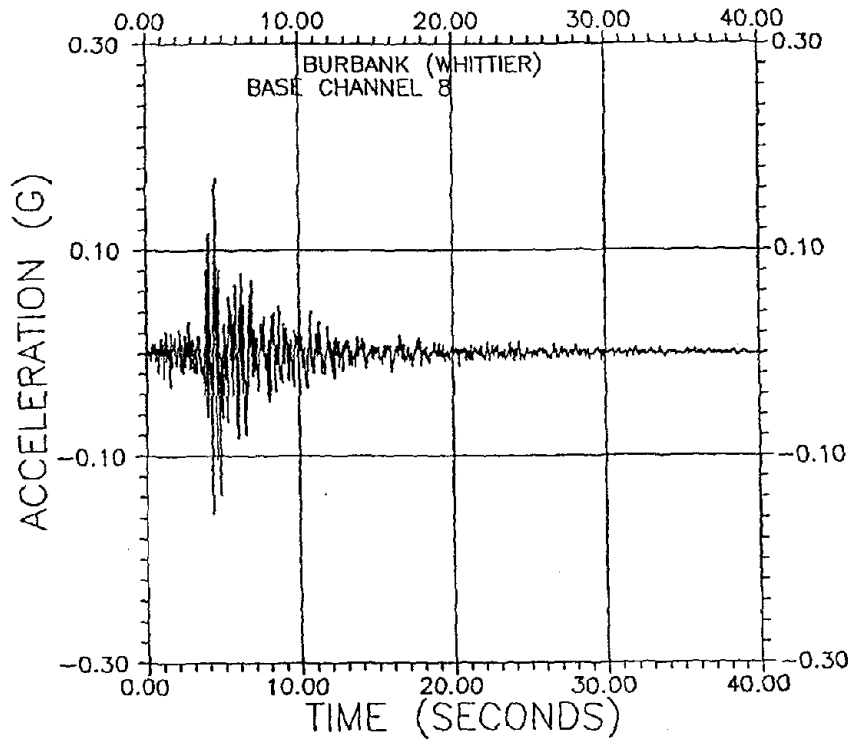


(a) Channel 1, Up, NW Corner

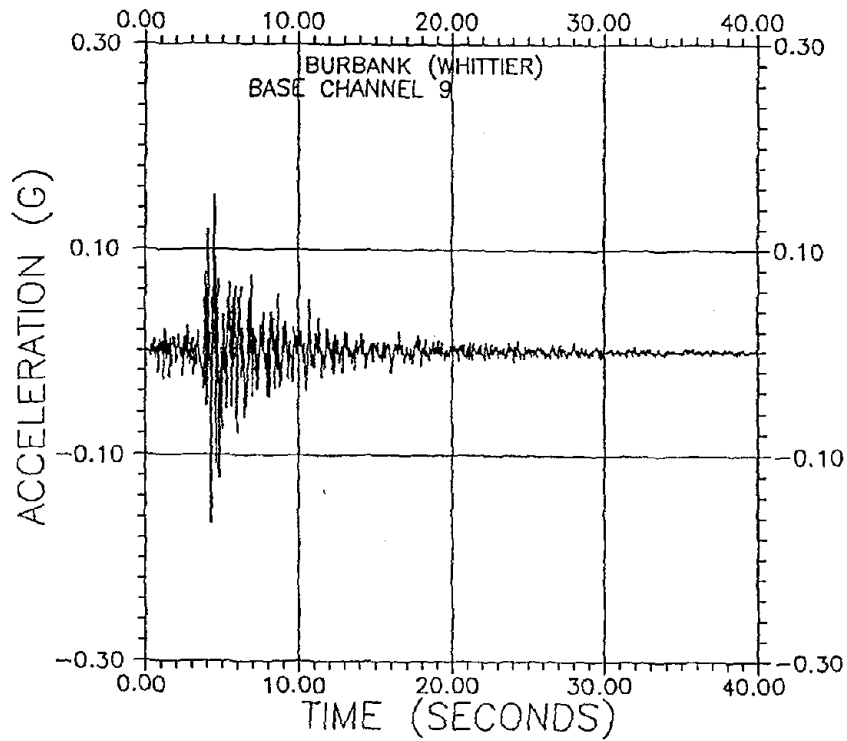


(b) Channel 13, N-S, NW Corner

Fig. 5 Recorded Acceleration at Ground Level

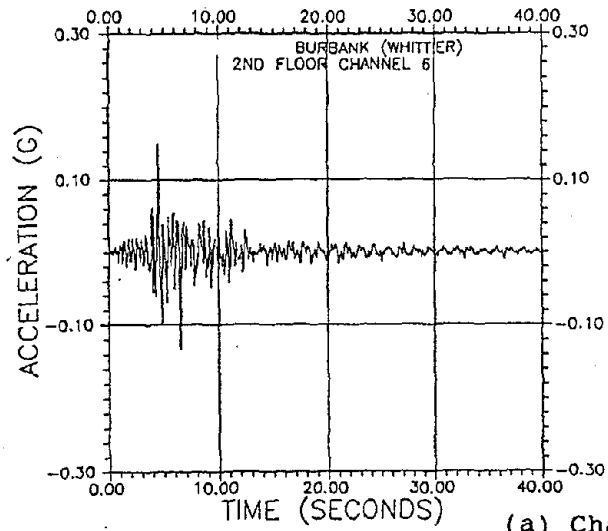


(a) Channel 8, E-W, NW Corner

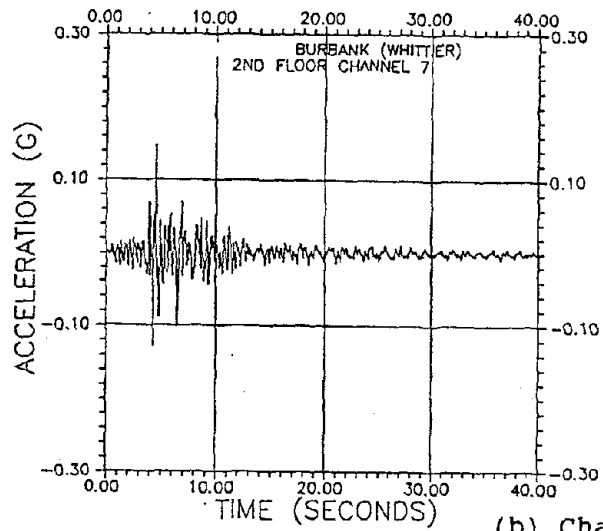


(b) Channel 9, E-W, SW Corner

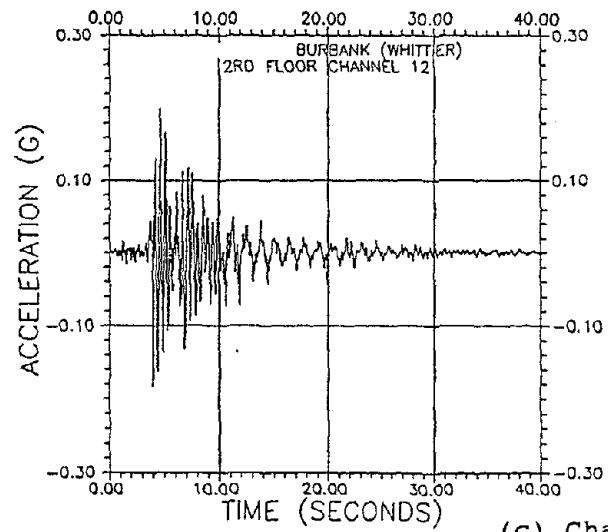
Fig. 6 Recorded Acceleration at Ground Level



(a) Channel 6, E-W, NW Corner

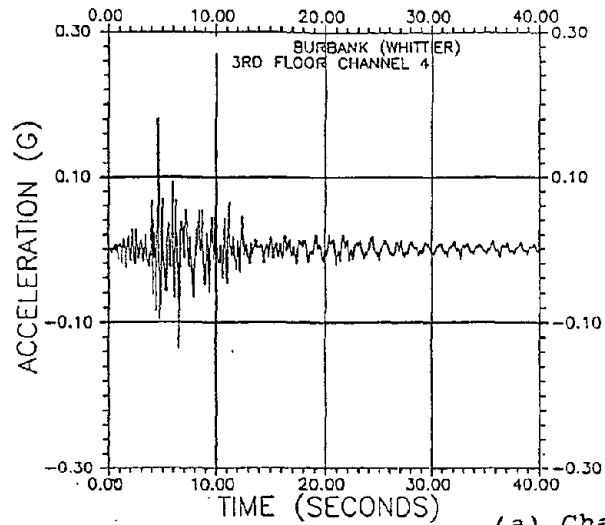


(b) Channel 7, E-W, SW Corner

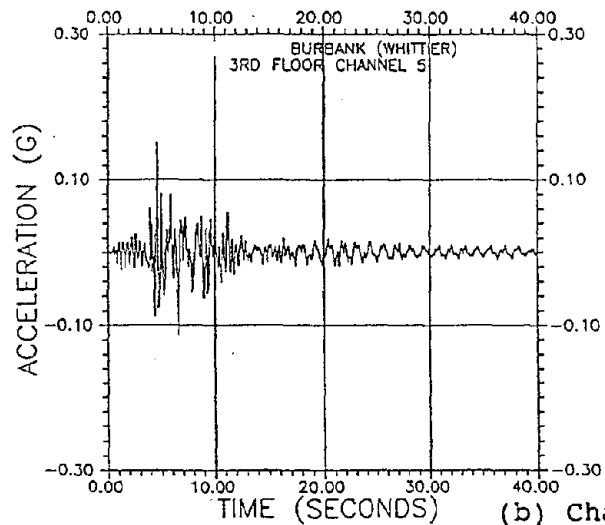


(c) Channel 12, N-S, NW Corner

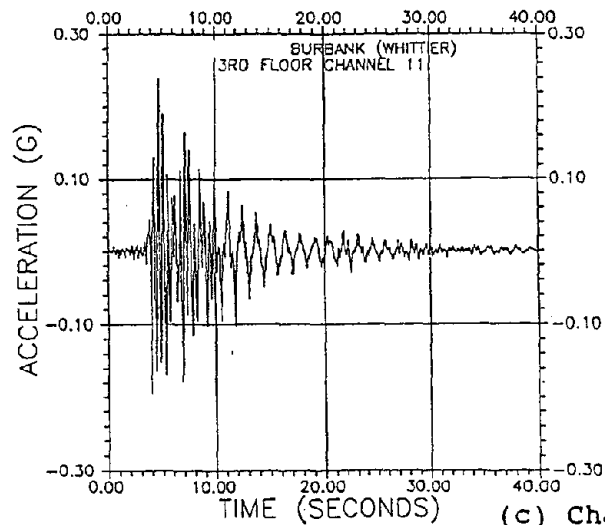
Fig. 7 Recorded Acceleration at Second Floor Level



(a) Channel 4, E-W, NW Corner



(b) Channel 5, E-W, SW Corner



(c) Channel 11, N-S, NW Corner

Fig. 8 Recorded Acceleration at Third Floor Level

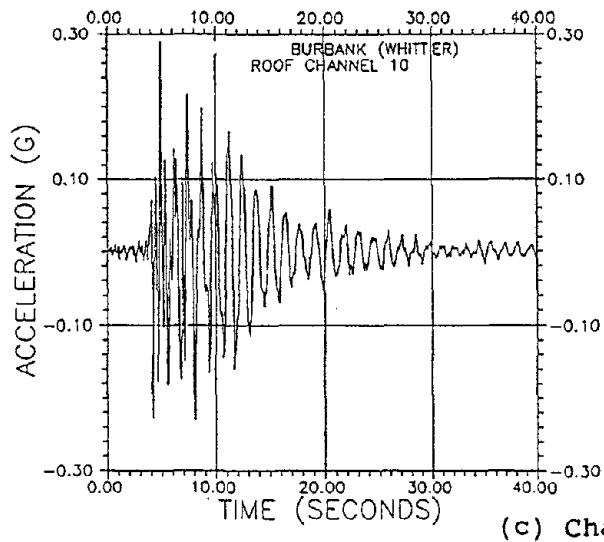
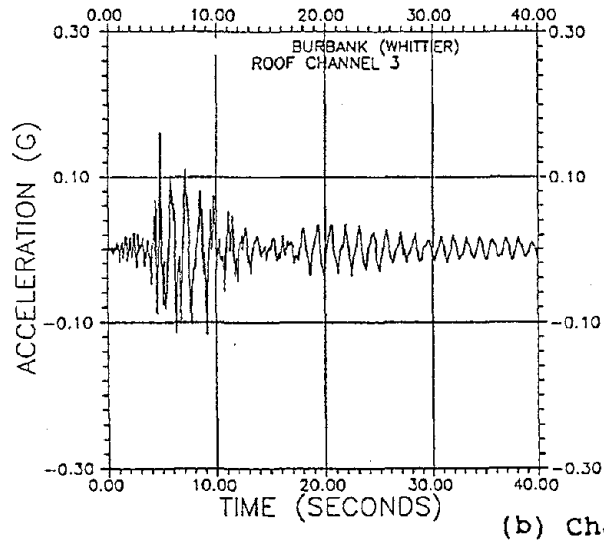
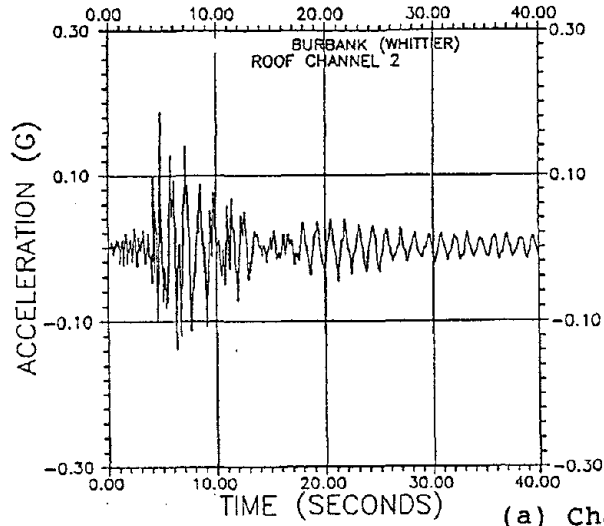
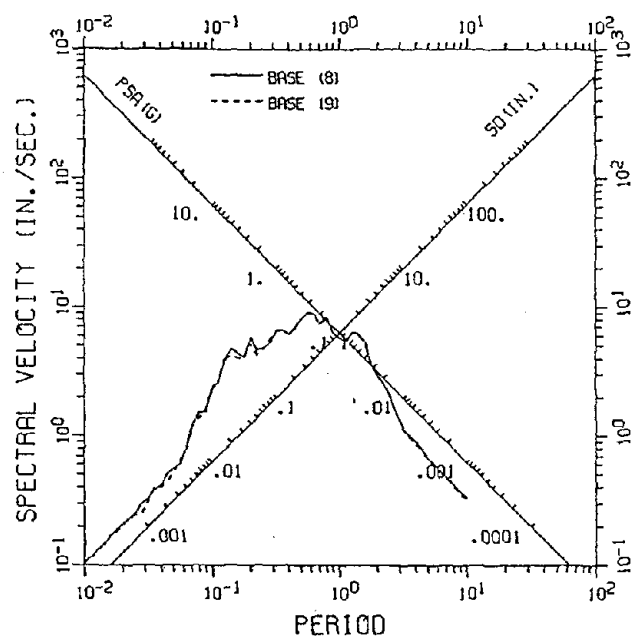
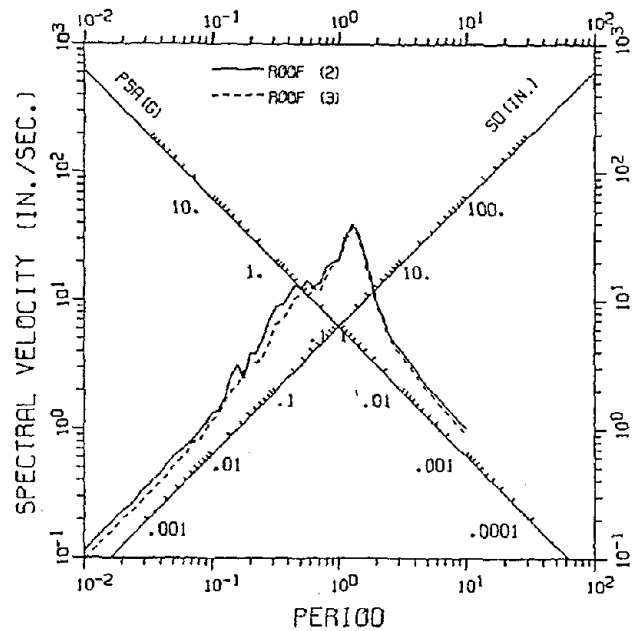


Fig. 9 Recorded Acceleration at Roof Level

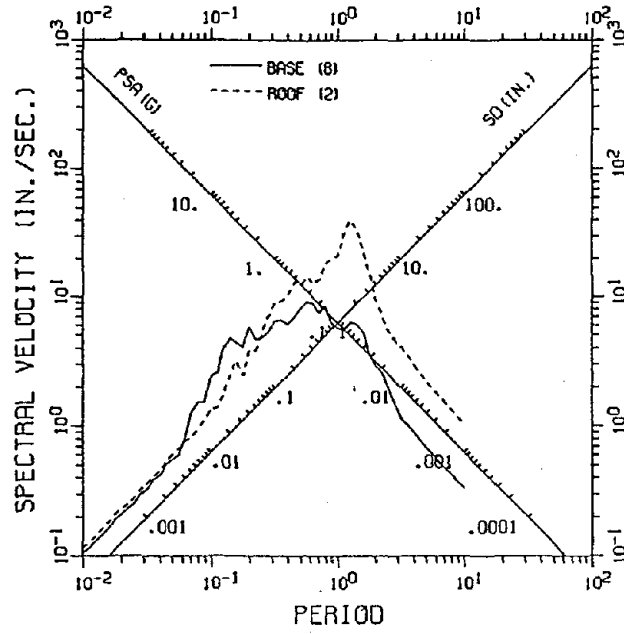


(a) Base

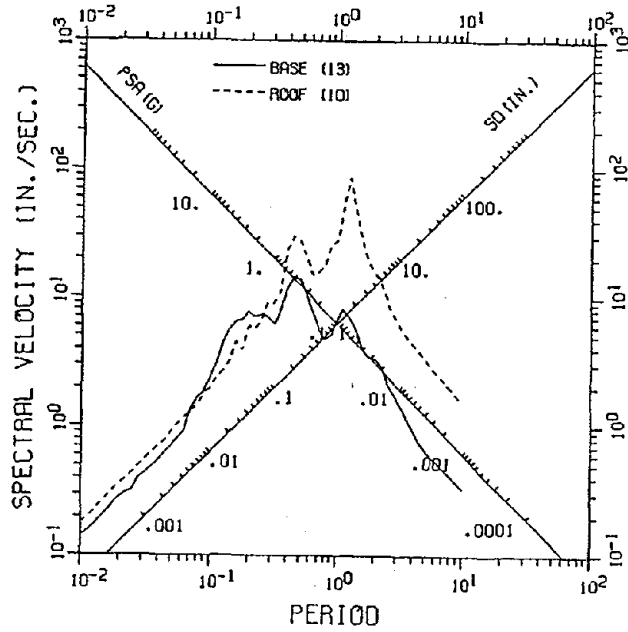


(b) Roof

Fig. 10 Spectra Comparison, Torsional Effects

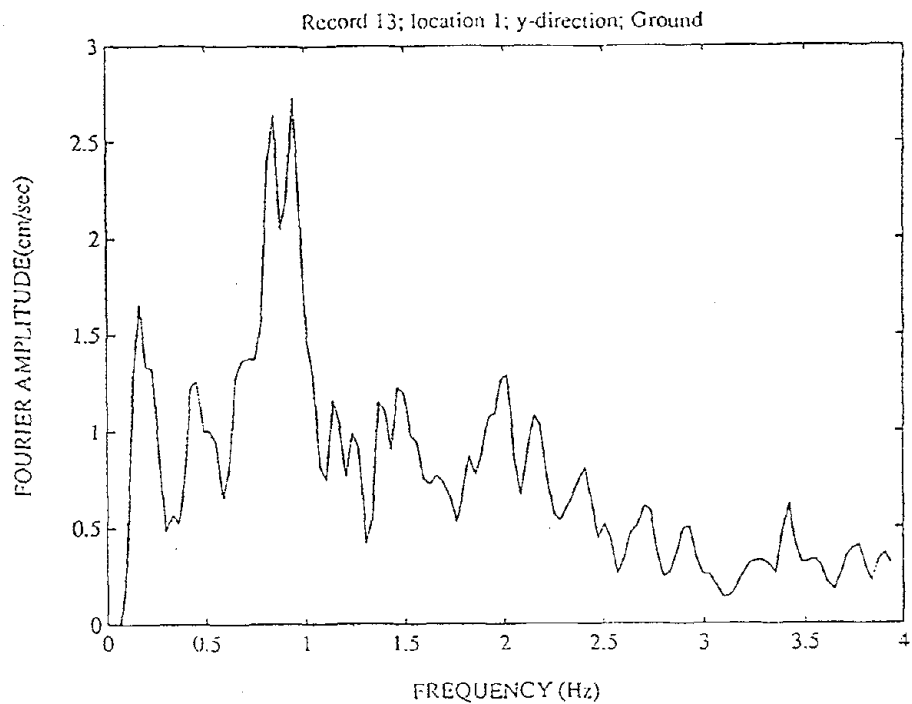


(a) E-W Motions

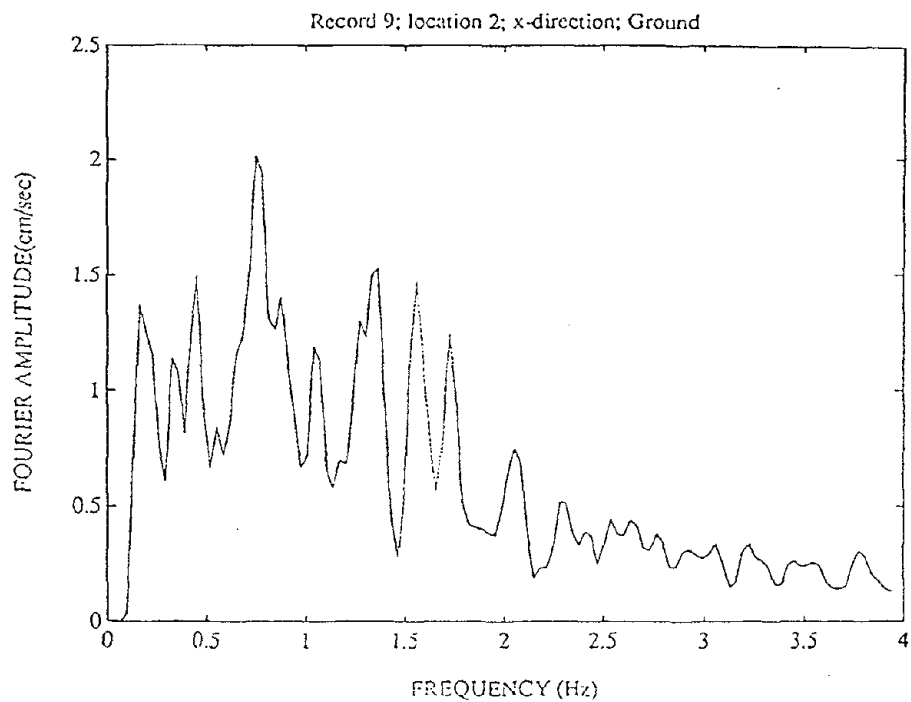


(b) N-S Motions

Fig. 11 Spectra Comparison, Amplification Effects

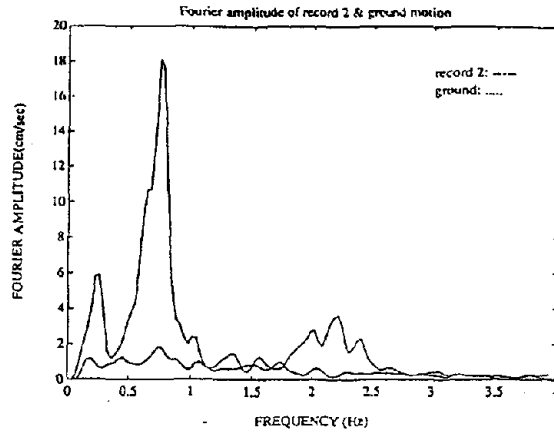


(a) North-South, Channel 13

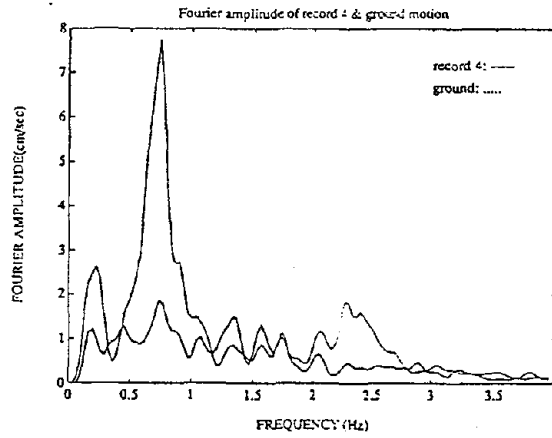


(b) East-West, Channel 9

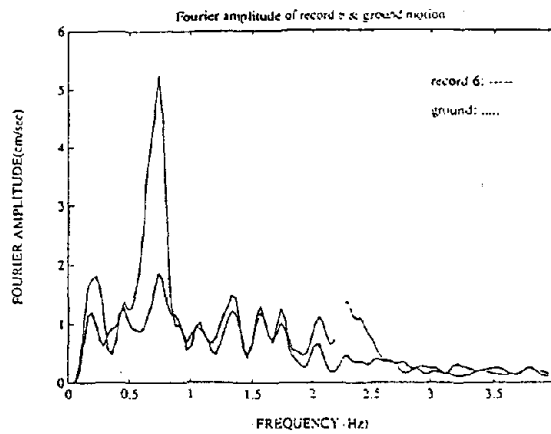
Fig. 12 Fourier Amplitude Spectra for Base Motions



(a) Roof Level

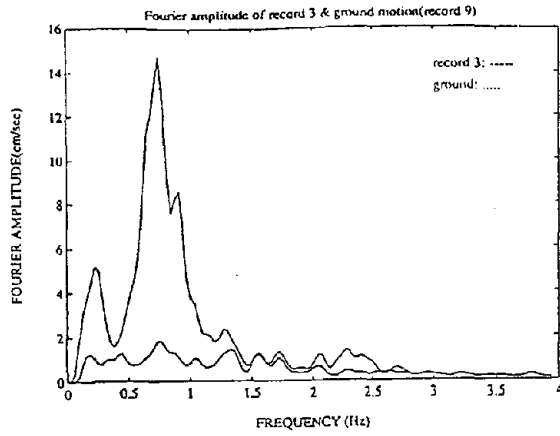


(b) Third Floor

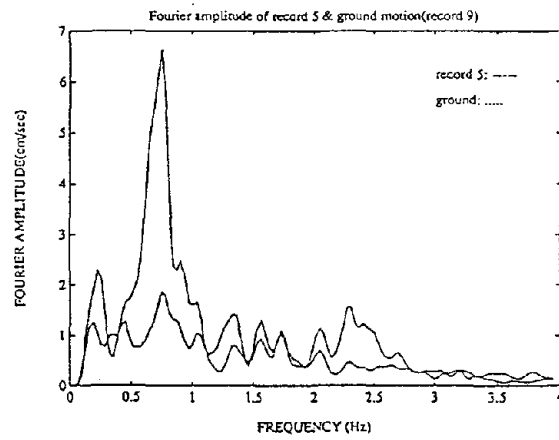


(c) Second Floor

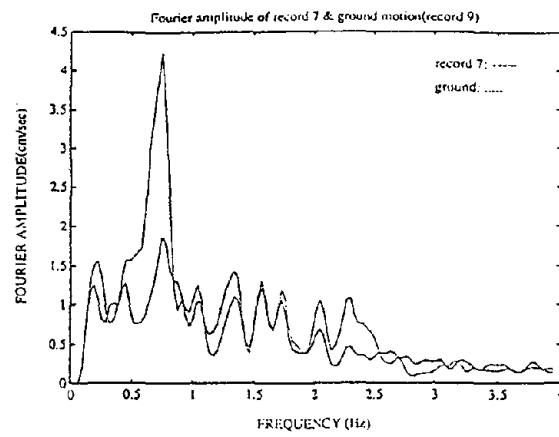
Fig. 13 Fourier Amplitude Spectra, E-W, NW Corner



(a) Roof Level

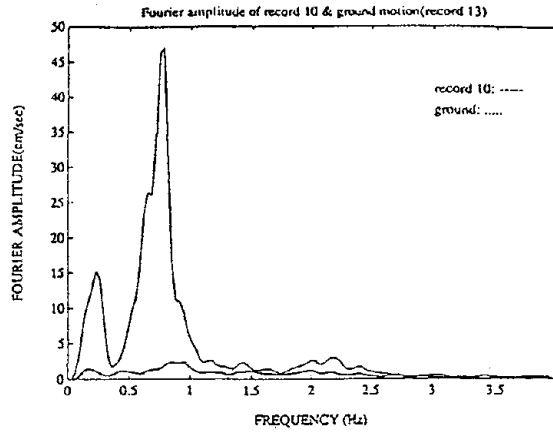


(b) Third Floor

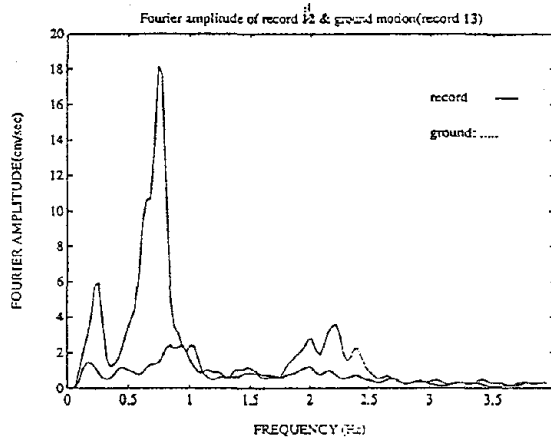


(c) Second Floor

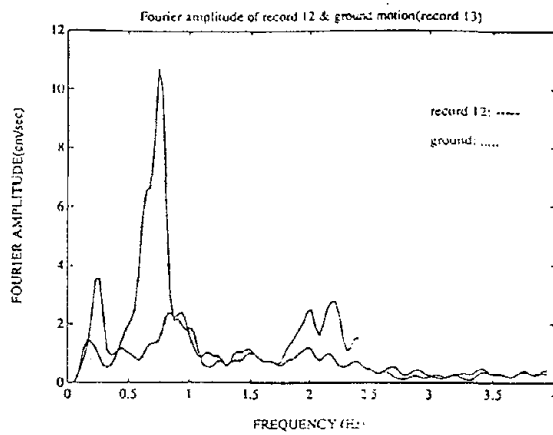
Fig. 14 Fourier Amplitude Spectra, E-W, SW Corner



(a) Roof Level

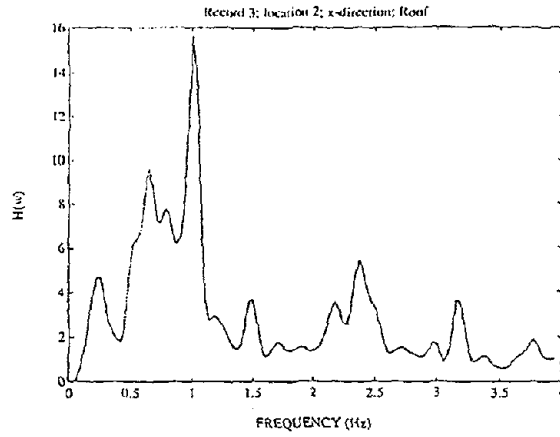


(b) Third Floor

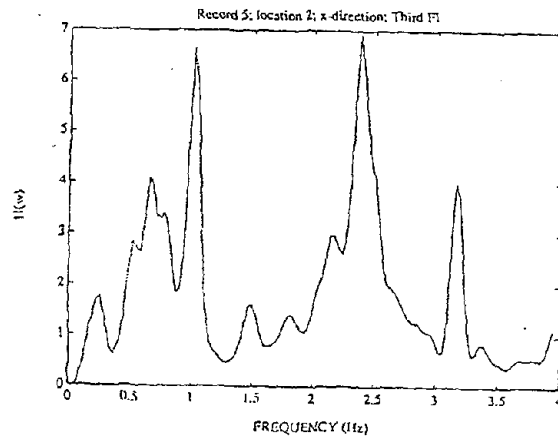


(c) Second Floor

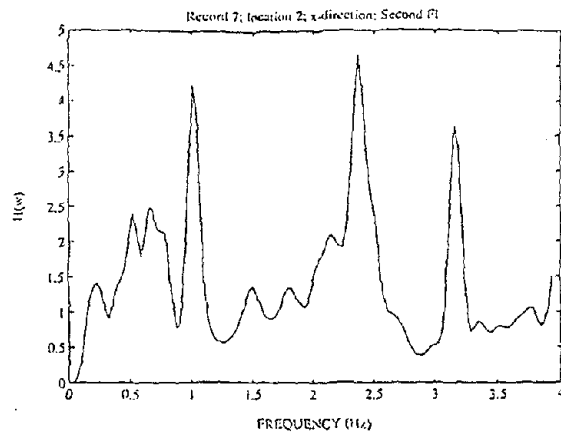
Fig. 15 Fourier Amplitude Spectra, N-S, NW Corner



(a) Roof Level

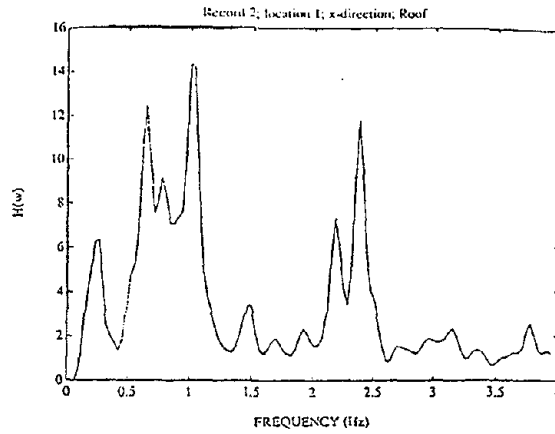


(b) Third Floor

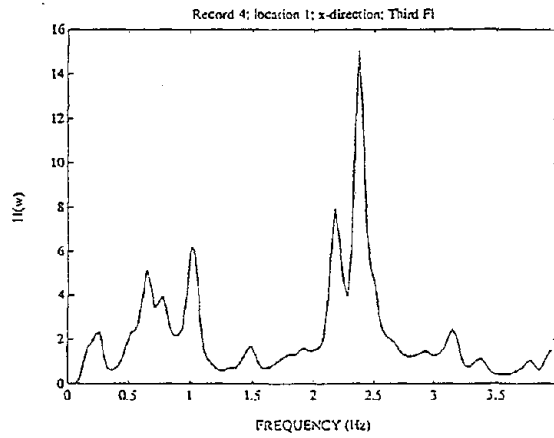


(c) Second Floor

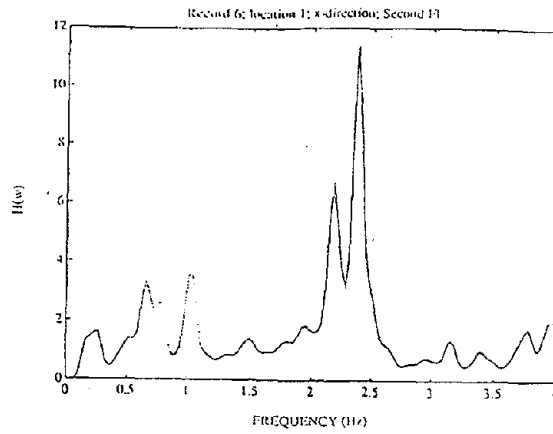
Fig. 16 Transfer Functions, E-W, SW Corner



(a) Roof Level

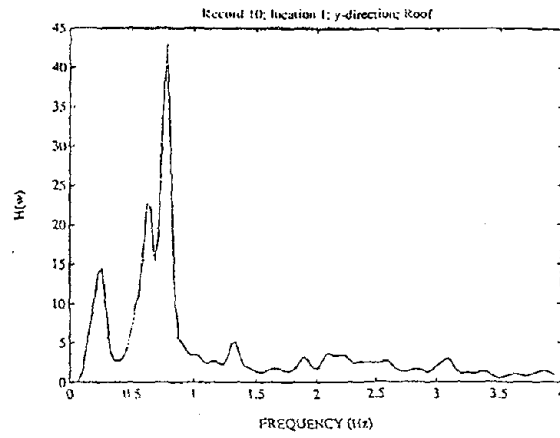


(b) Third Floor

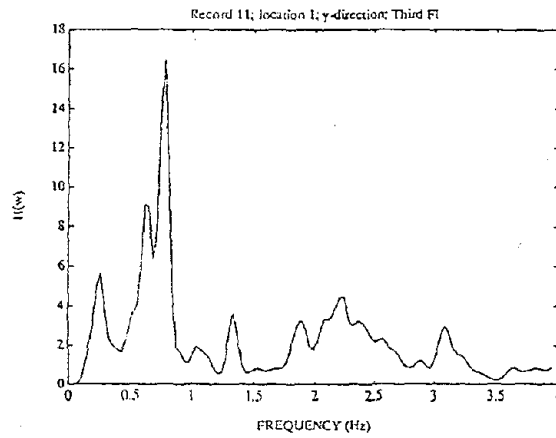


(c) Second Floor

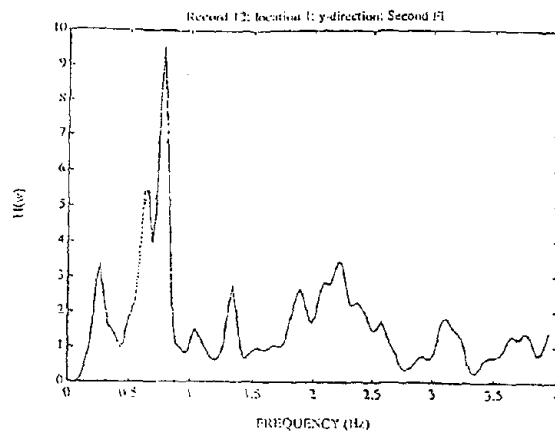
Fig. 17 Transfer Functions, E-W, NW Corner



(a) Roof Level



(b) Third Floor



(c) Second Floor

Fig. 18 Transfer Functions, N-S, NW Corner

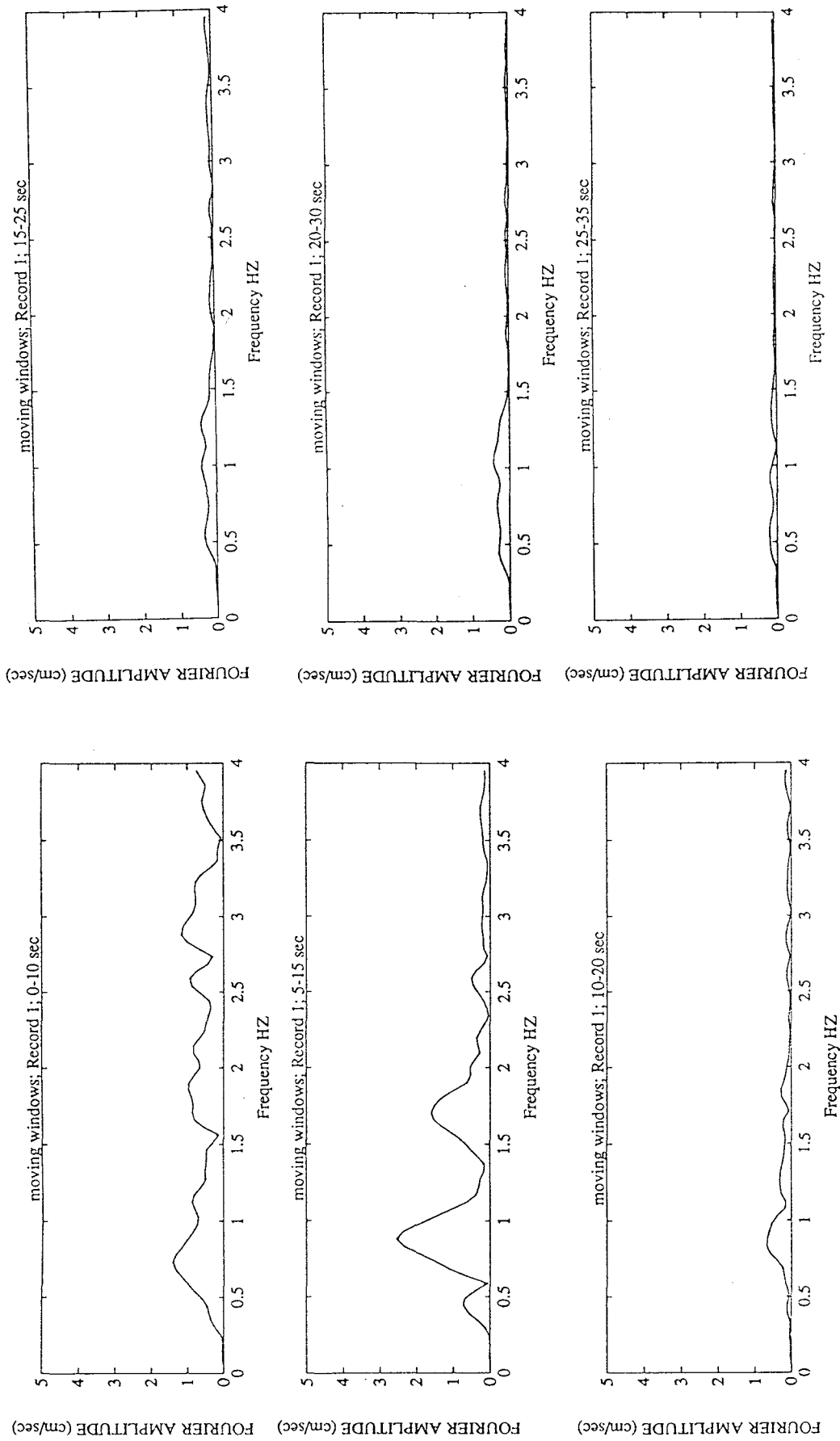


Fig. 19 Moving Window Fourier Analyses, Base, Vertical

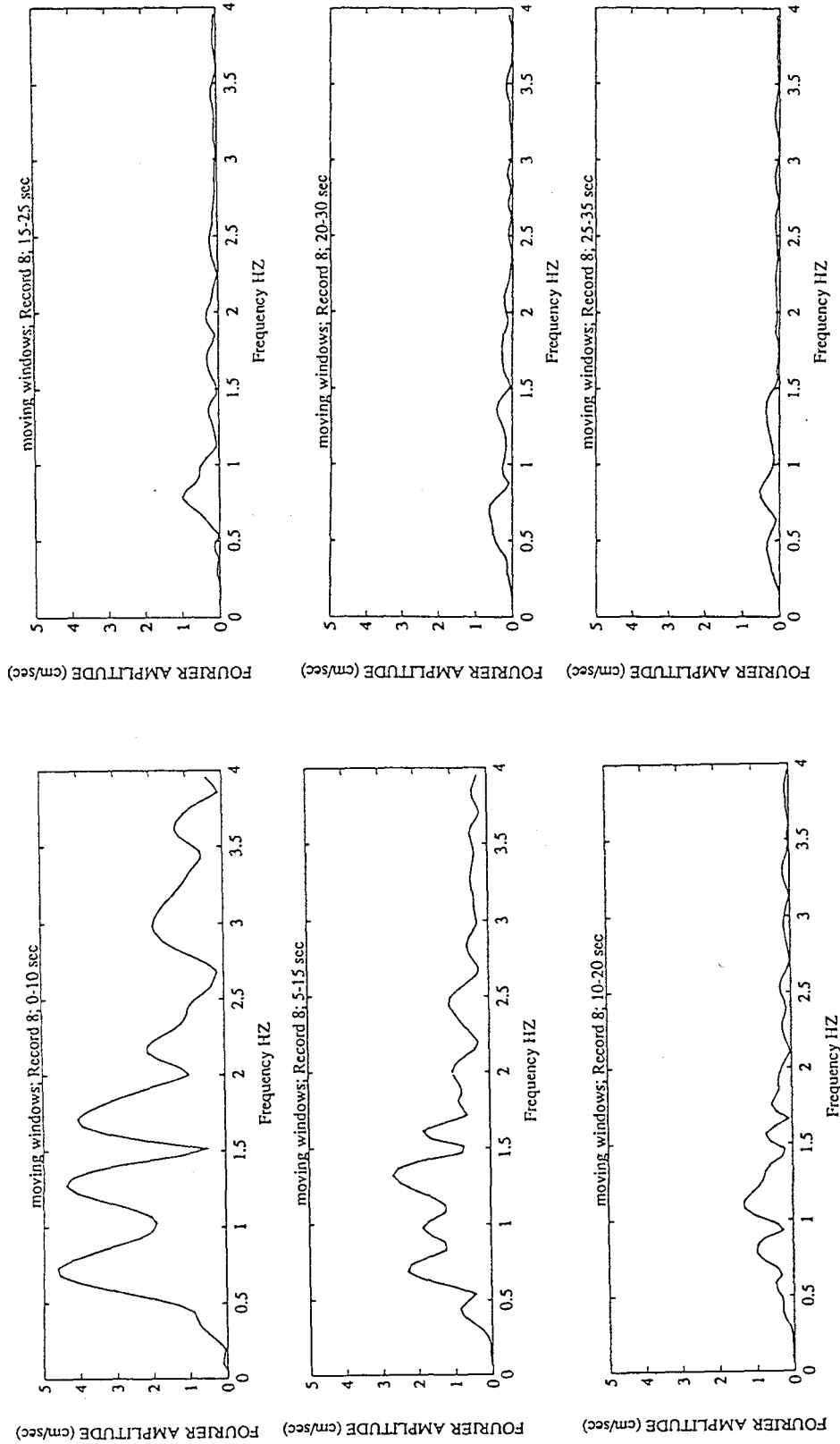


Fig. 20 Moving Window Fourier Analyses, Base, E-W

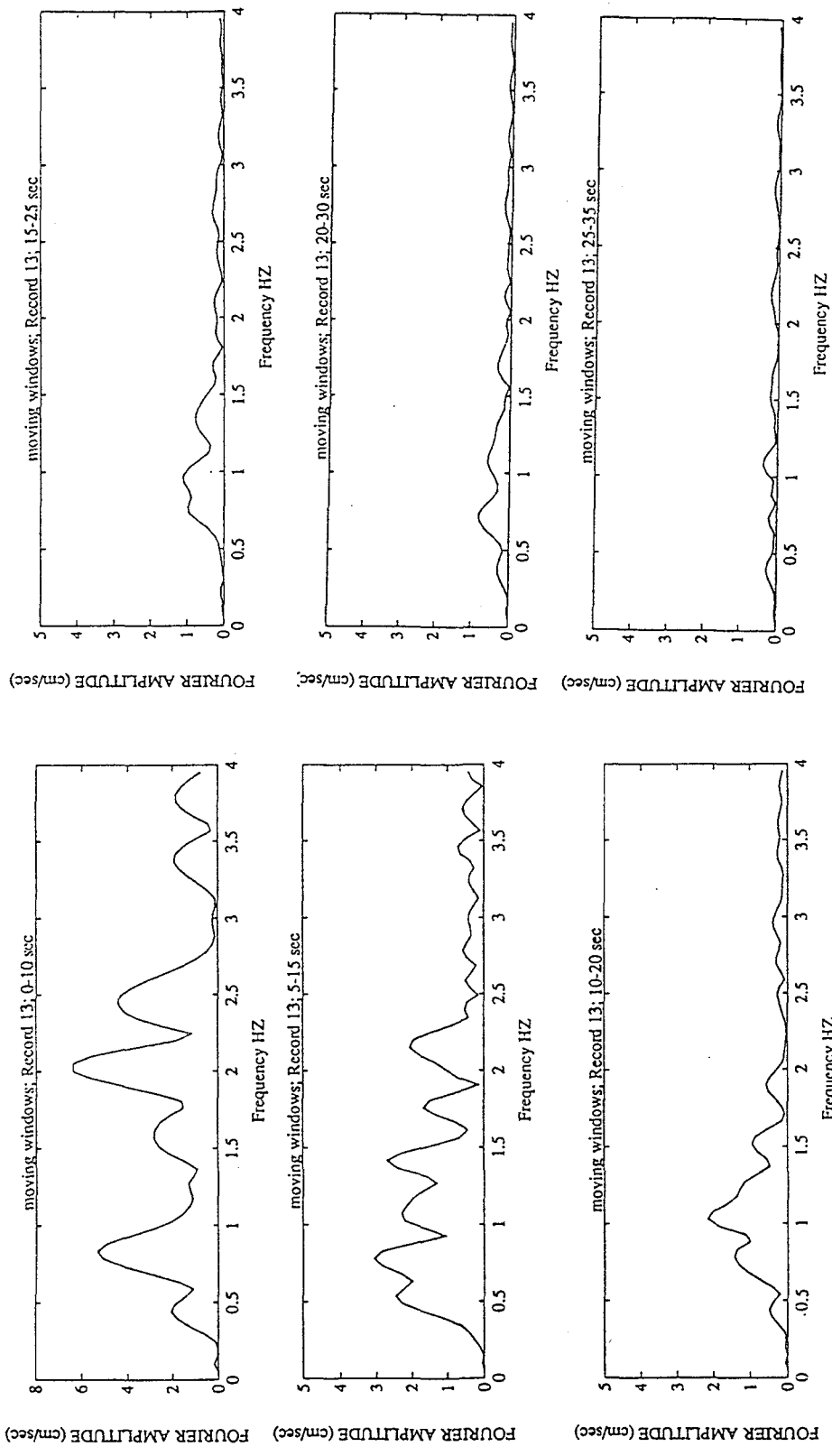


Fig. 21 Moving Window Fourier Analyses, Base, N-S

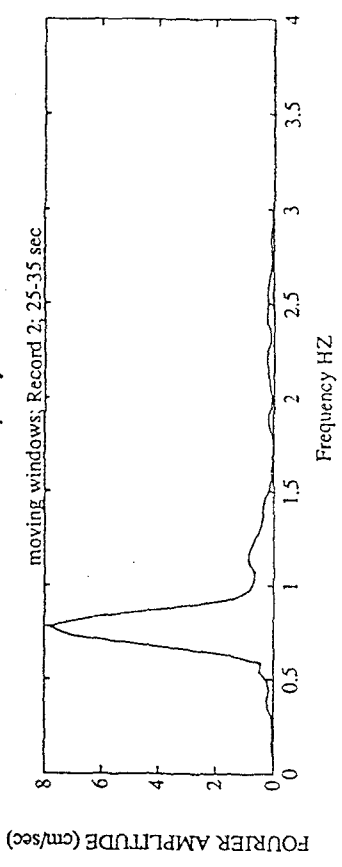
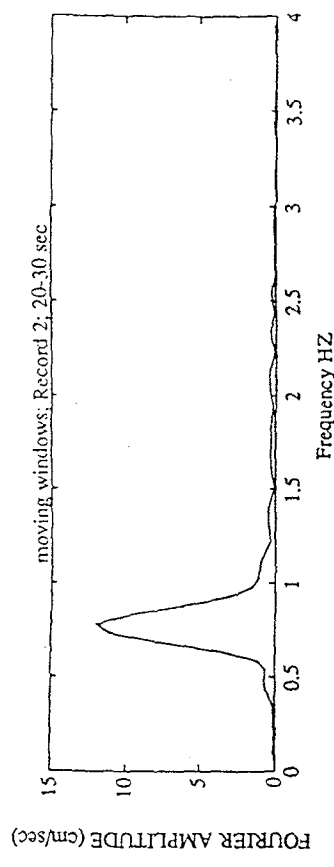
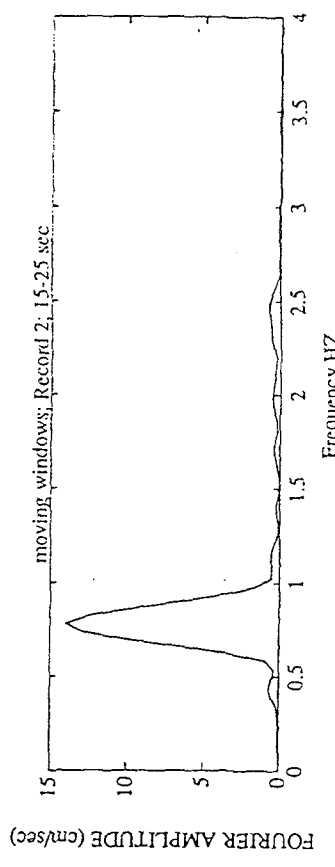
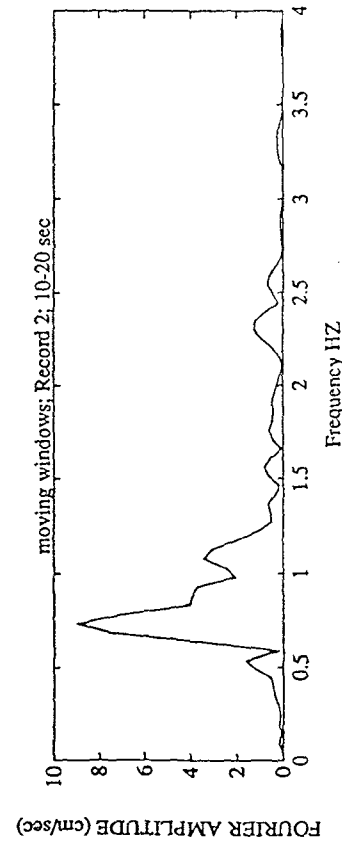
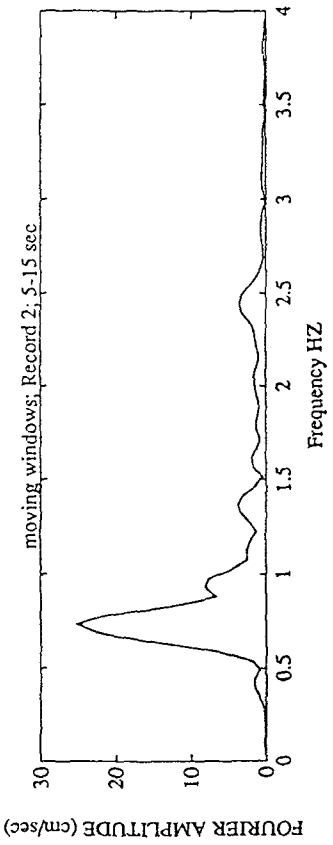
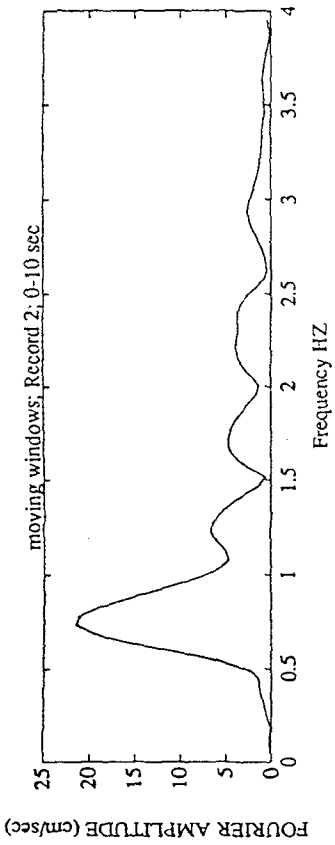


Fig. 22 Moving Window Fourier Analyses, E-W, Roof Level

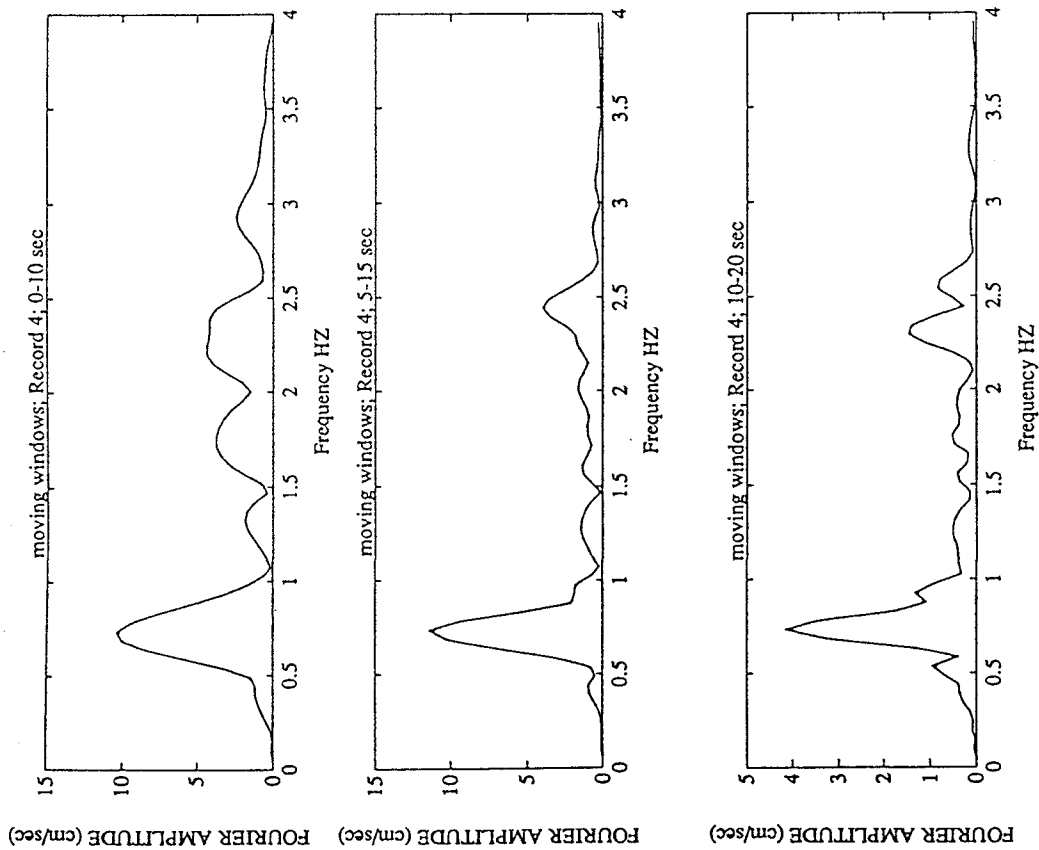
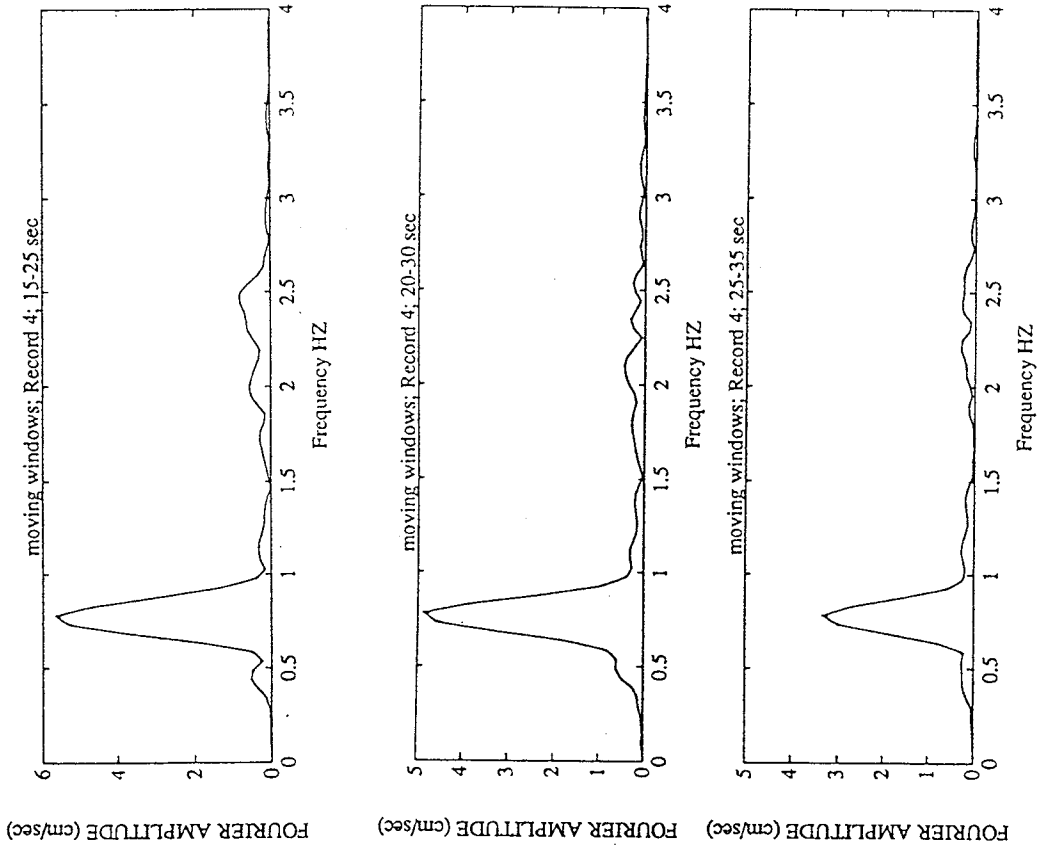


Fig. 23 Moving Window Fourier Analyses, Third Floor, E-W

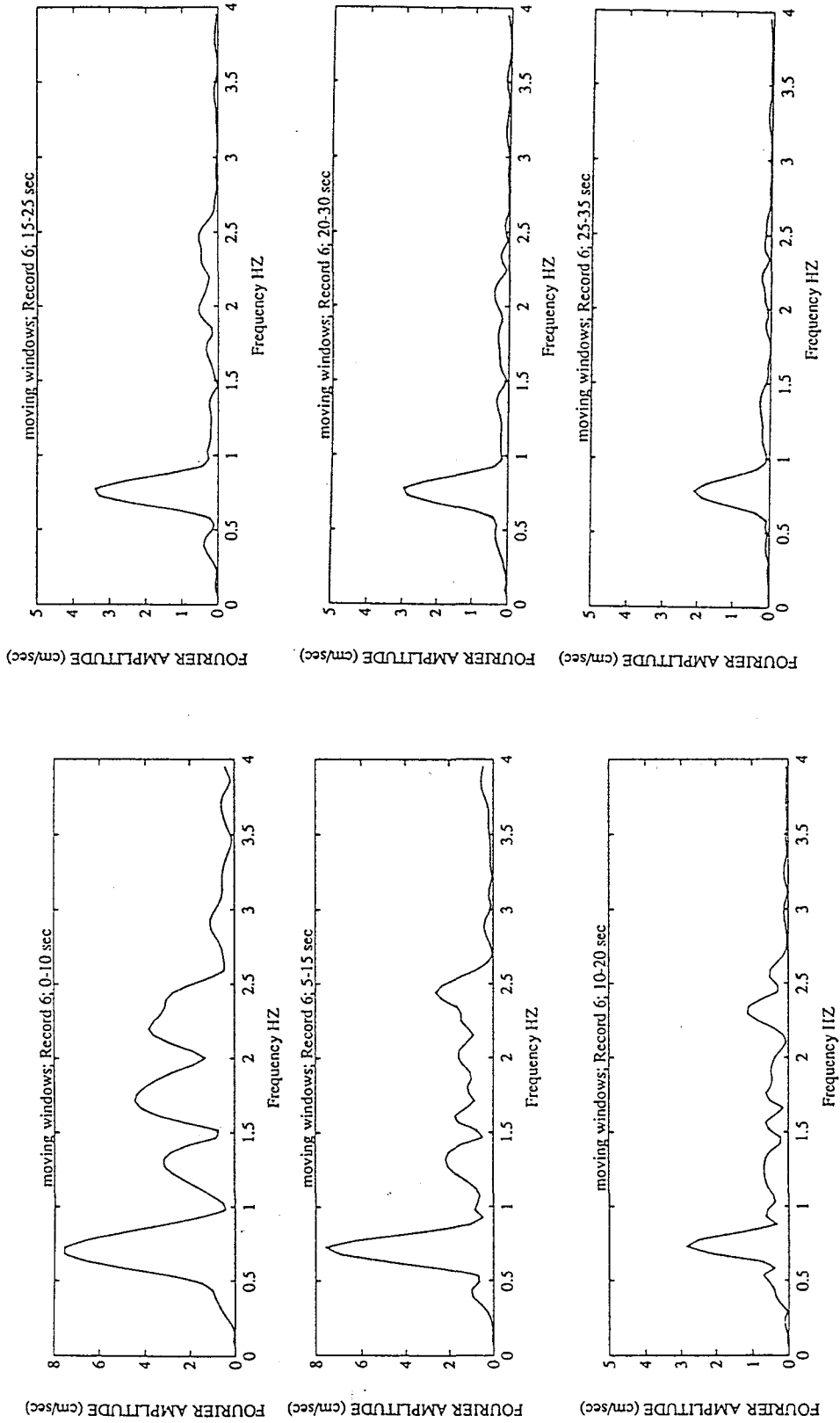


Fig. 24 Moving Window Fourier Analyses, E-W, Second Floor

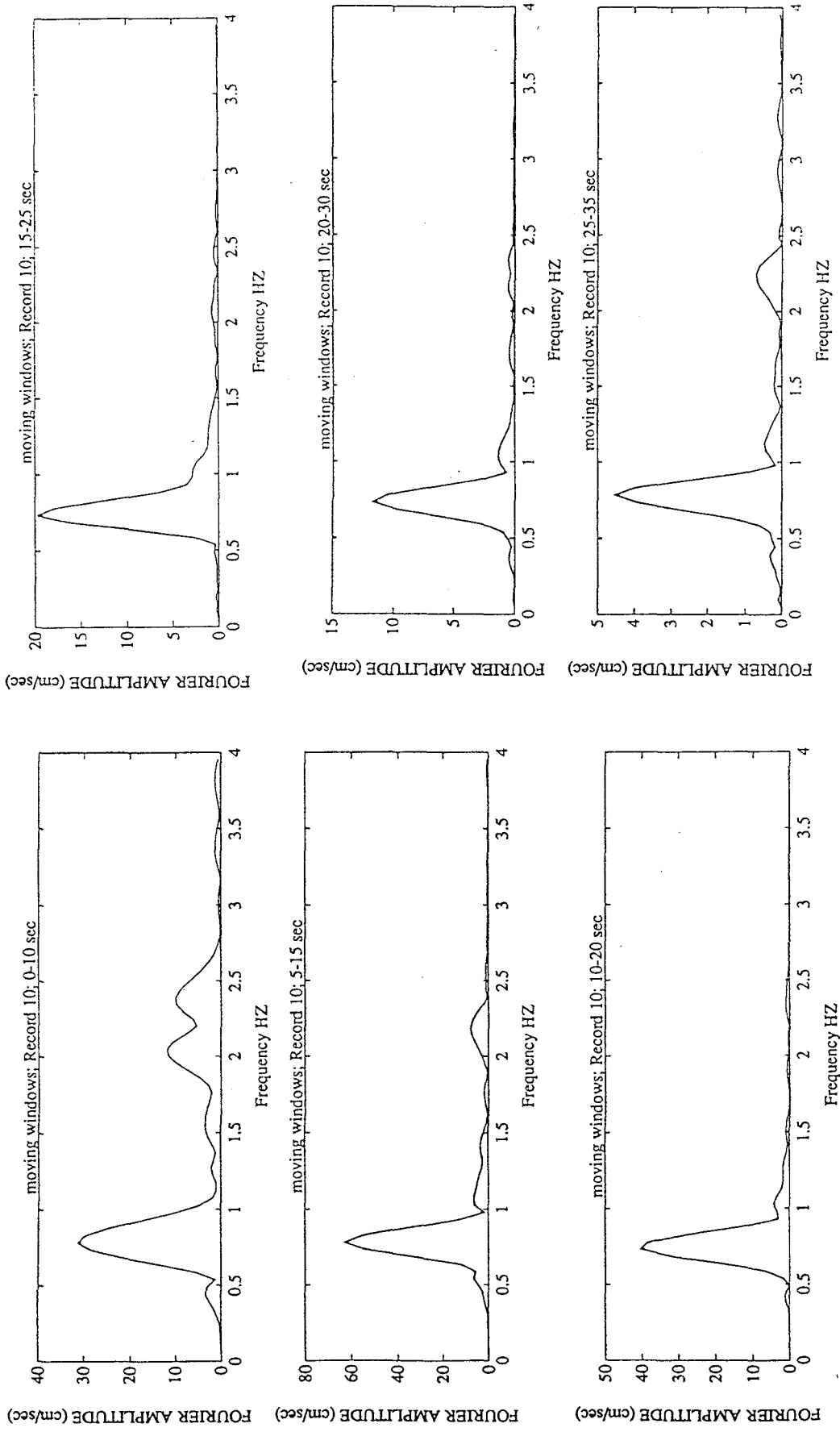


Fig. 25 Moving Window Fourier Analyses, N-S, Roof Level

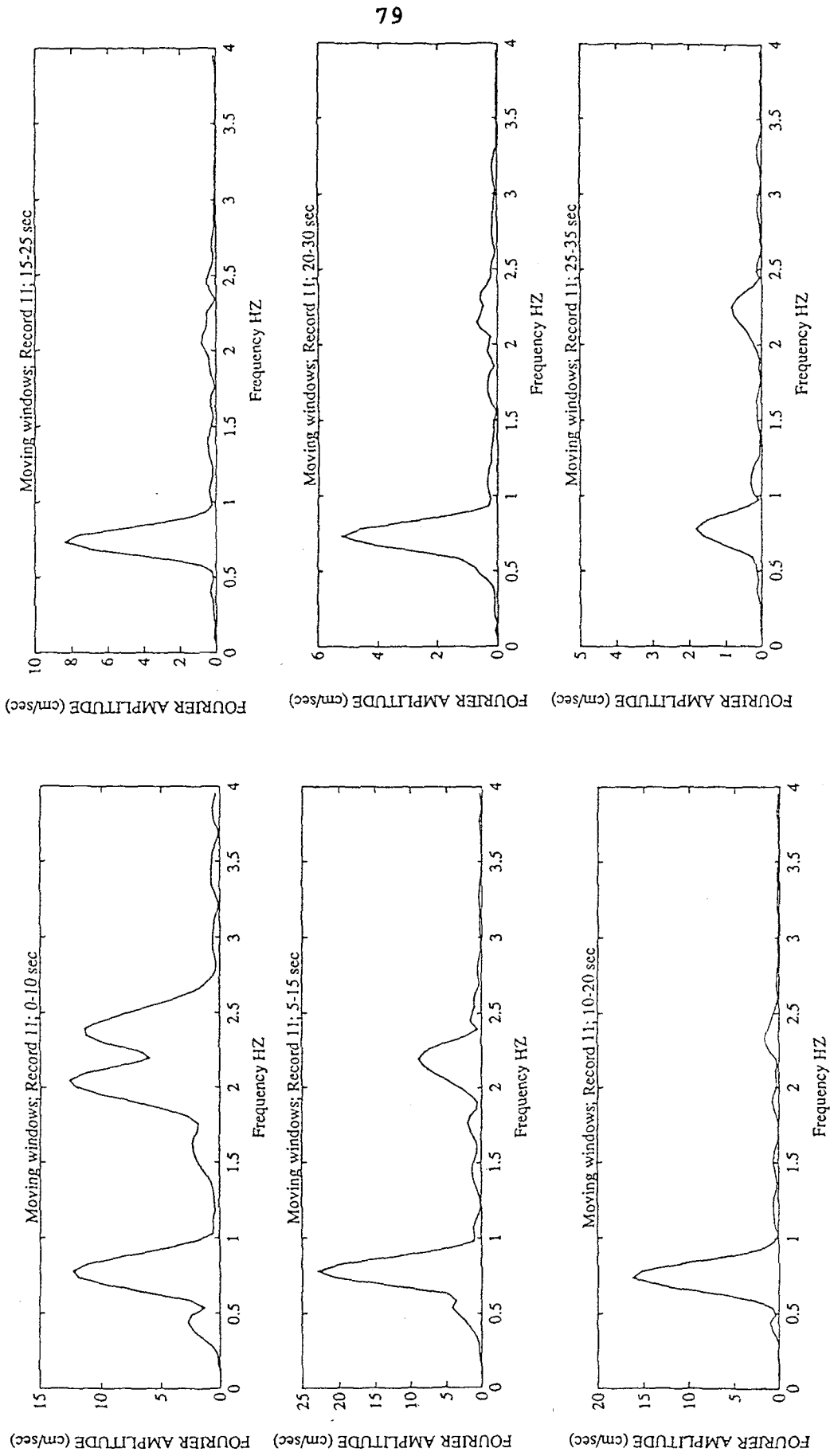


Fig. 26 Moving Window Fourier Analyses, N-S, Third Floor

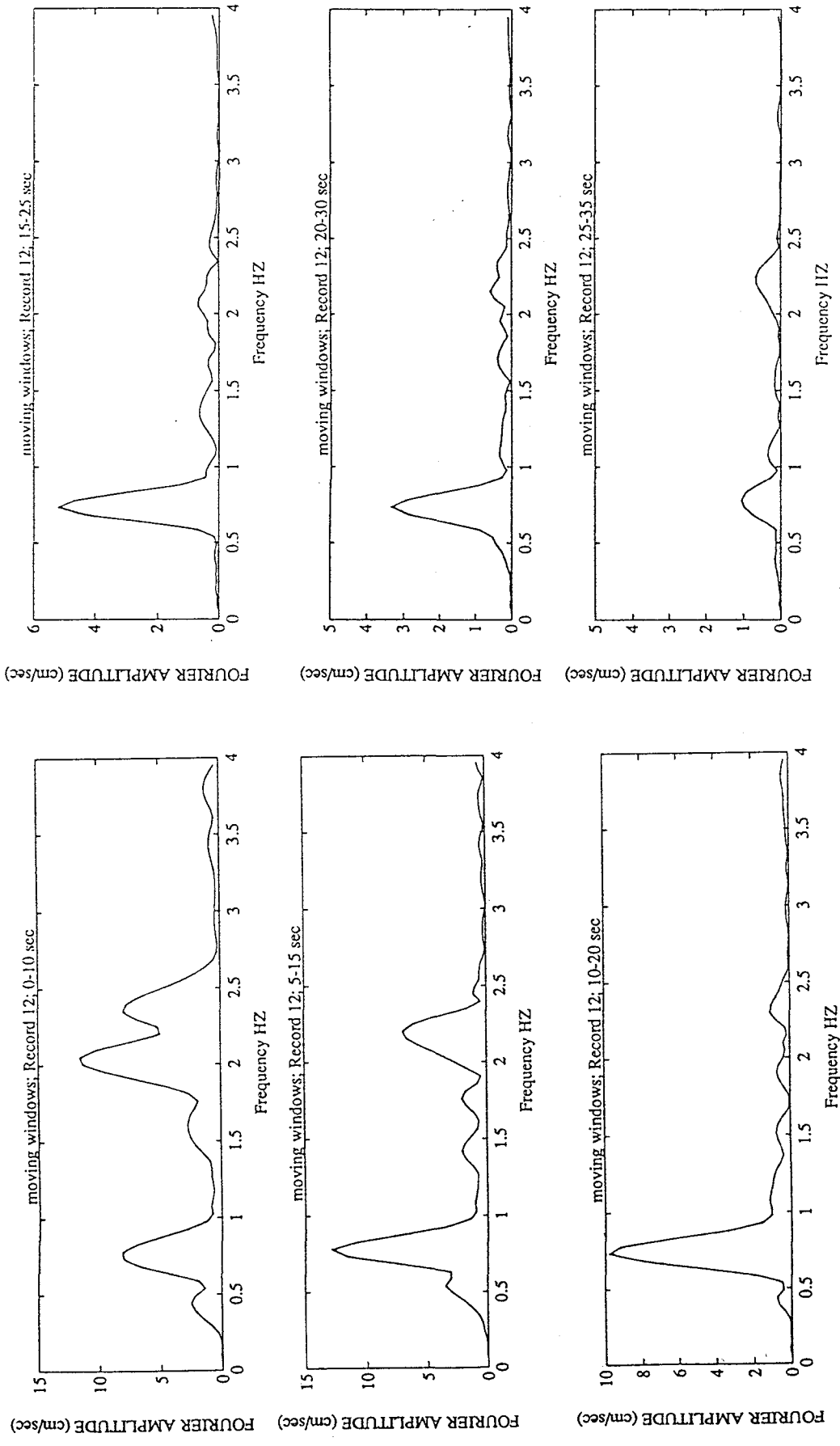


Fig. 27 Moving Window Fourier Analyses, N-S, Second Floor

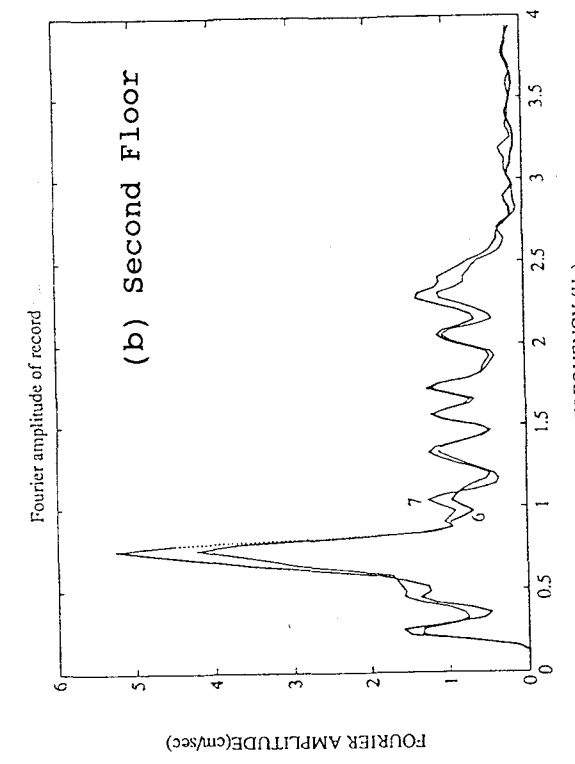
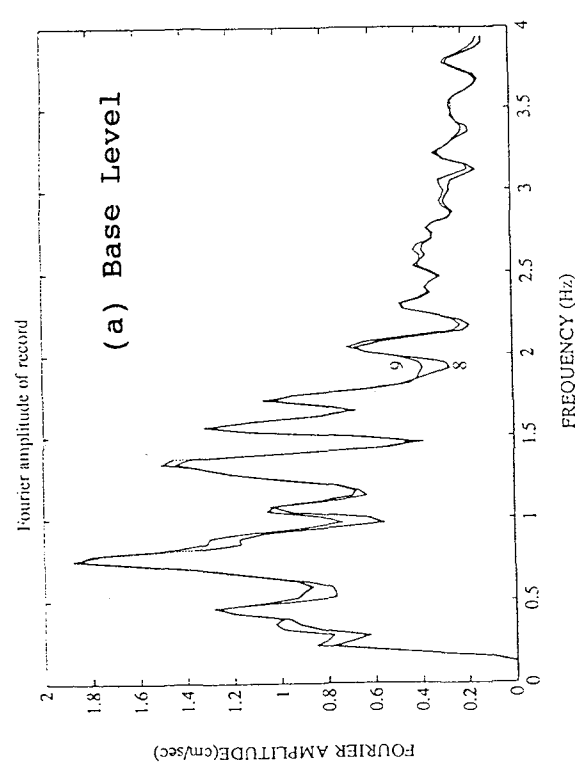
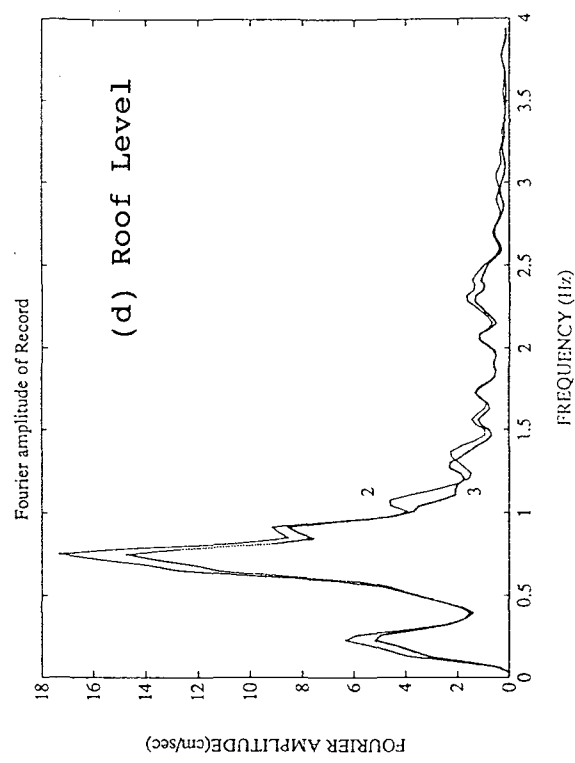
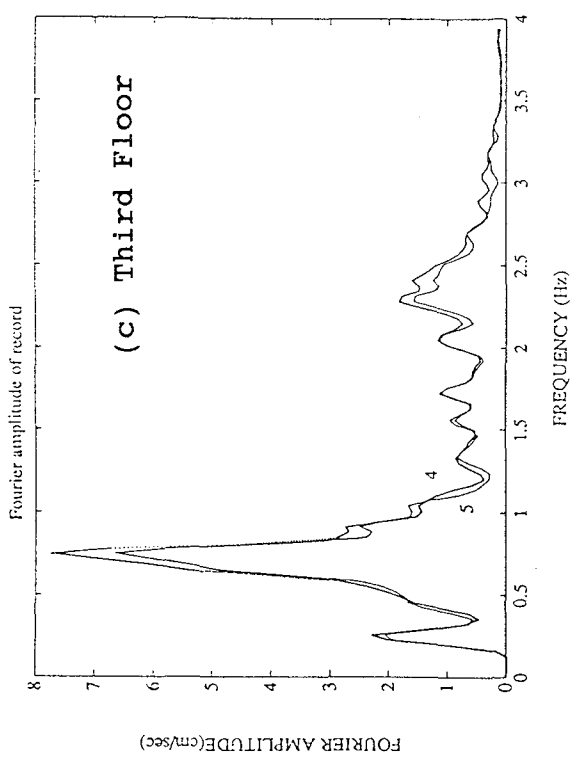
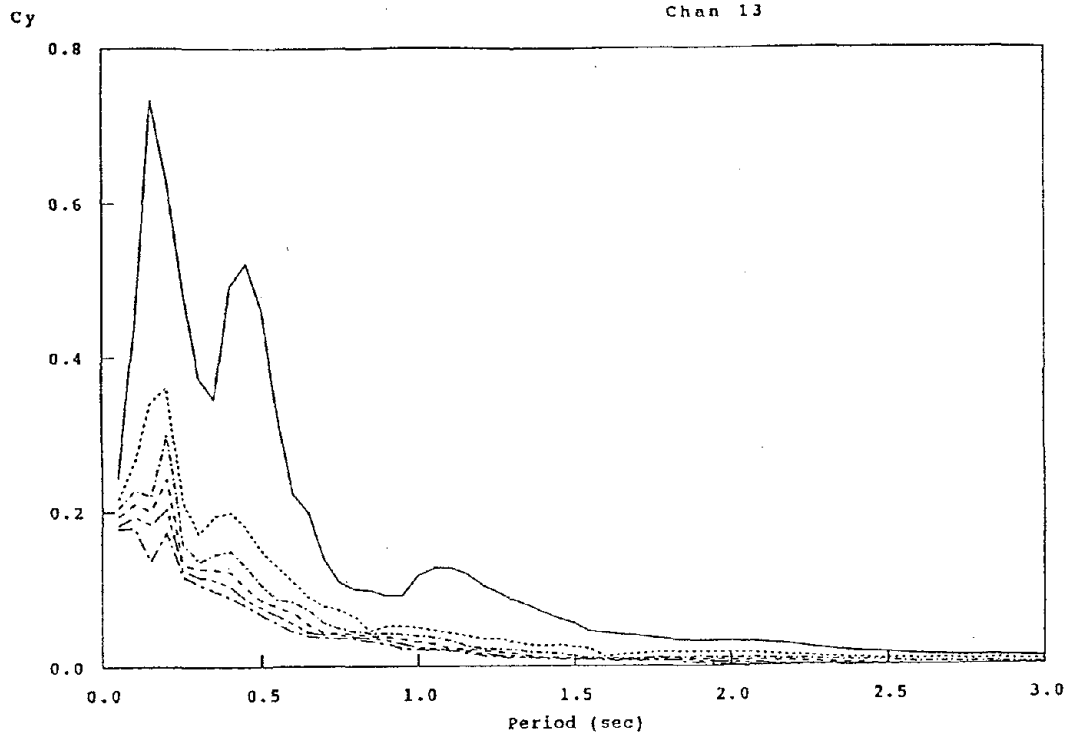
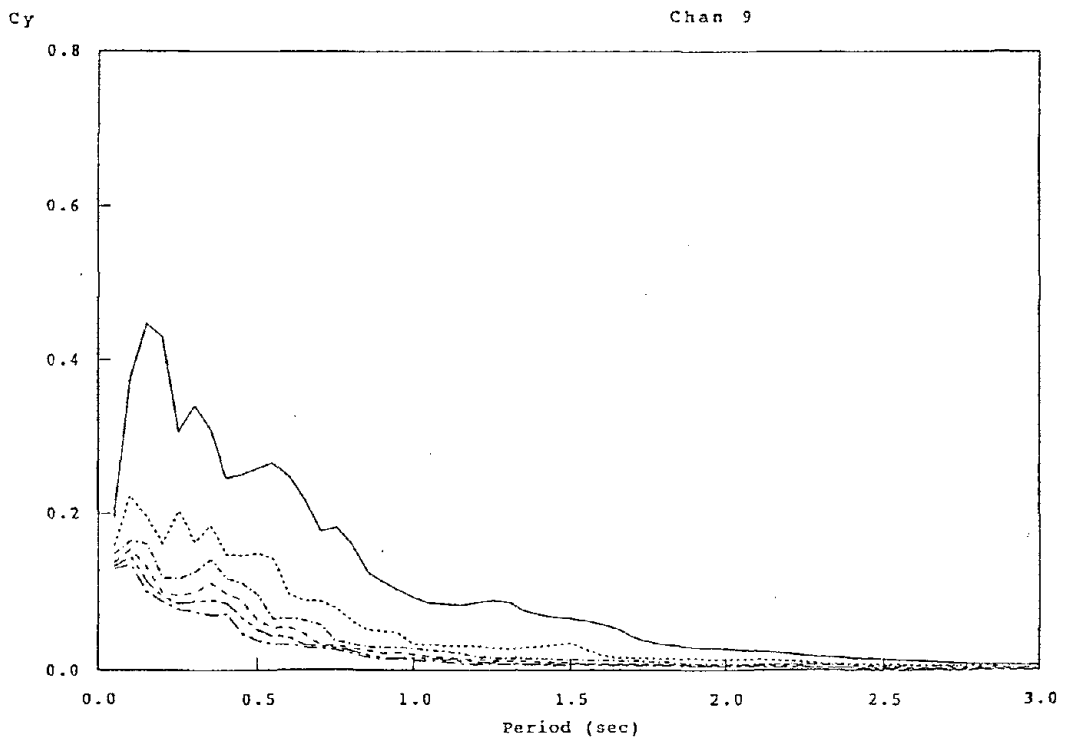


Fig. 28 Fourier Amplitude Spectra, Torsional Effects

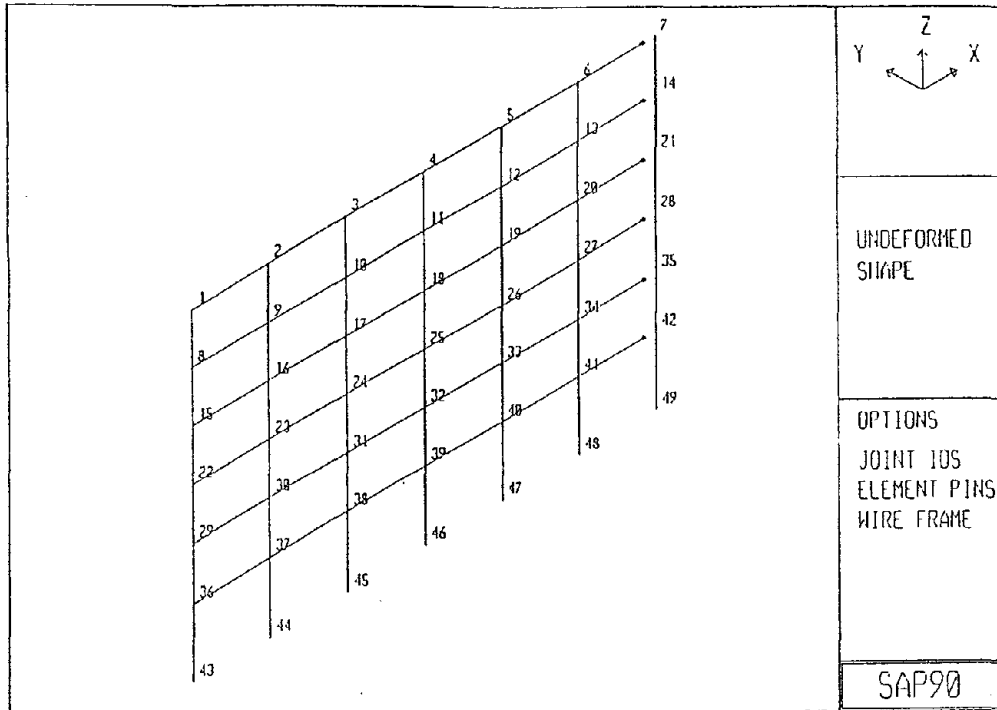


(a) Recorded Base Motion, N-S

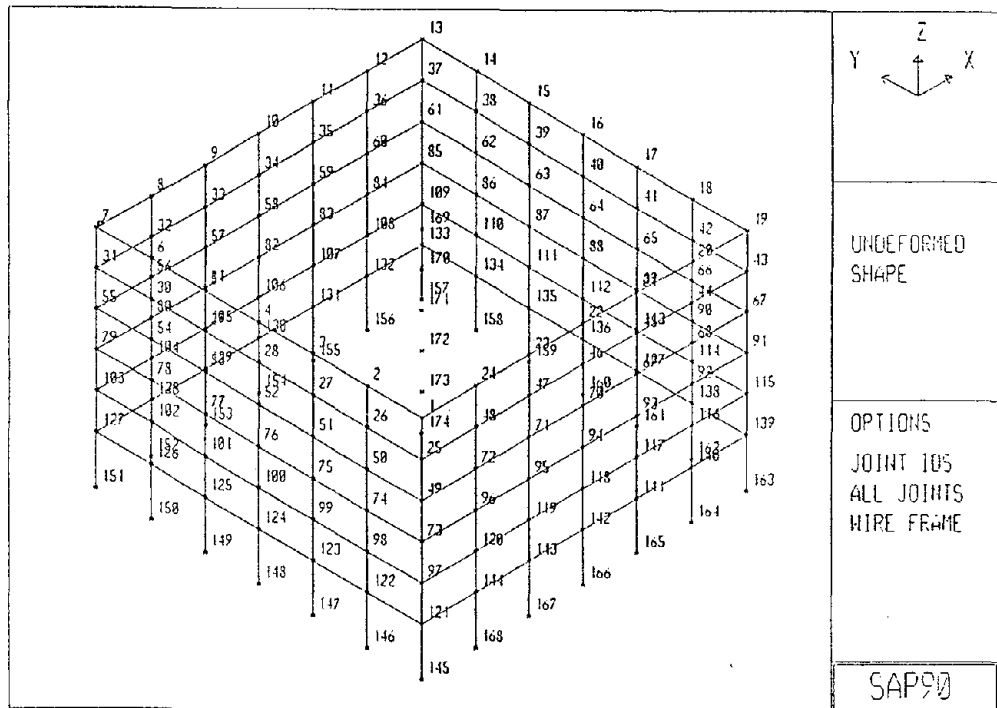


(b) Recorded Base Motion, E-W

Fig. 29 Inelastic Response Spectra

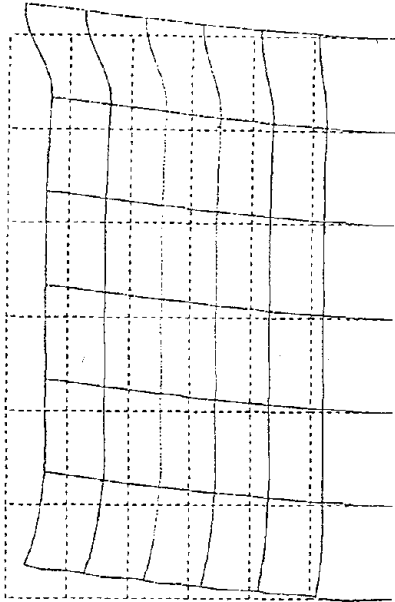


(a) Two Dimensional

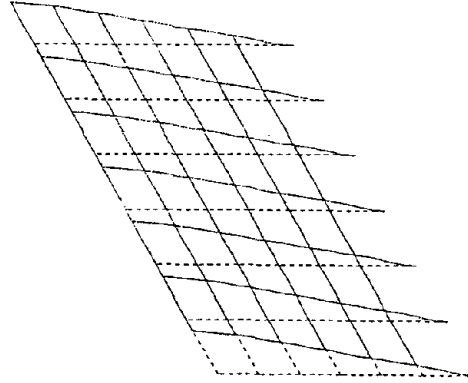


(b) Three Dimensional

Fig. 30 Elastic Finite Element Building Models



(a) Gravity Loading



(b) Deformed Shape, Gravity Load



(c) Lateral Seismic Loading (d) Deformed Shape, Lateral Seismic Load

Fig. 31 Code Loading and Resulting Deformations

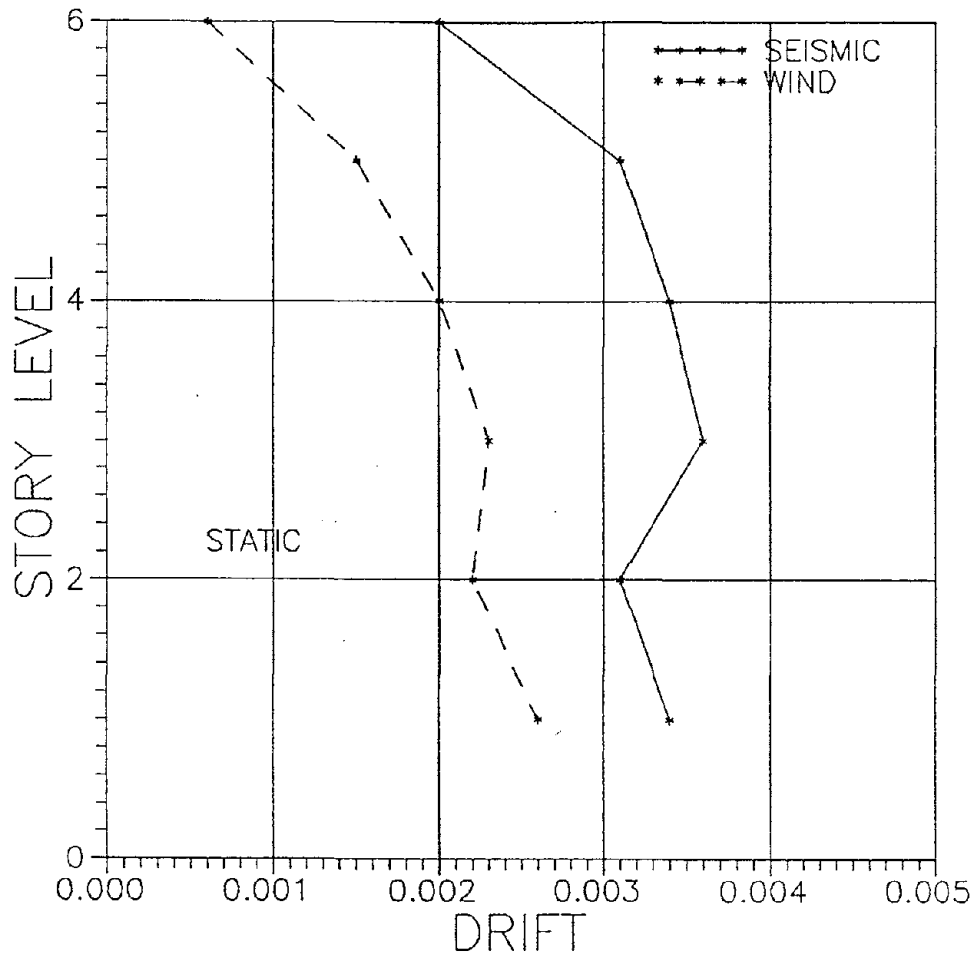
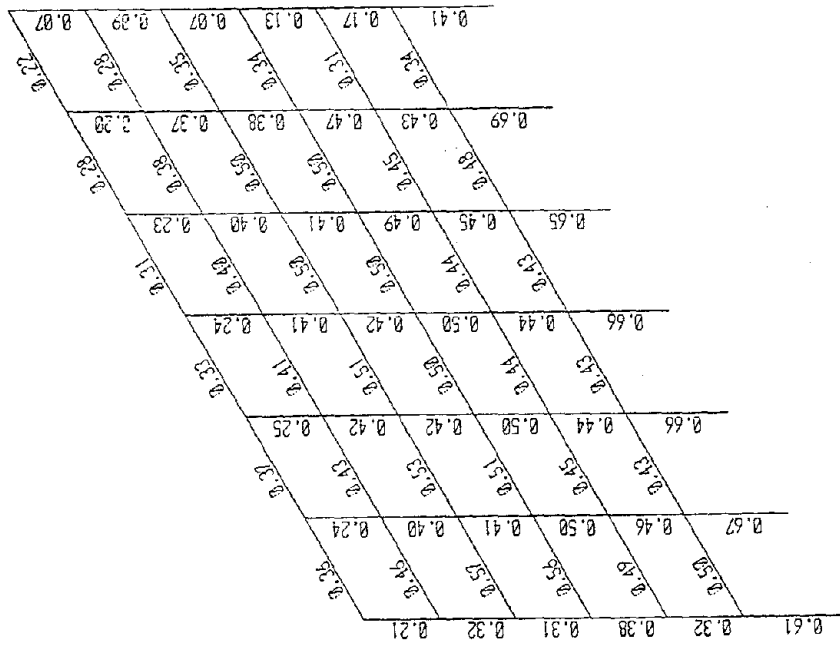


Fig. 32 Interstory Drift Index, Code Lateral Loads

(a) Gravity Load



(b) Gravity Load plus Lateral Seismic Load

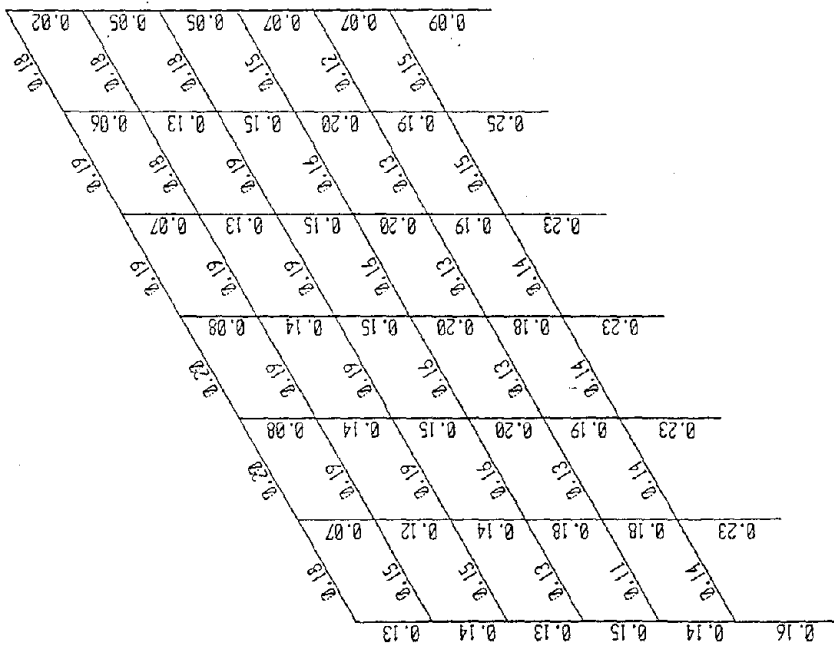


Fig. 33 Stress Ratios for Code Loads

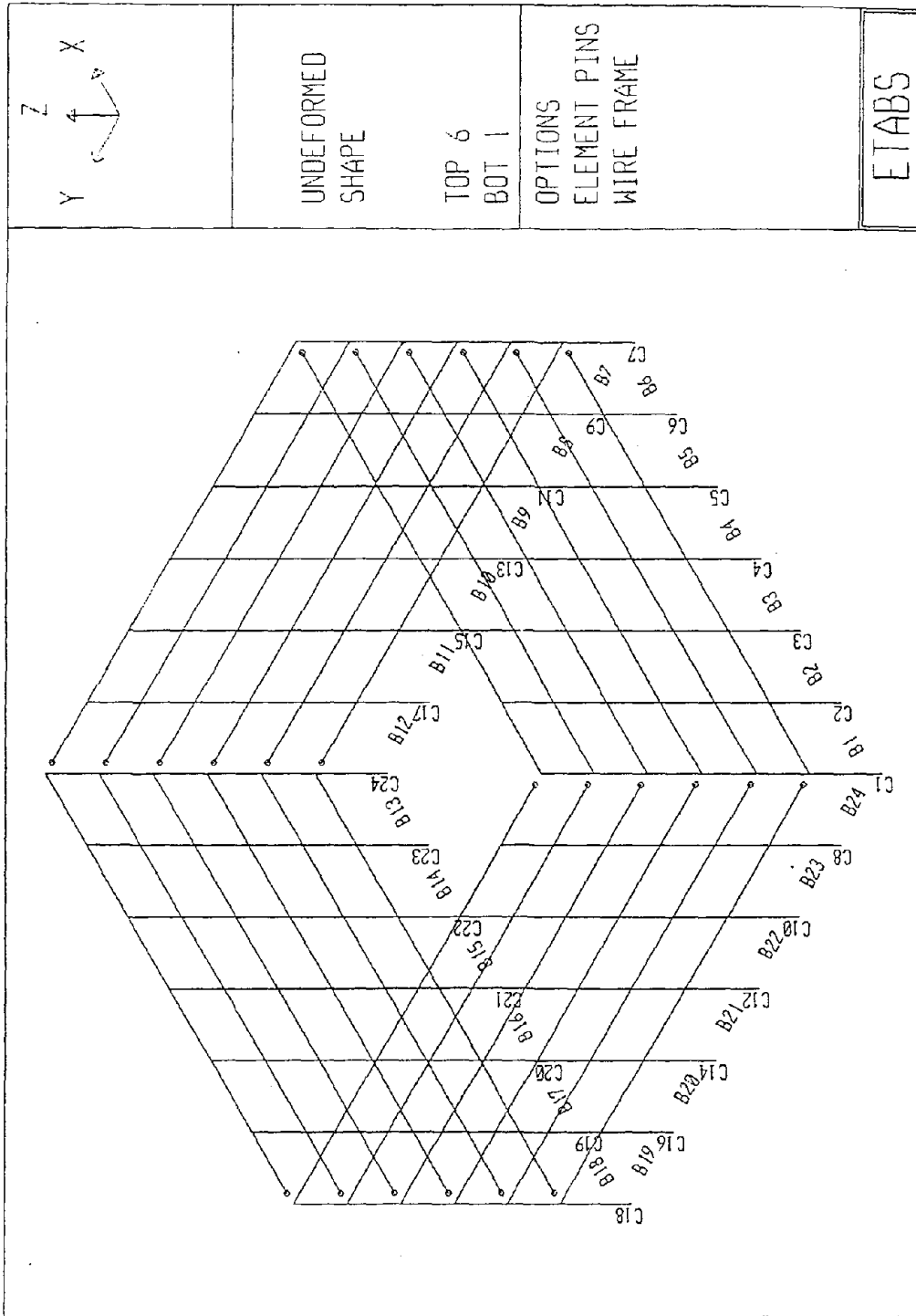
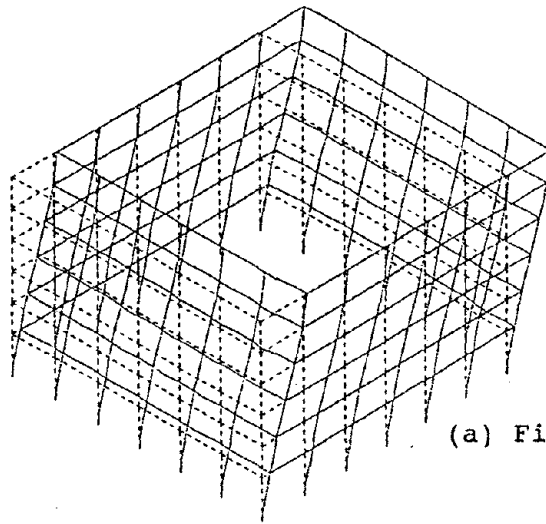
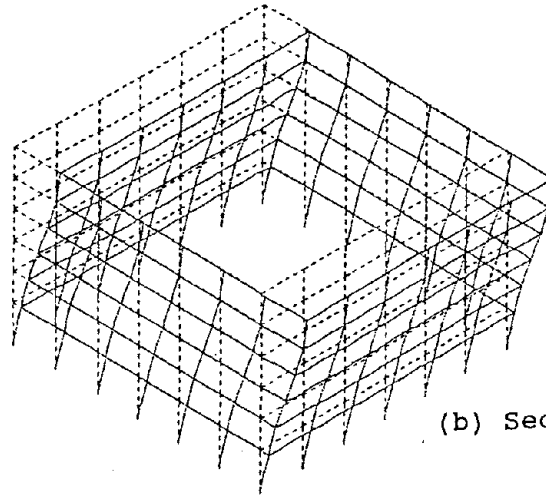


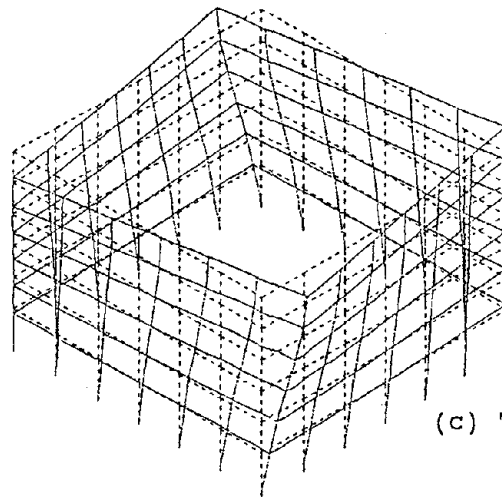
Fig. 34 Three Dimensional ETABS Building Model



(a) First Mode



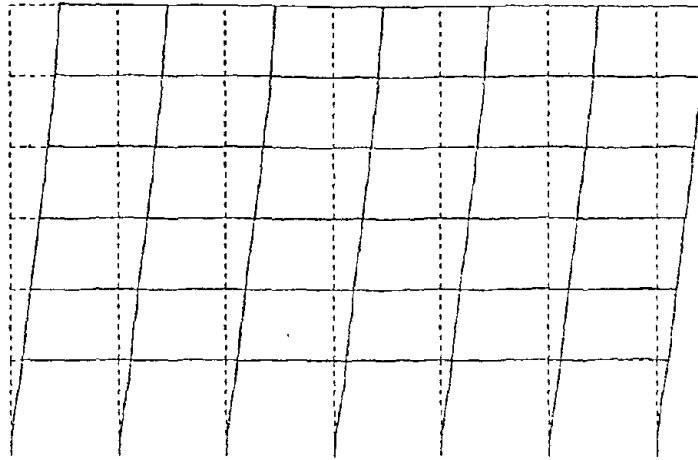
(b) Second Mode



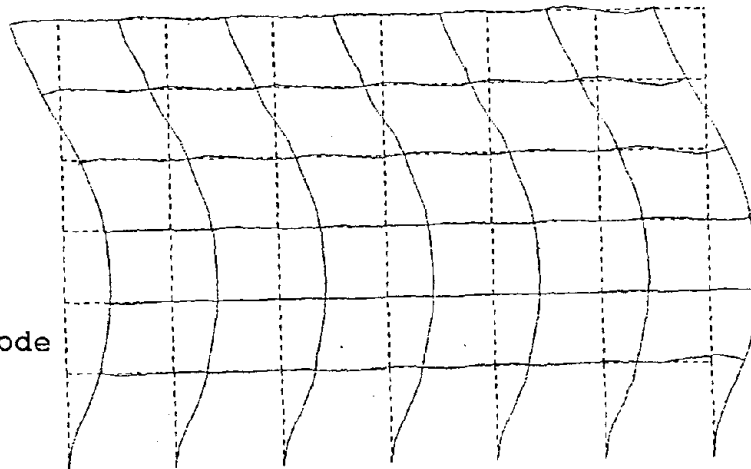
(c) Third Mode

Fig. 35 Mode Shapes, 3D Building Model

(a) First Mode



(b) Second Mode



(c) Third Mode

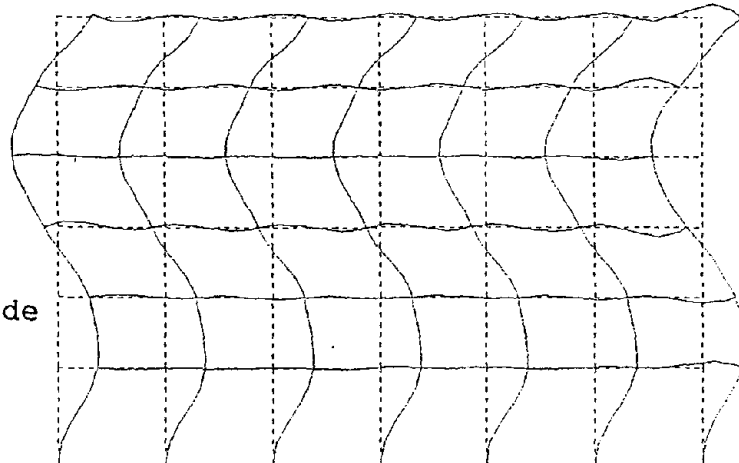


Fig. 36 Mode Shapes, 2D Building Model

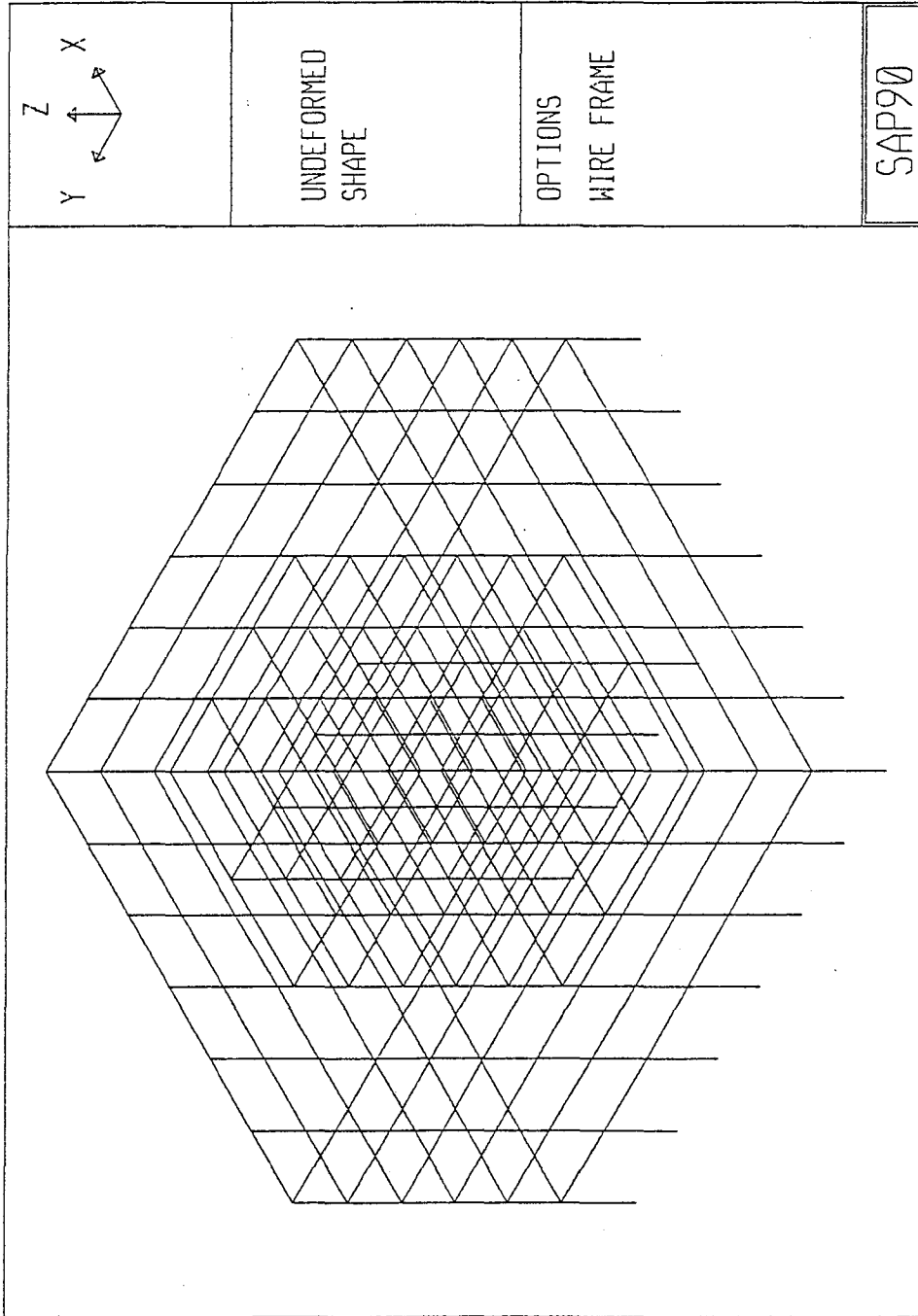
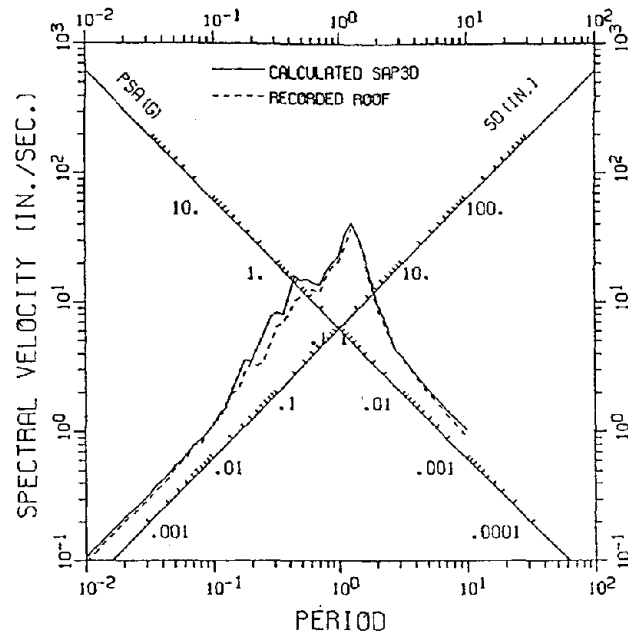
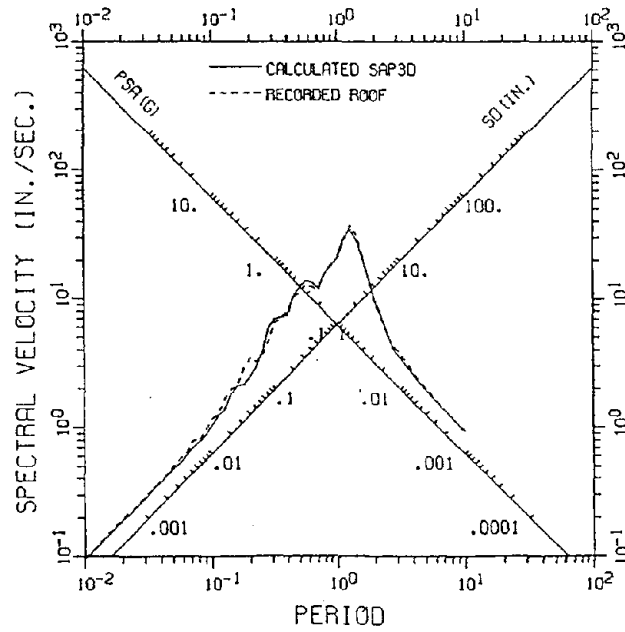


Fig. 37 Building Model Including Interior Gravity Frame



(a) Damping Ratios = 5%, 5%, 5%, 5%



(b) Damping Ratios = 7%, 10%, 13%, 15%

Fig. 38 Roof Response spectra

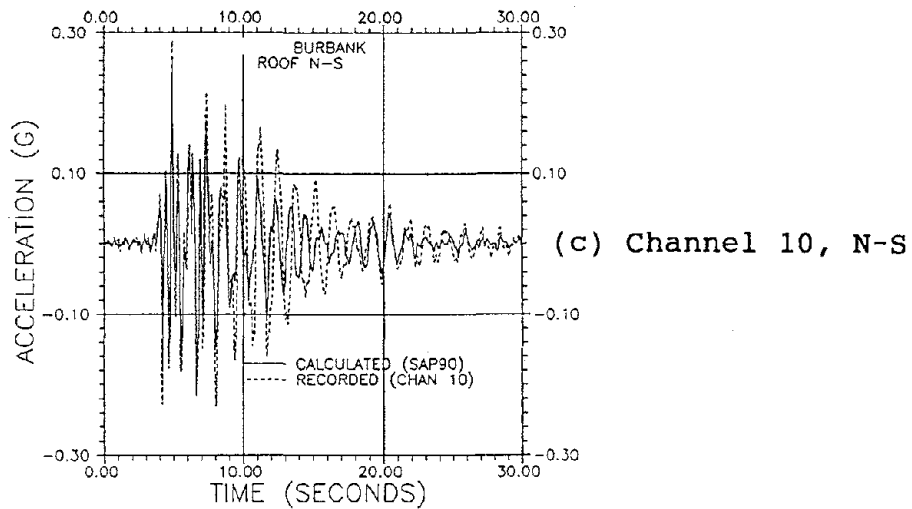
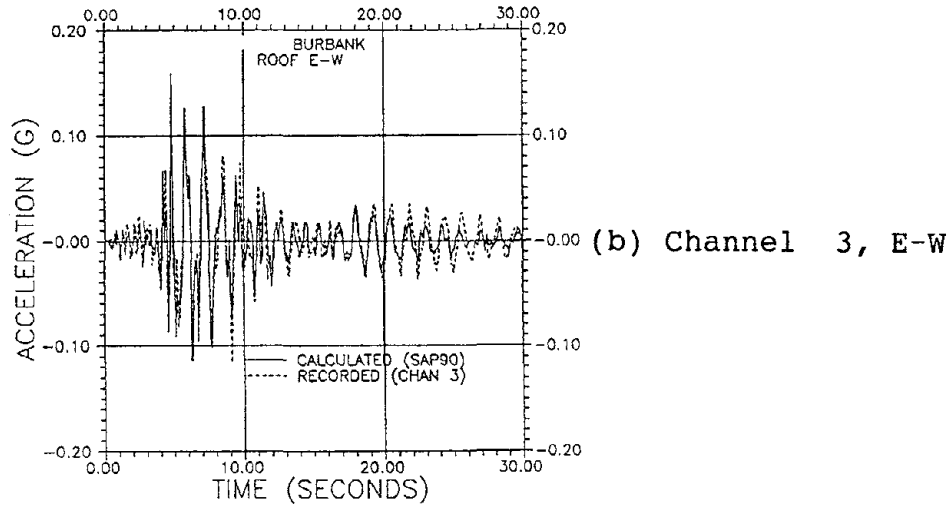
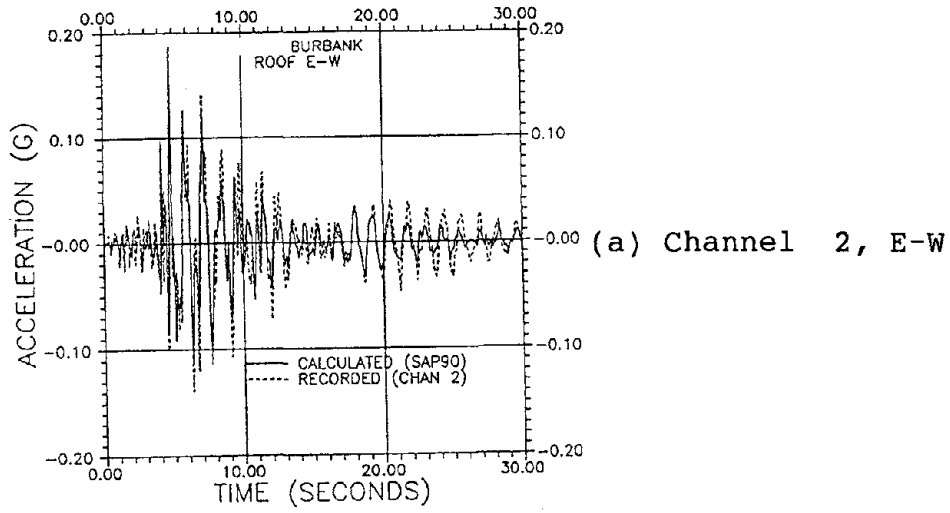
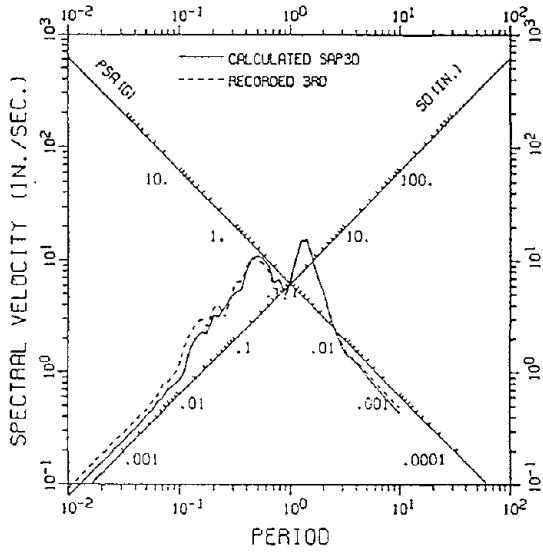
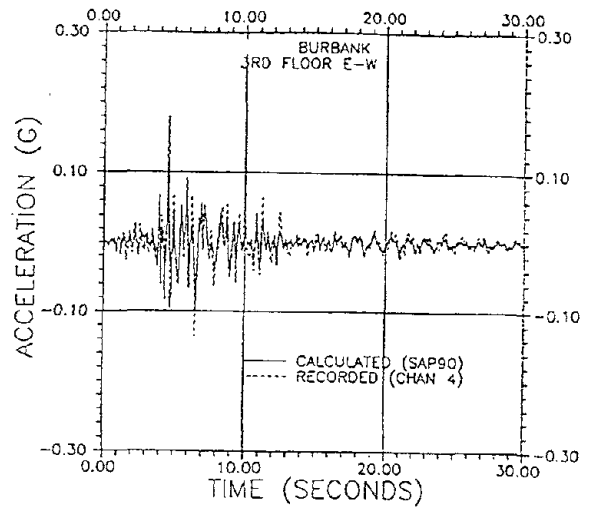


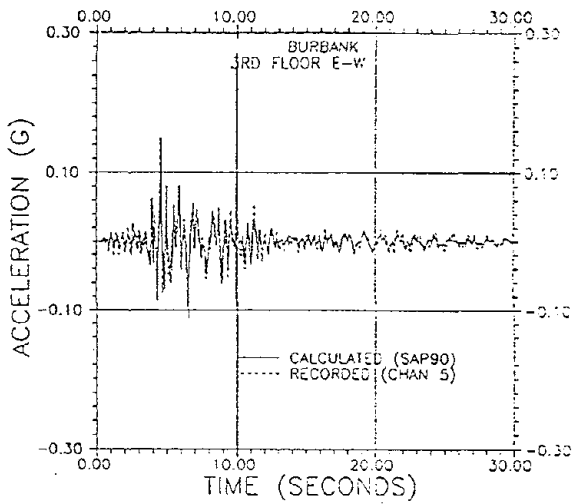
Fig. 39 Acceleration Time Histories, Roof Level



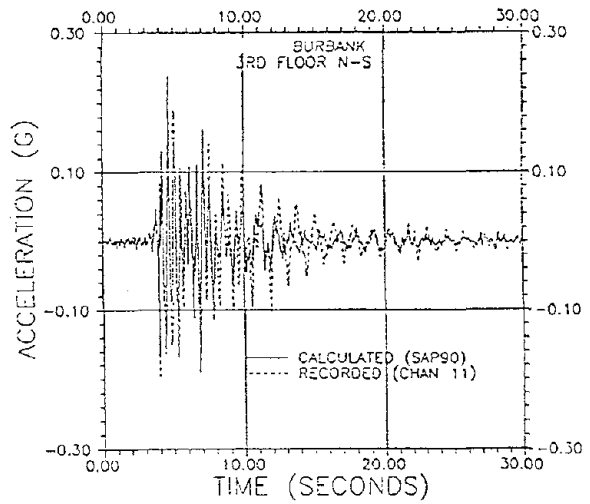
(a) Floor Response Spectra



(b) Channel 4, E-W



(c) Channel 5, E-W



(d) Channel 11, N-S

Fig. 40 Third Floor Response Comparisons



STRESS RATIOS

TOP 6

BOT 1

LEGEND

ETABS

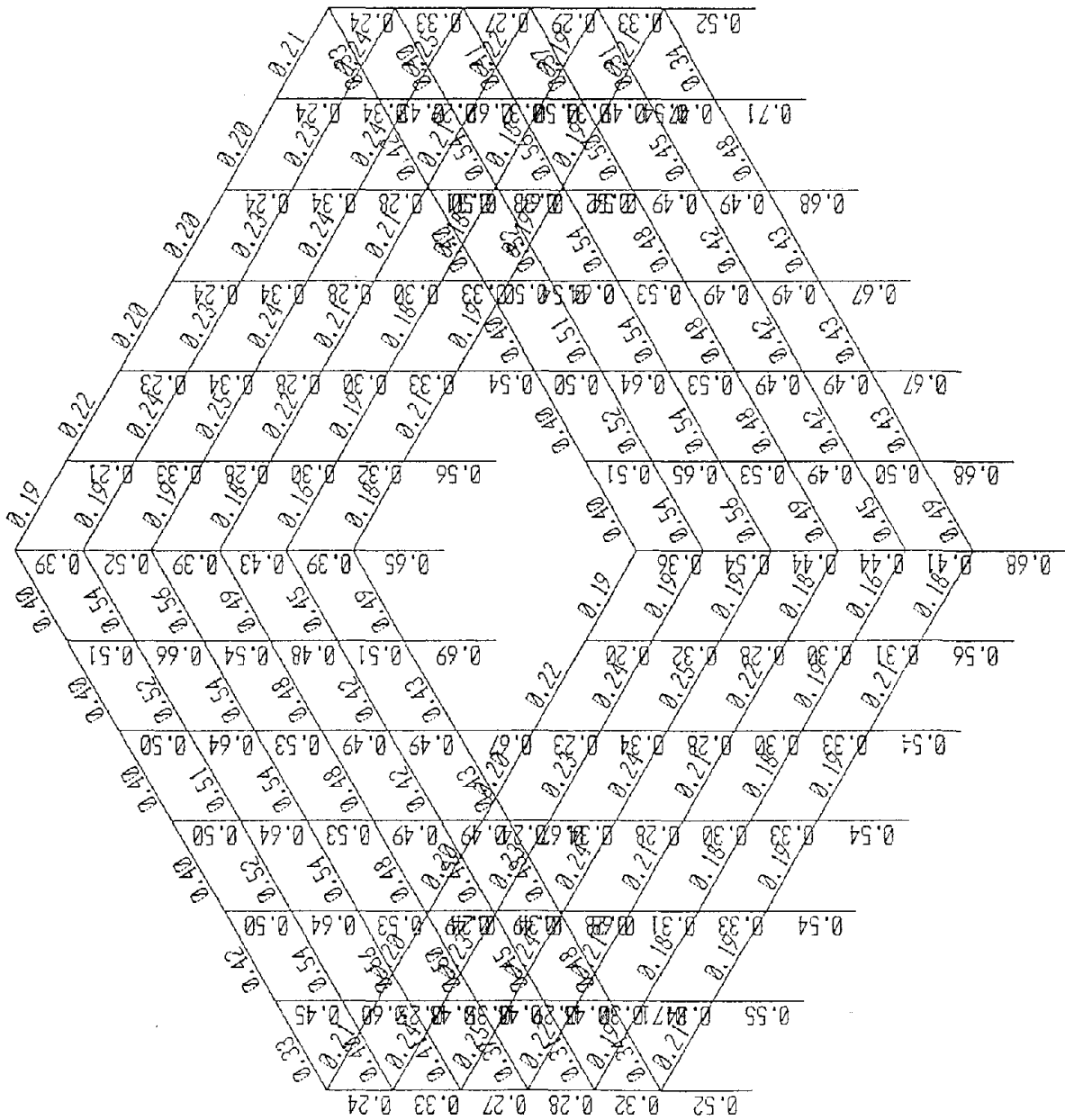
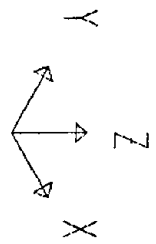
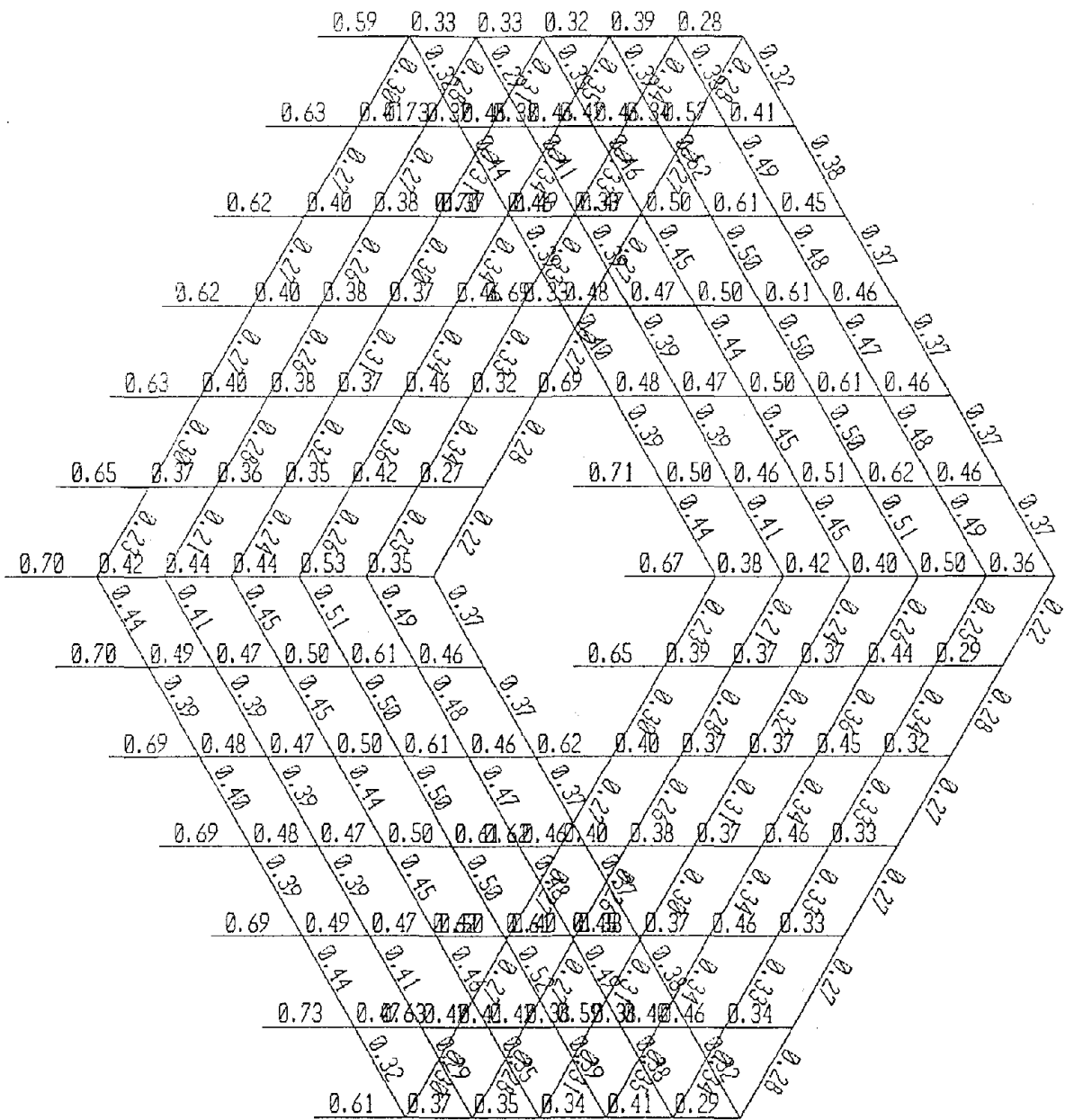


Fig. 42 Stress Ratios, Input Angle = 15°

Fig. 43 Stress Ratios, Input Angle = 30°



STRESS RATIOS

TOP 6  
BOT 1

LEGEND

	OTHER
	0.0
	0.5
	0.7
	0.9
	1.0

ETABS

STRESS RATIOS

TOP 6

BOT 1

LEGEND

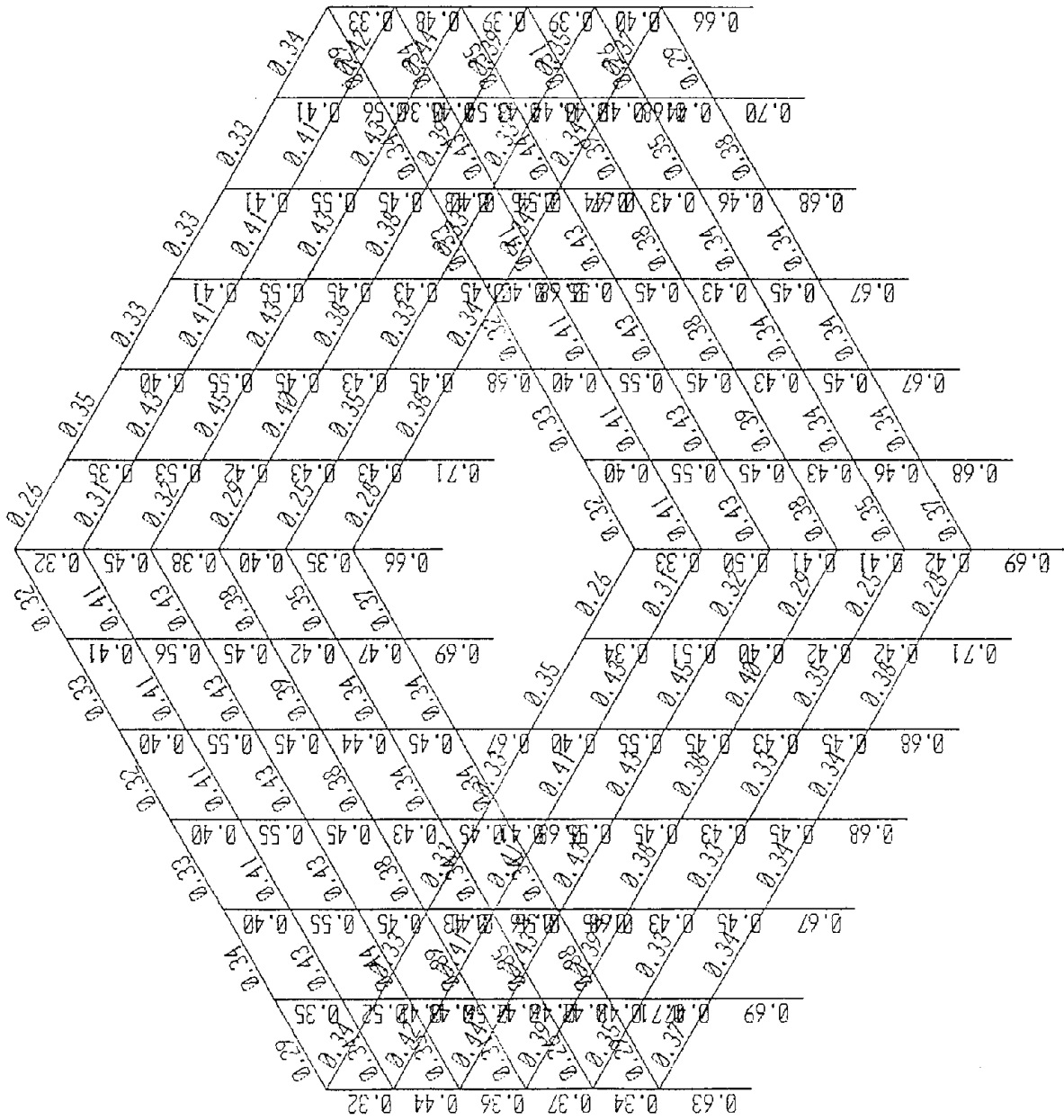


Fig. 44 Stress Ratios, Input Angle = 45°



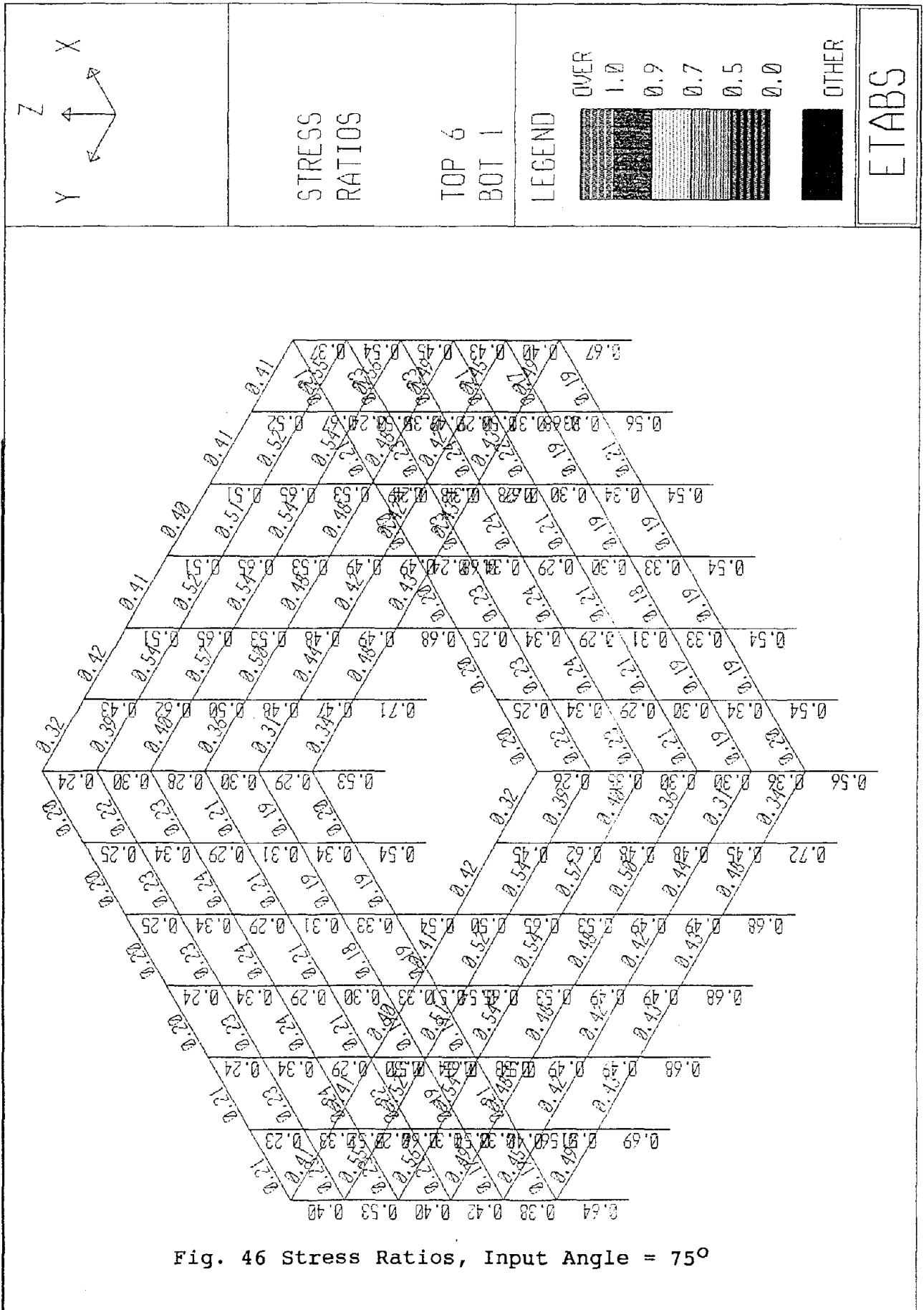
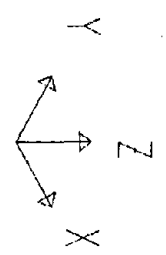
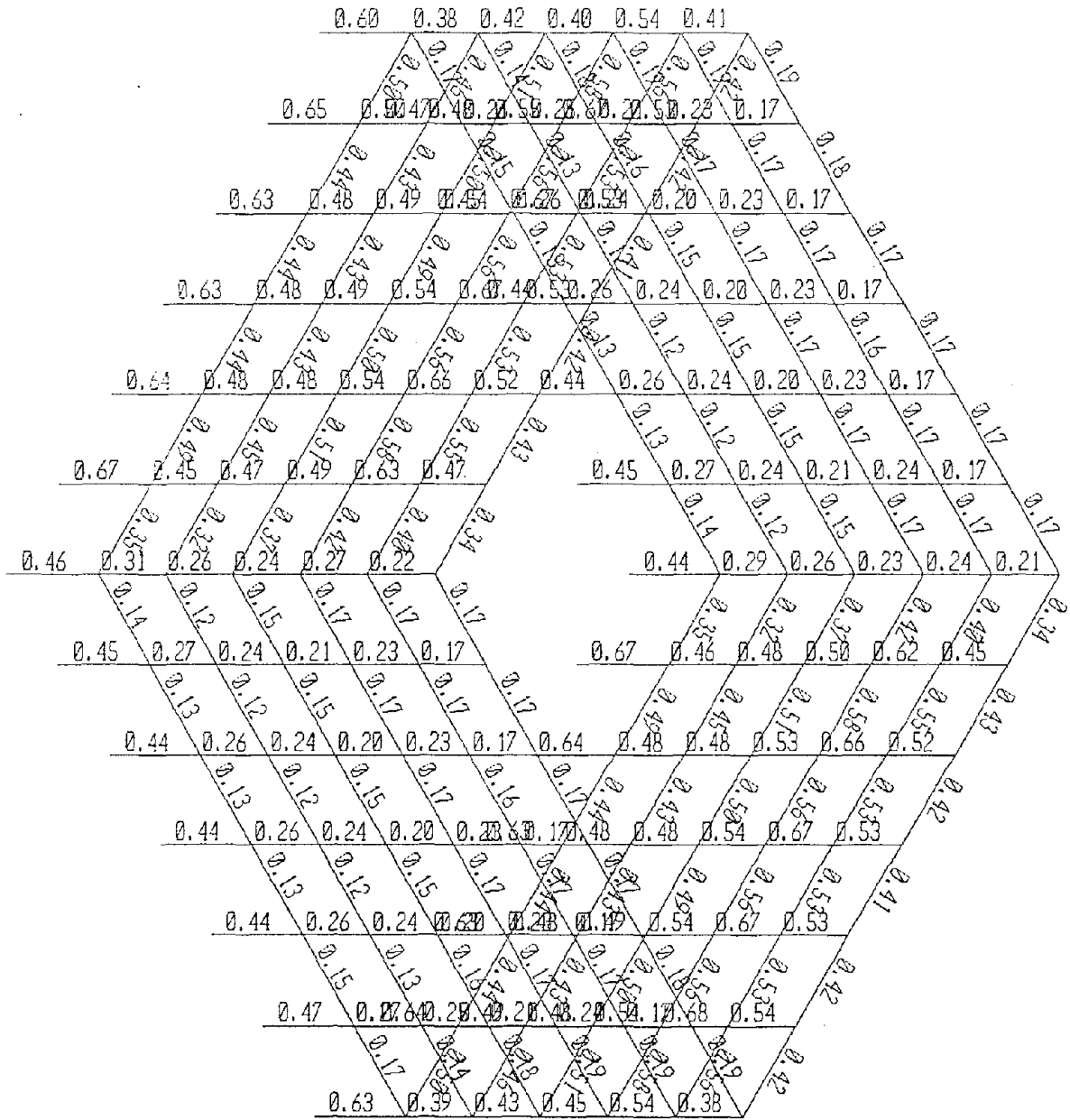


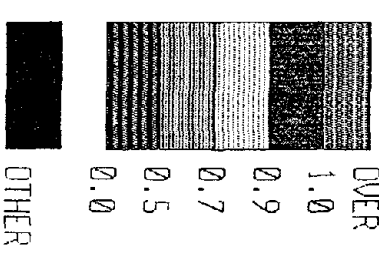
Fig. 47 Stress Ratios, Input Angle = 90°



STRESS RATIOS

TOP 6  
BOT 1

LEGEND



ETABS

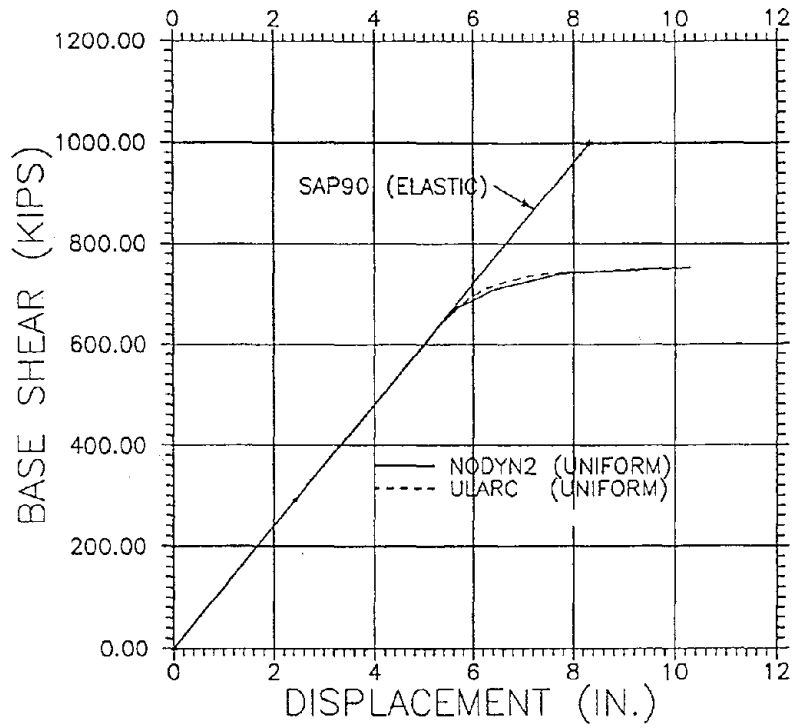


Fig. 48 Roof Displacement vs. Base Shear, Uniform Lateral

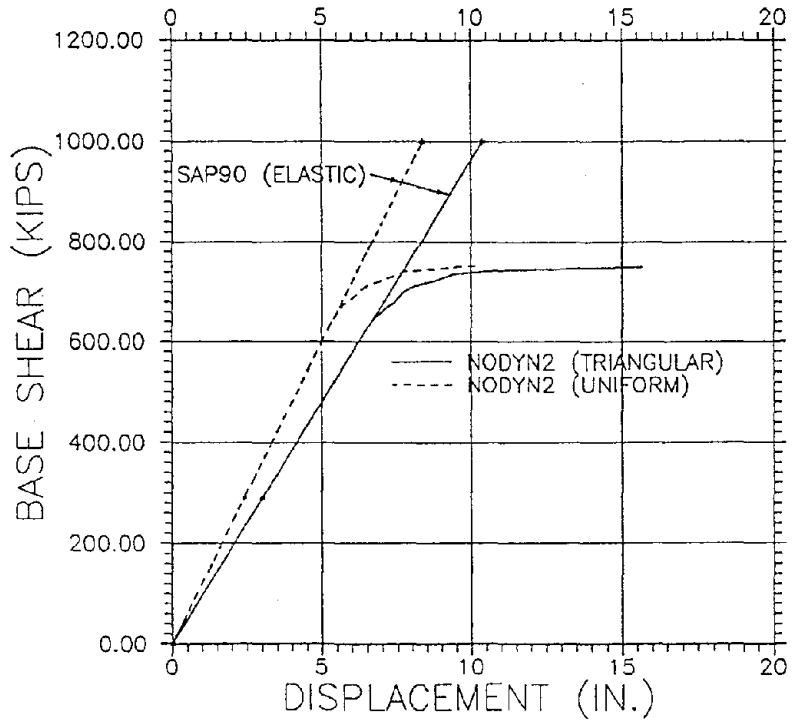


Fig. 49 Uniform vs. Triangular Lateral Loading

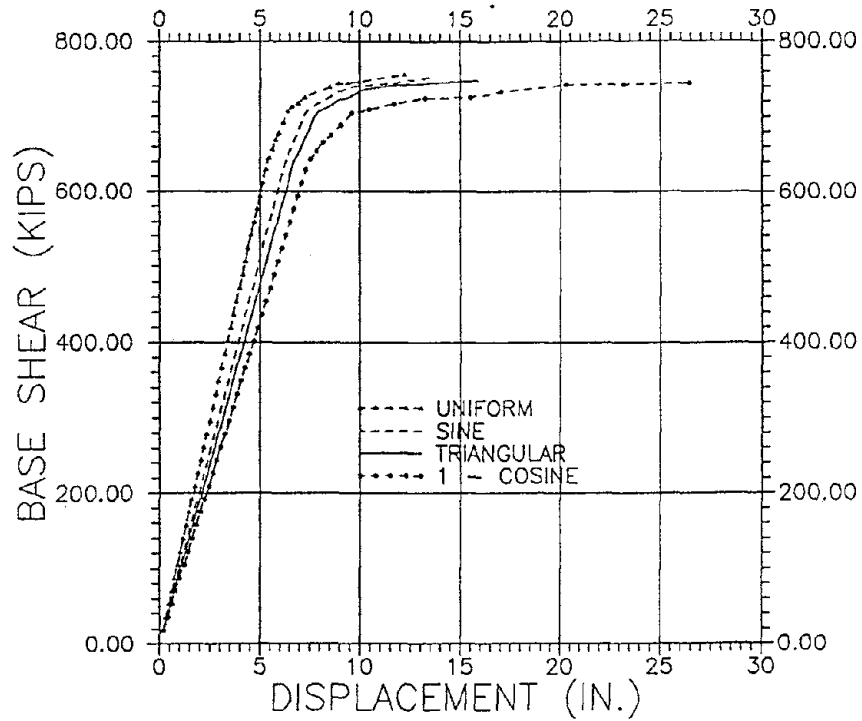


Fig. 50 Lateral Load Distribution and Lateral Resistance

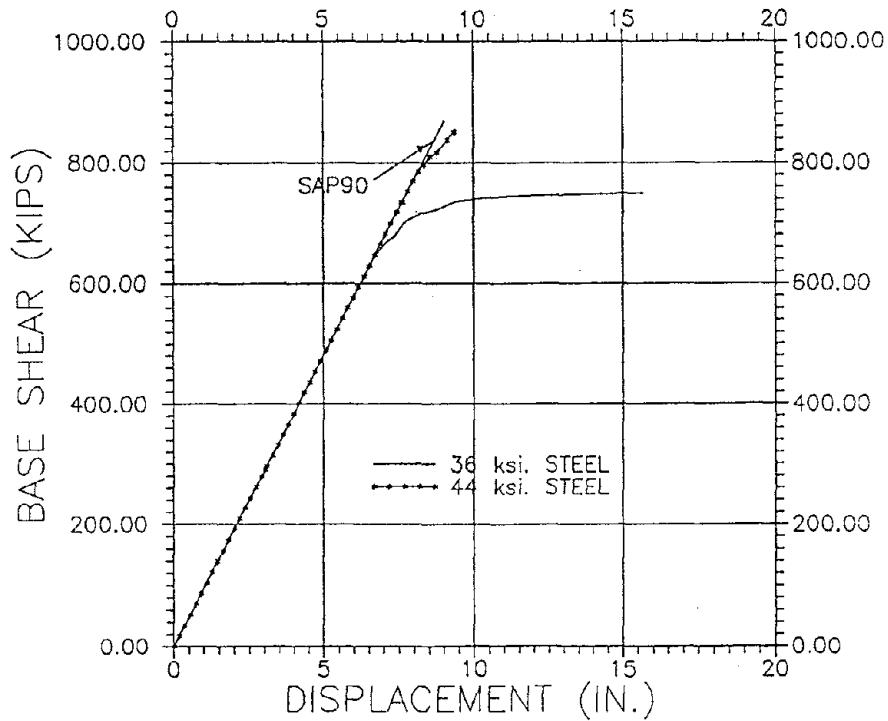


Fig. 51 Resistance, Nominal vs. Actual Steel Strength

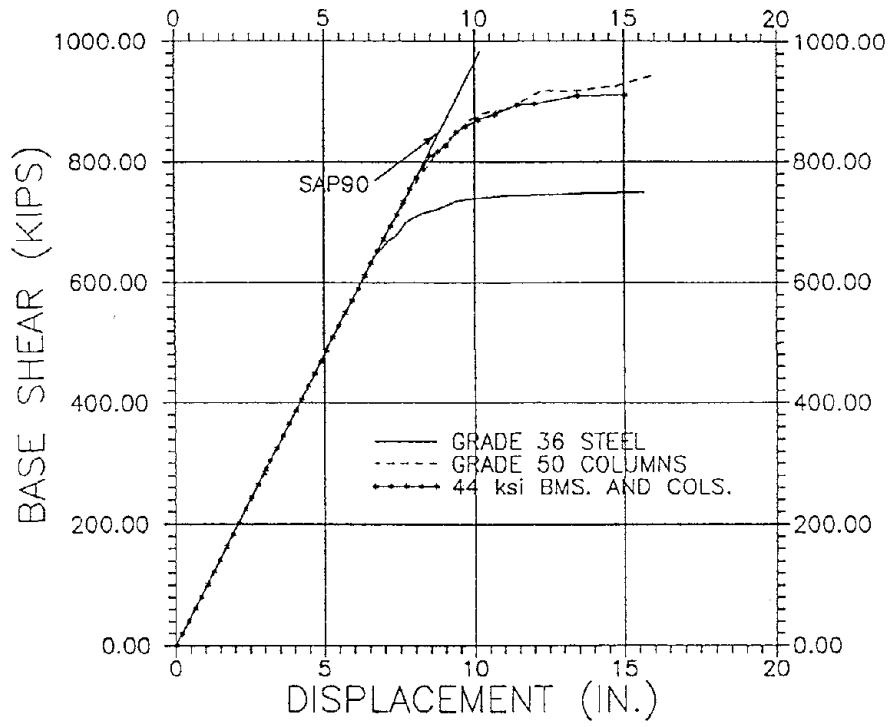


Fig. 52 Steel Strength and Lateral Resistance

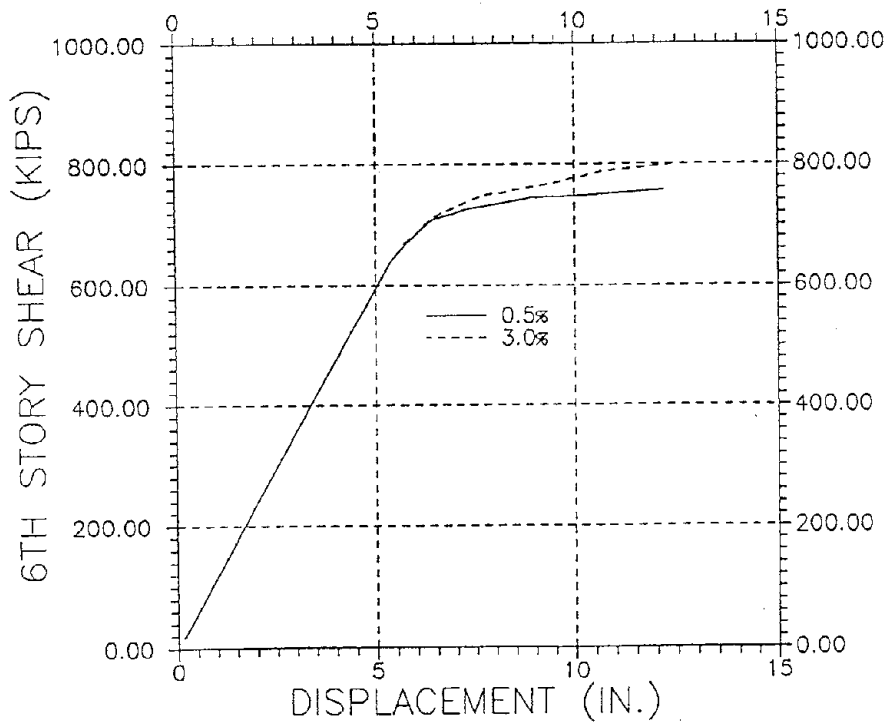


Fig. 53 Strain Hardening and Lateral Resistance

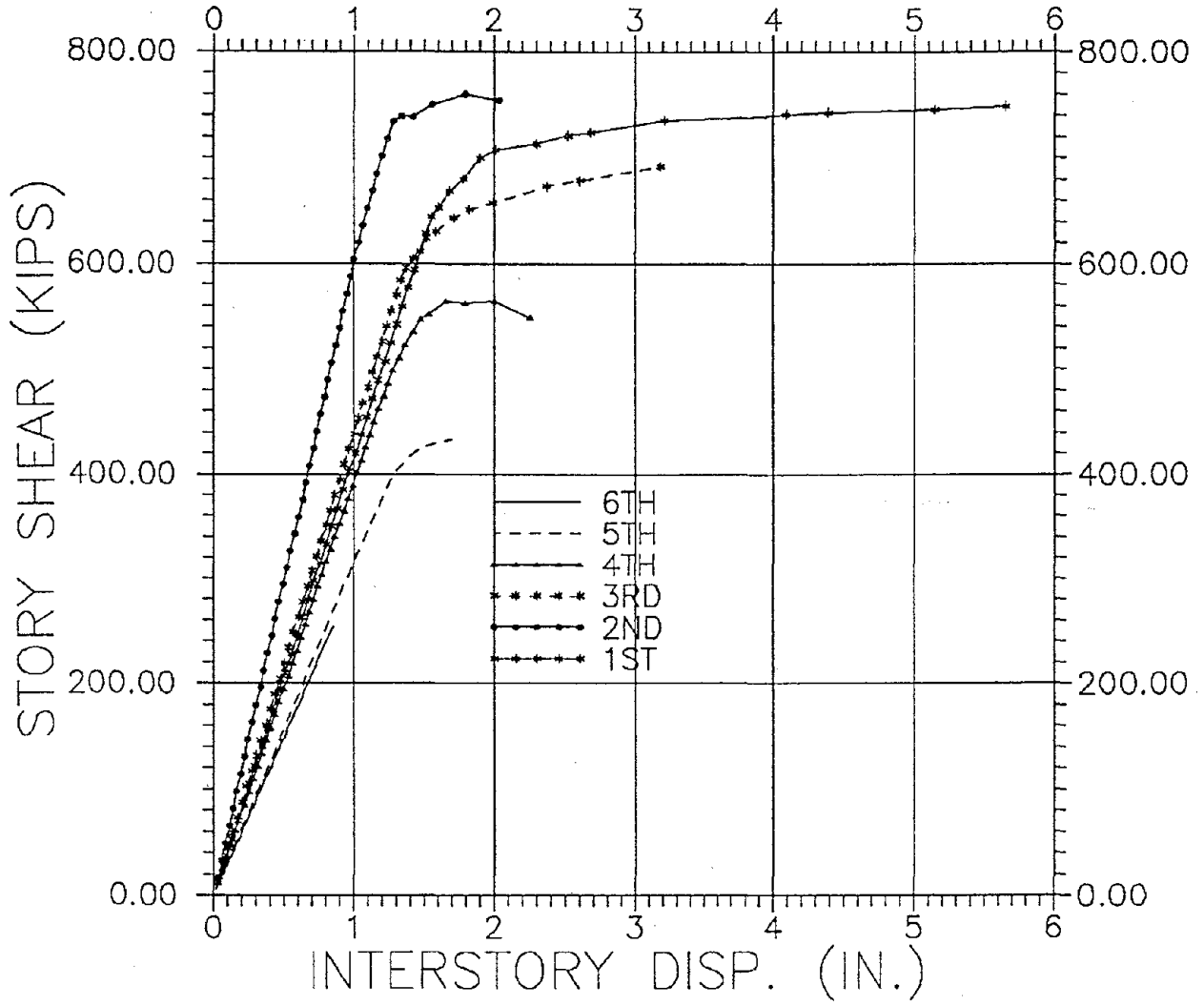


Fig. 54 Interstory Shear vs. Displacement, Triangular Load

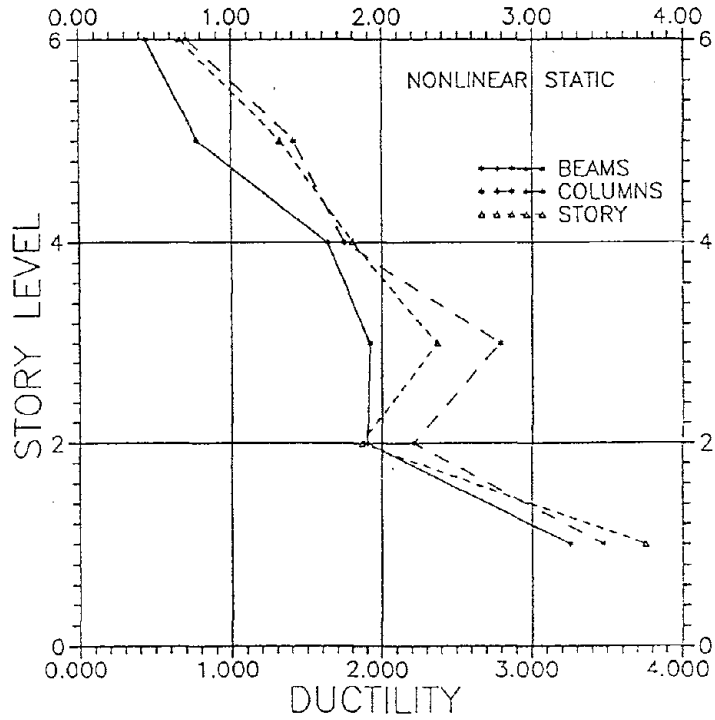


Fig. 55 Ductility Requirements vs. Story Level

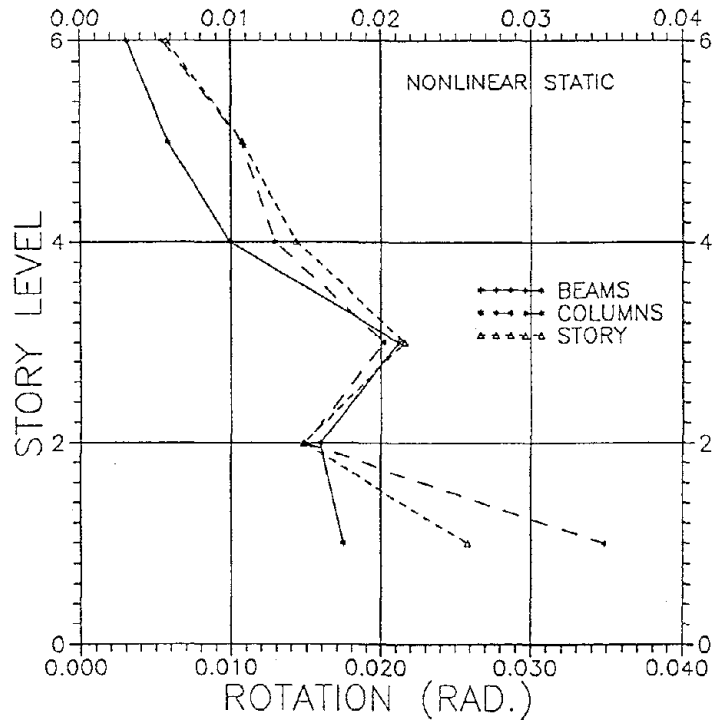


Fig. 56 Rotation Requirements vs. Story Level

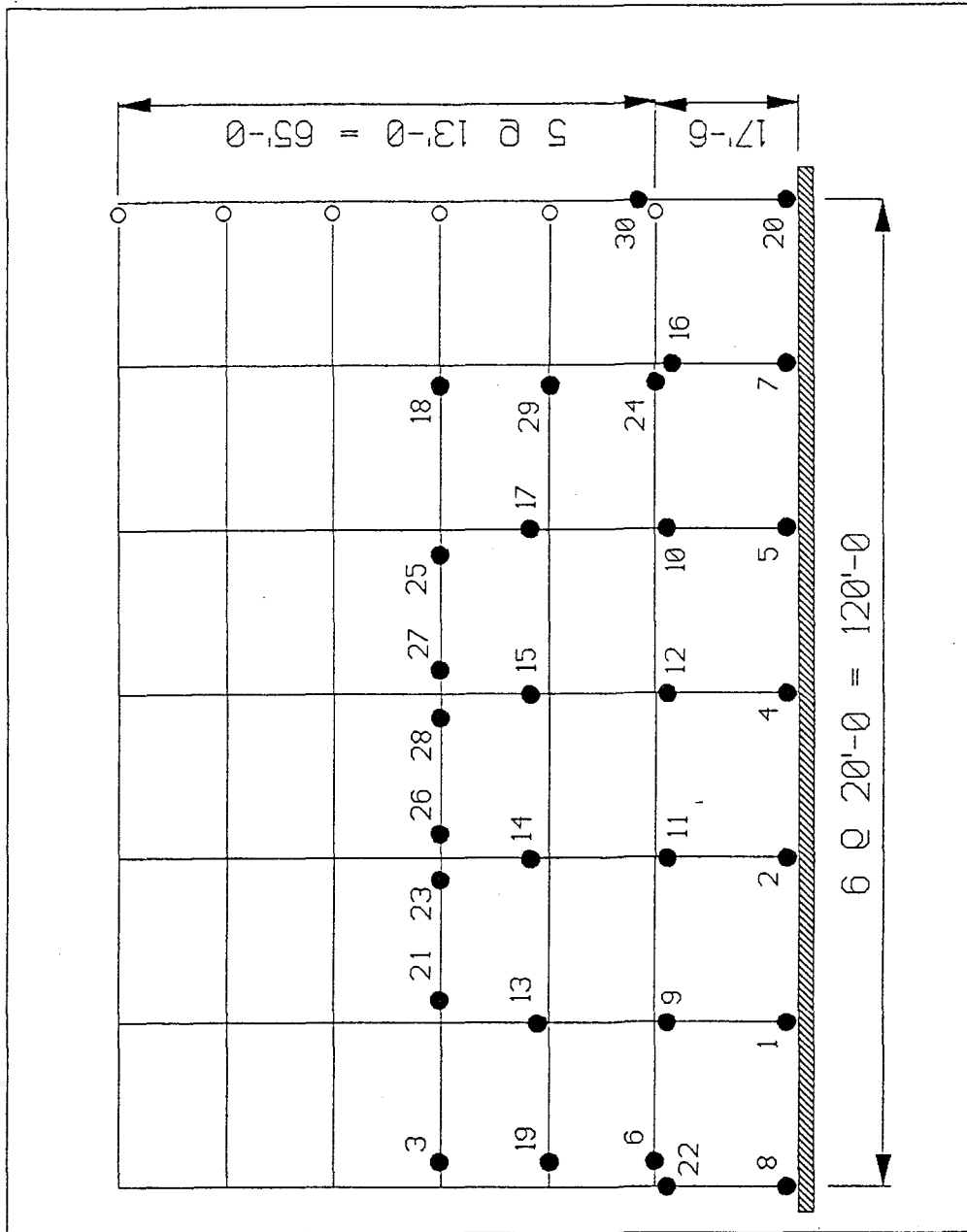


Fig. 57 Sequence of Plastic Hinge Formation

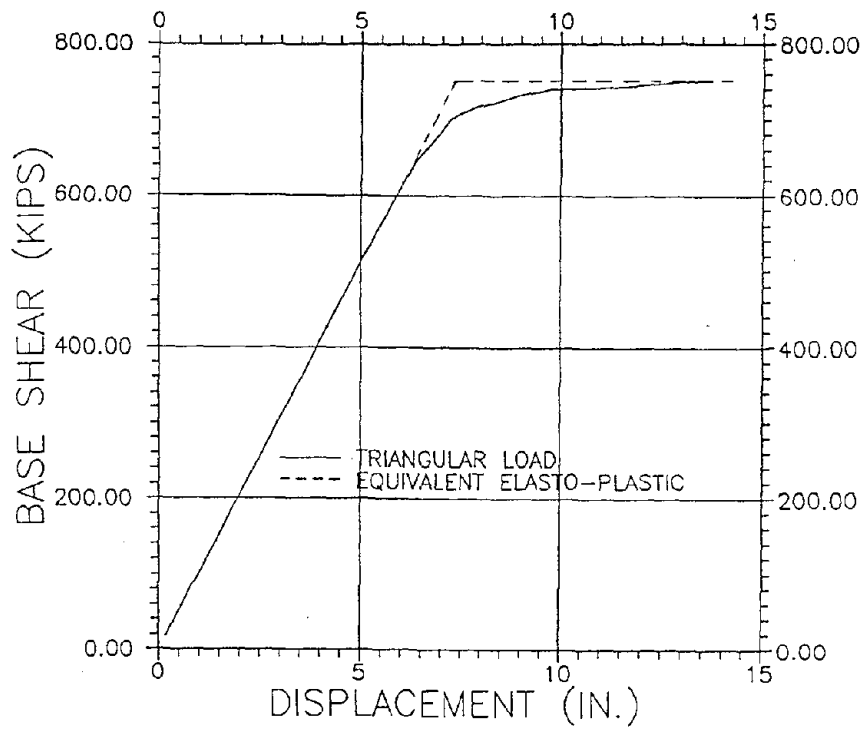


Fig. 58 Idealized Elastic-Plastic Shear vs. Displacement

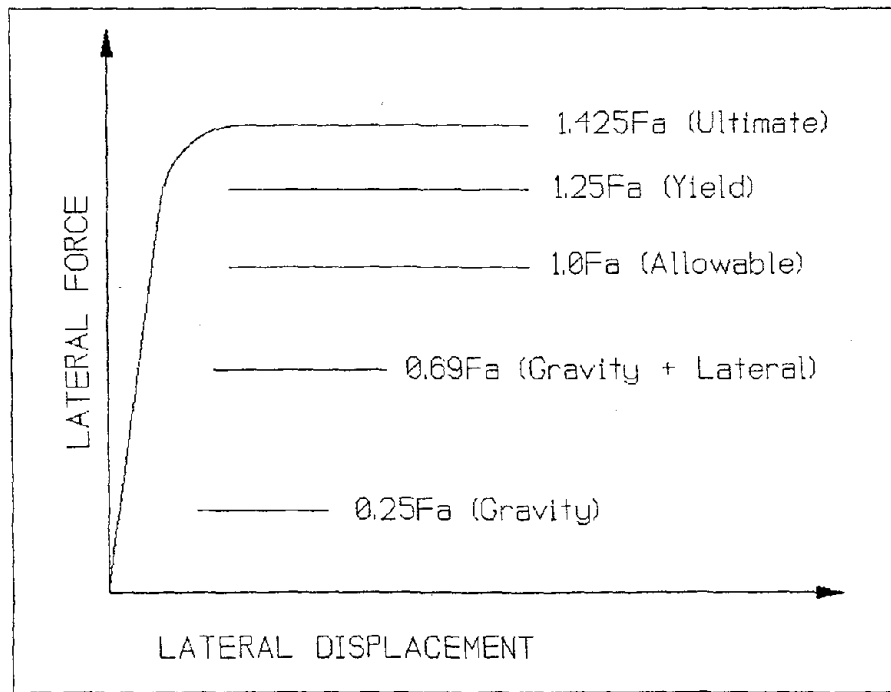


Fig. 59 Stresses in an Idealized Member

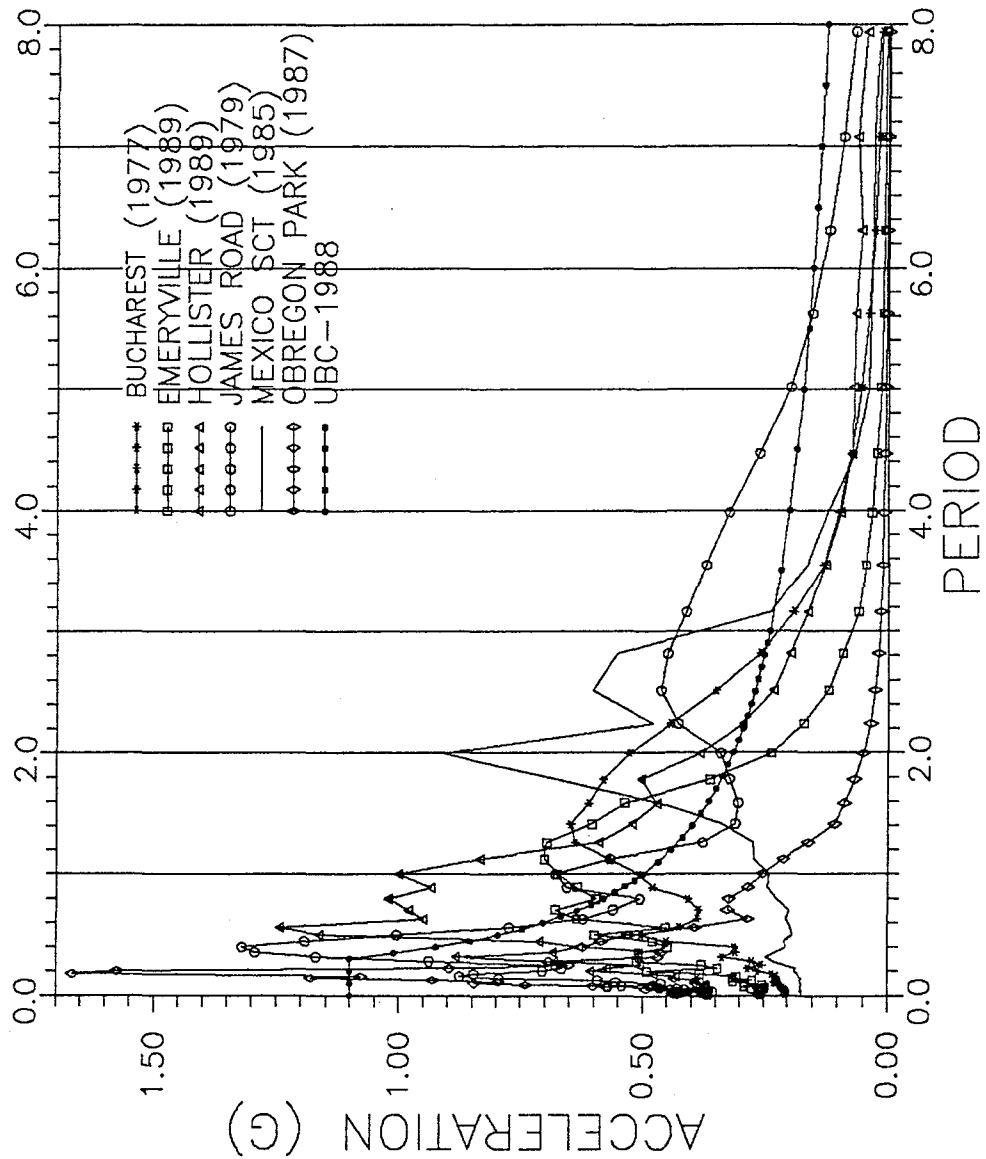
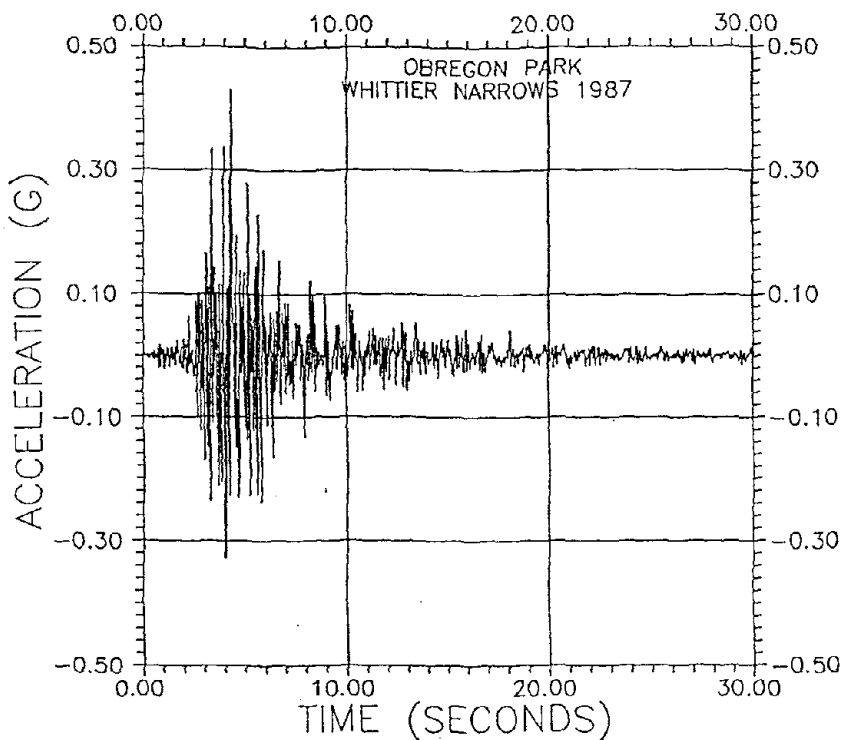
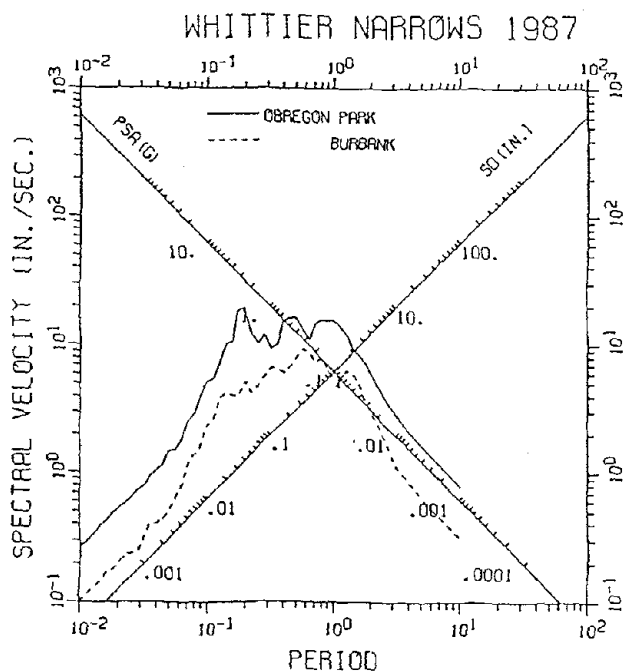


Fig. 60 LERS for Recent Earthquakes

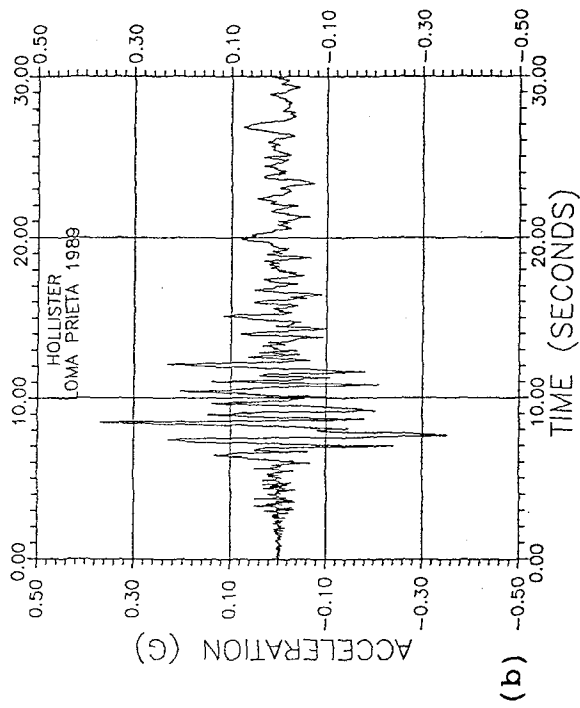


(a) Acceleration Time History

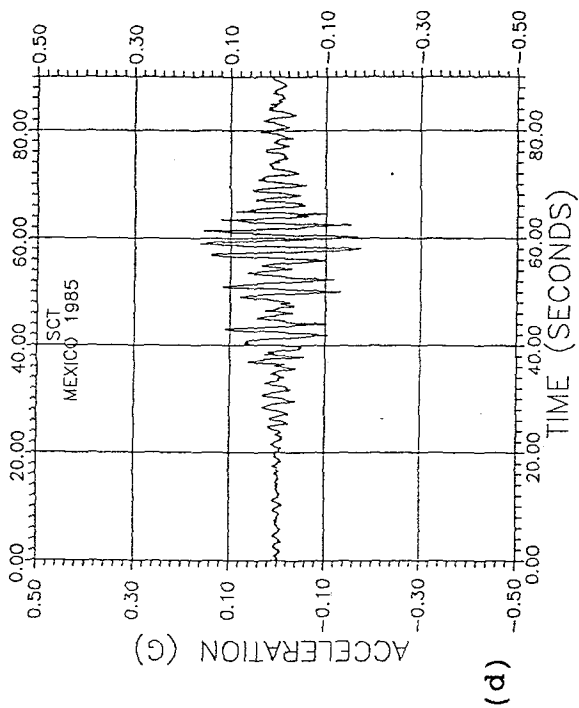


(b) Response Spectra Comparison

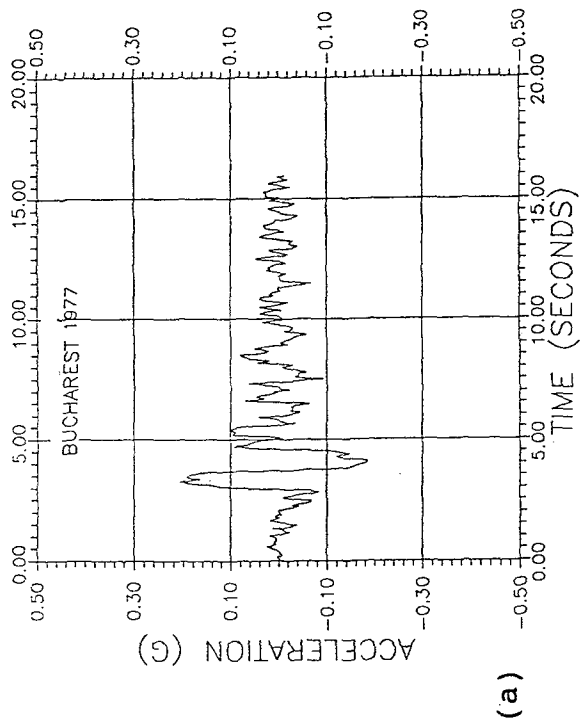
Fig. 61 Motion Recorded at Obregon Park, Whittier Narrows



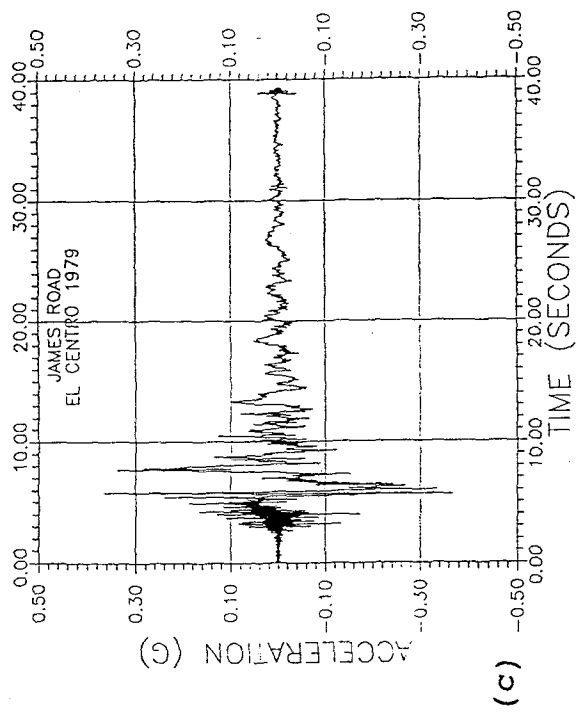
(a)



(b)



(c)



(d)

Fig. 62 Acceleration Time Histories of Recent Earthquakes

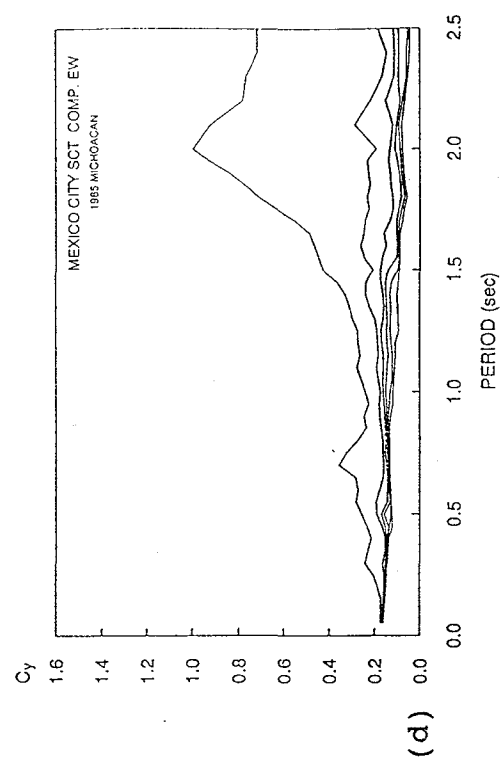
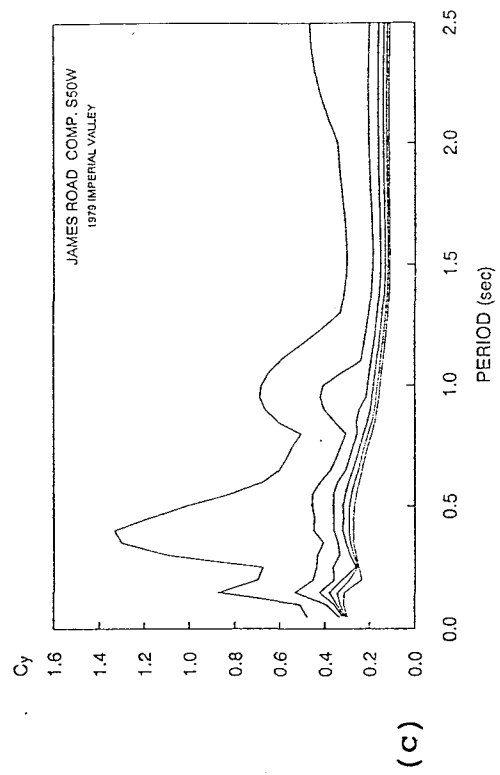
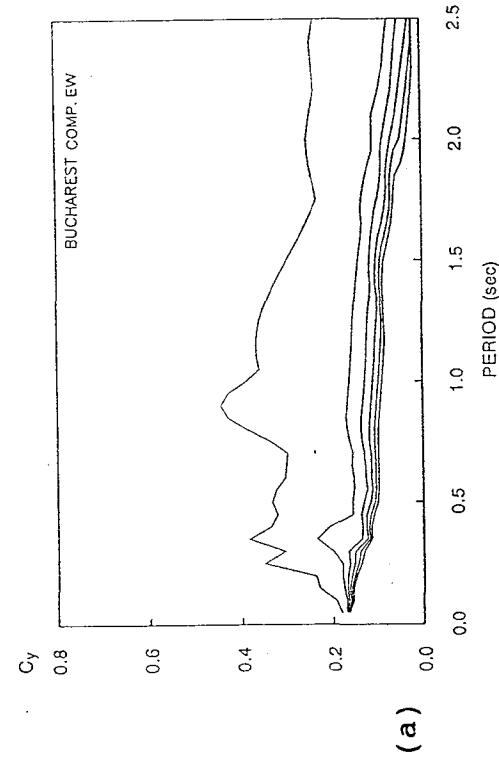
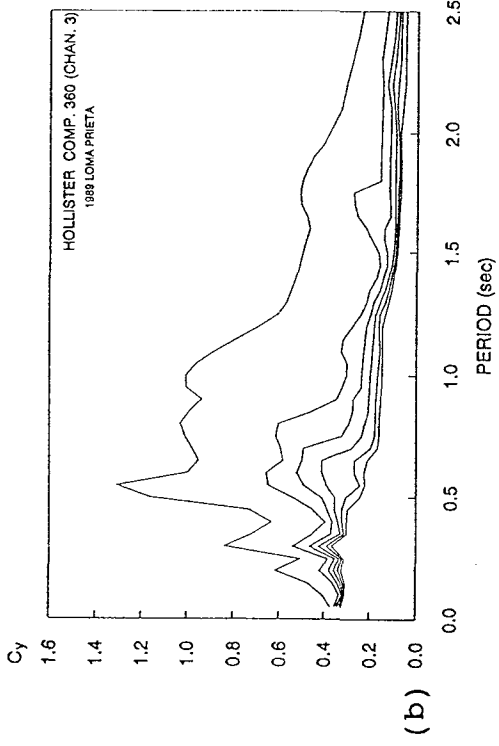
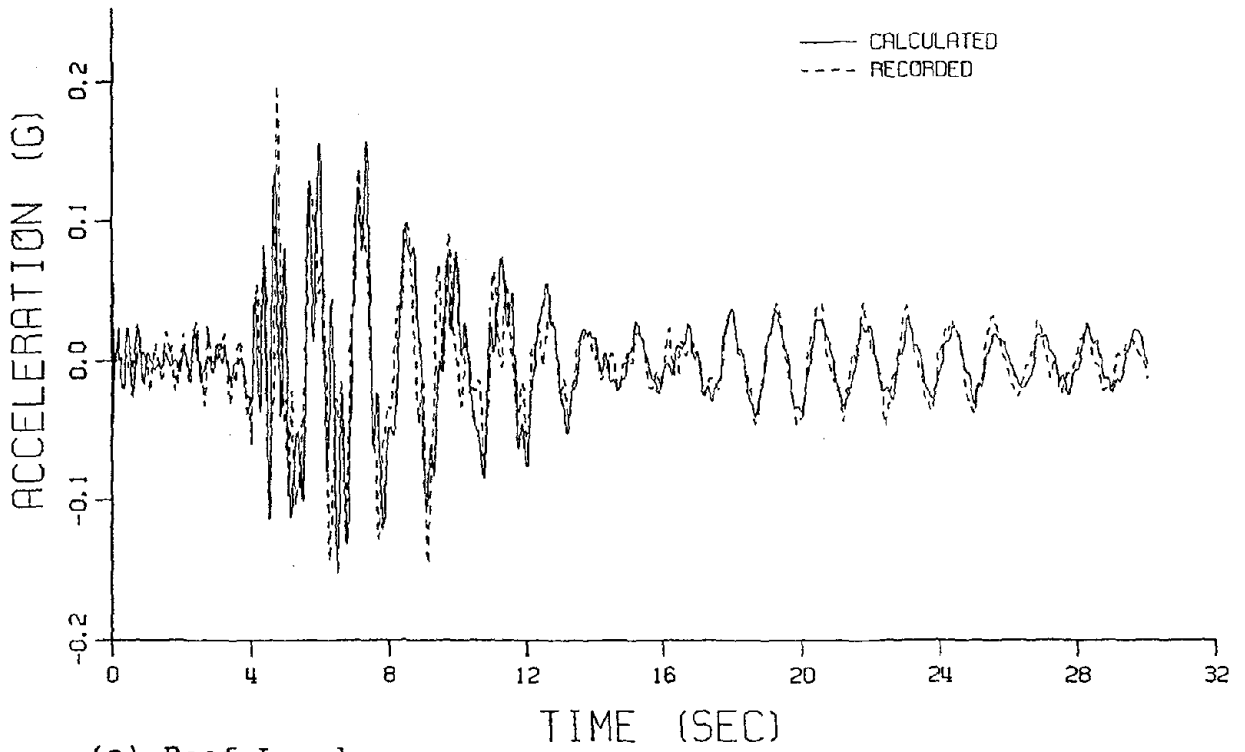
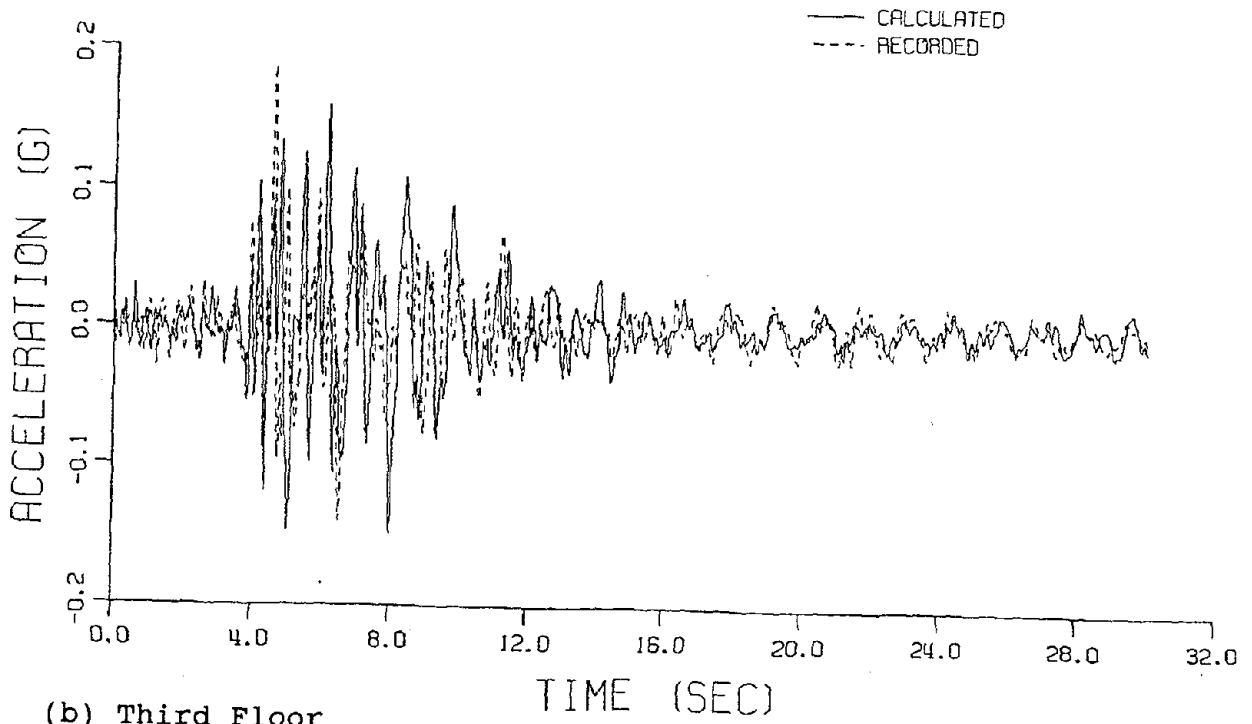


Fig. 63 Inelastic Response Spectra

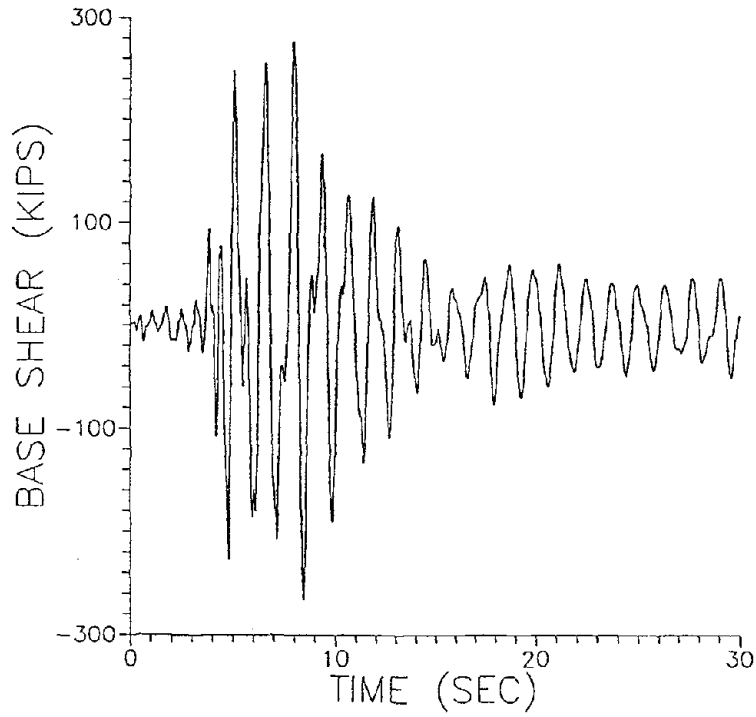


(a) Roof Level

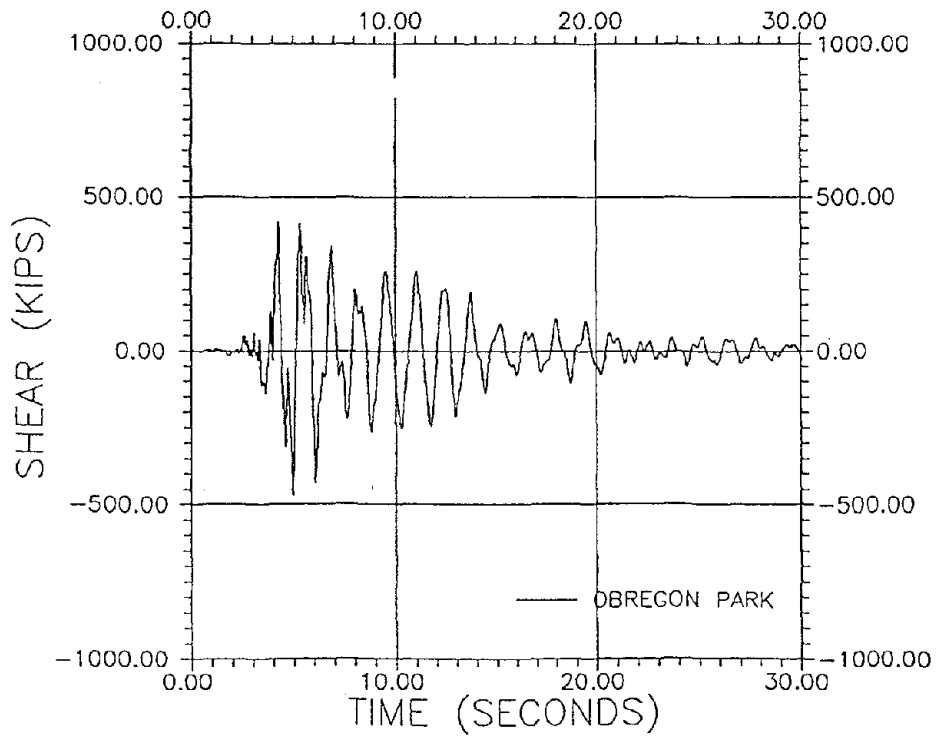


(b) Third Floor

Fig. 64 Acceleration Comparisons, Nonlinear Model



(a) Building Base



(b) Obregon Park

Fig. 65 Base Shear Time Histories, Whittier Narrows

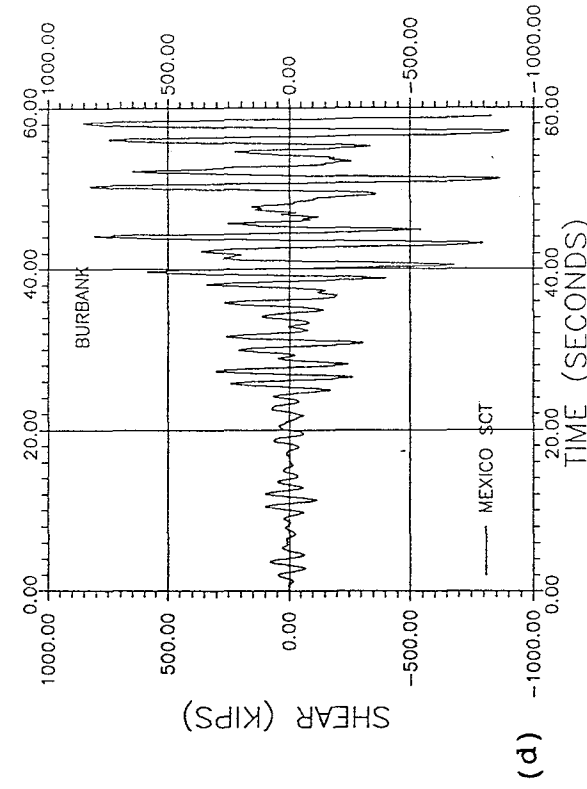
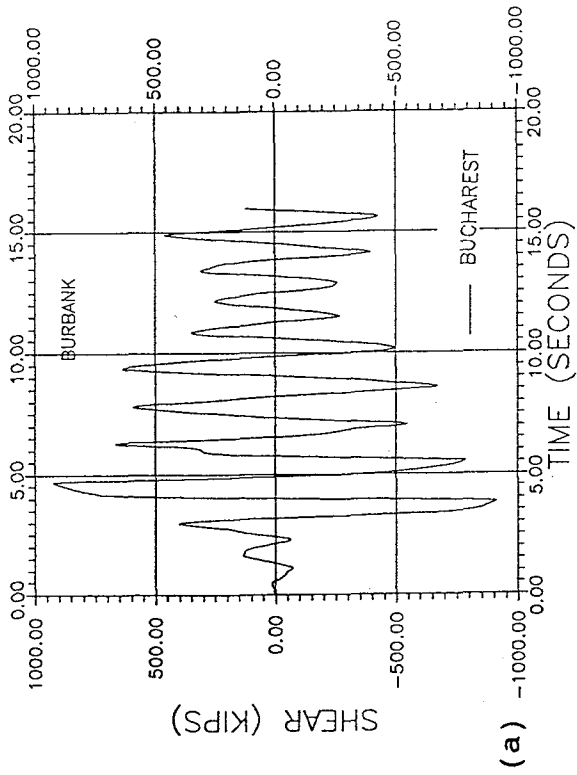
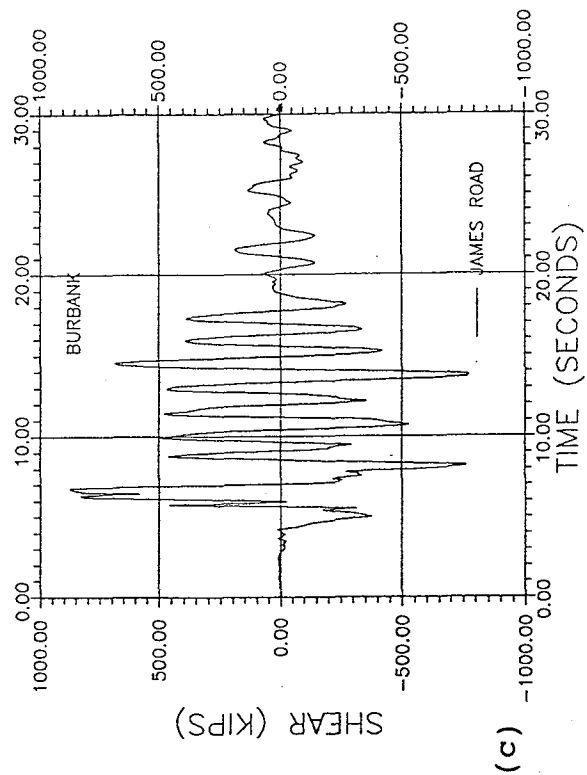
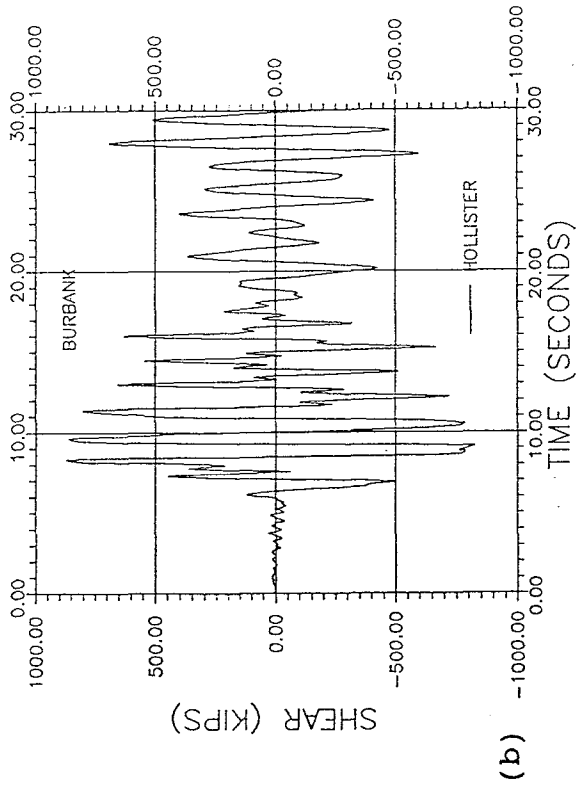
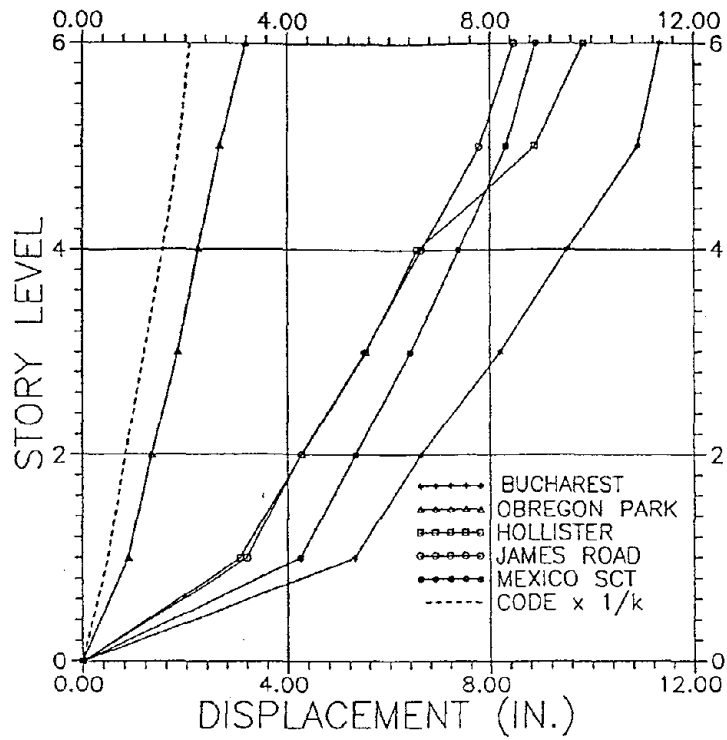
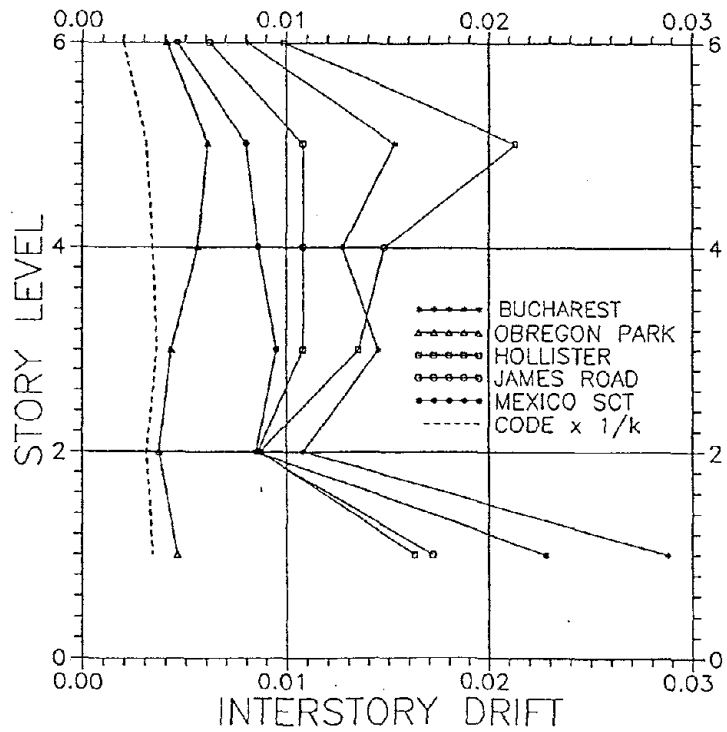


Fig. 66 Base Shear Time Histories, Recent Earthquakes

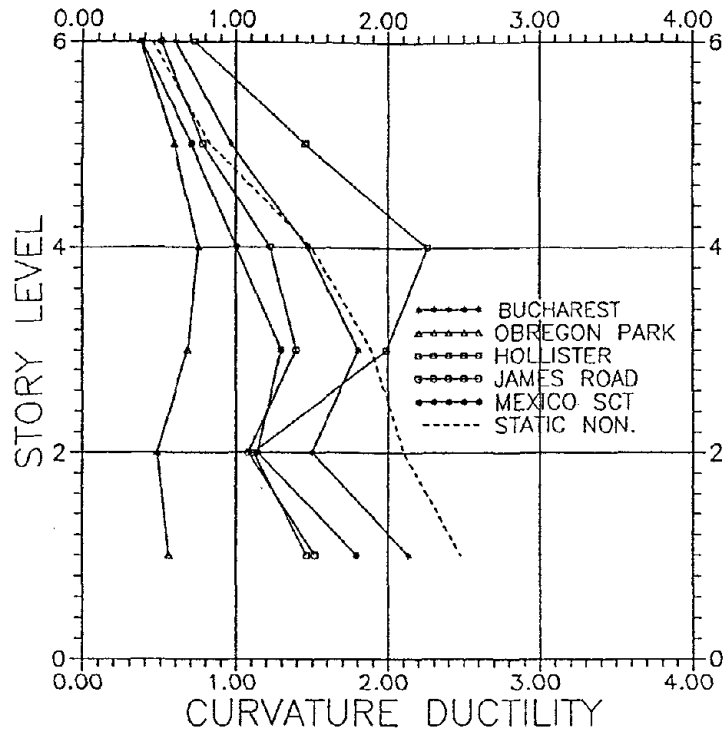


(a) Lateral Displacement

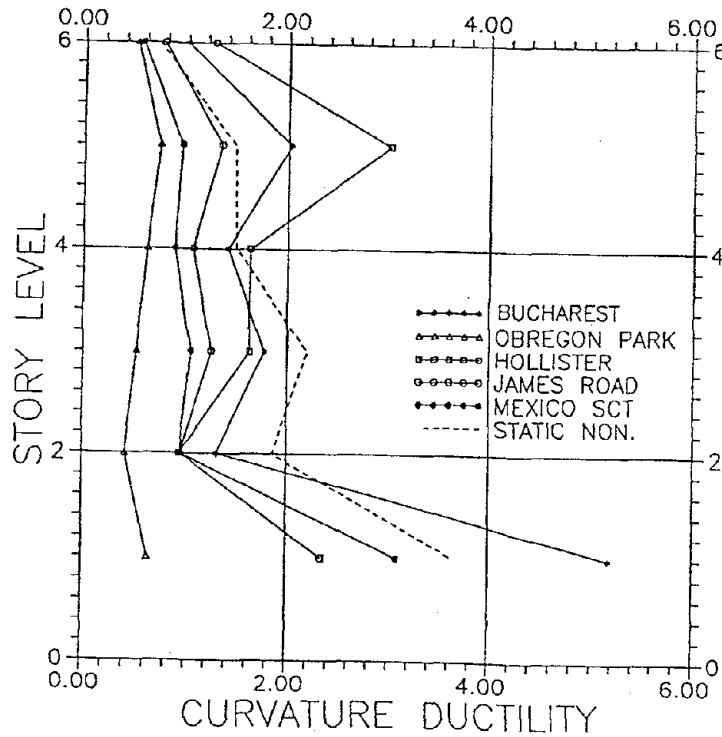


(b) Interstory Drift Index

Fig. 67 Maximum Displacement Response

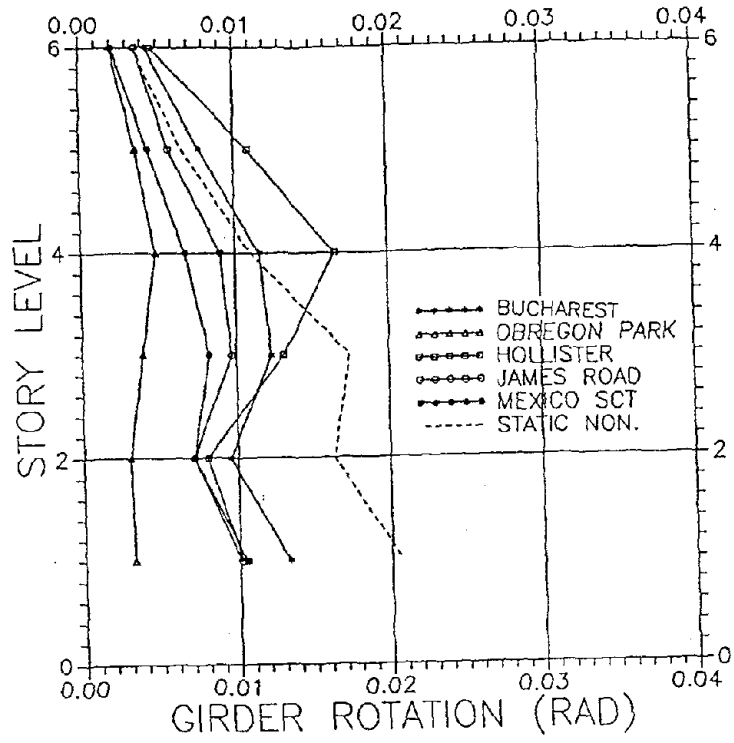


(a) Girders

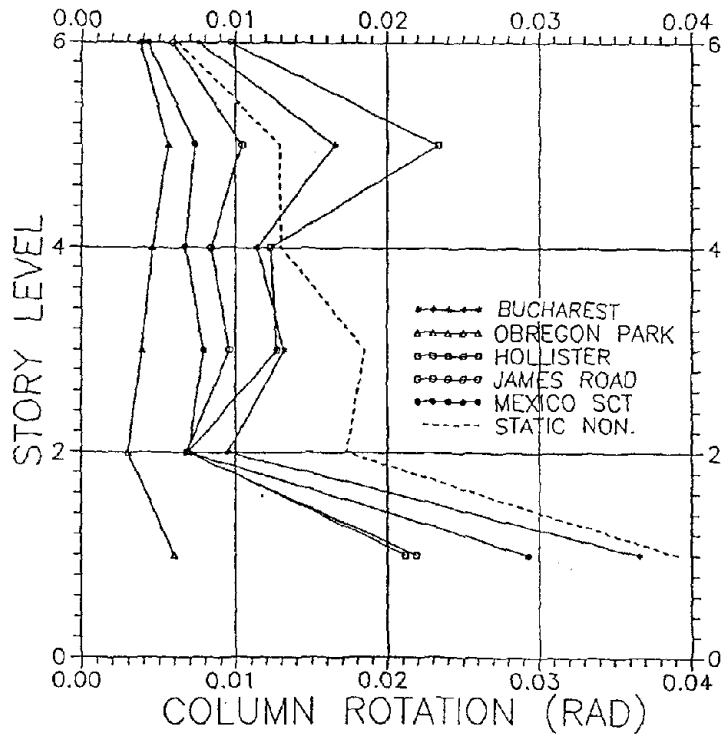


(b) Columns

Fig. 68 Curvature Ductility Demand



(a) Girders



(b) Columns

Fig. 69 Maximum Rotation Demand

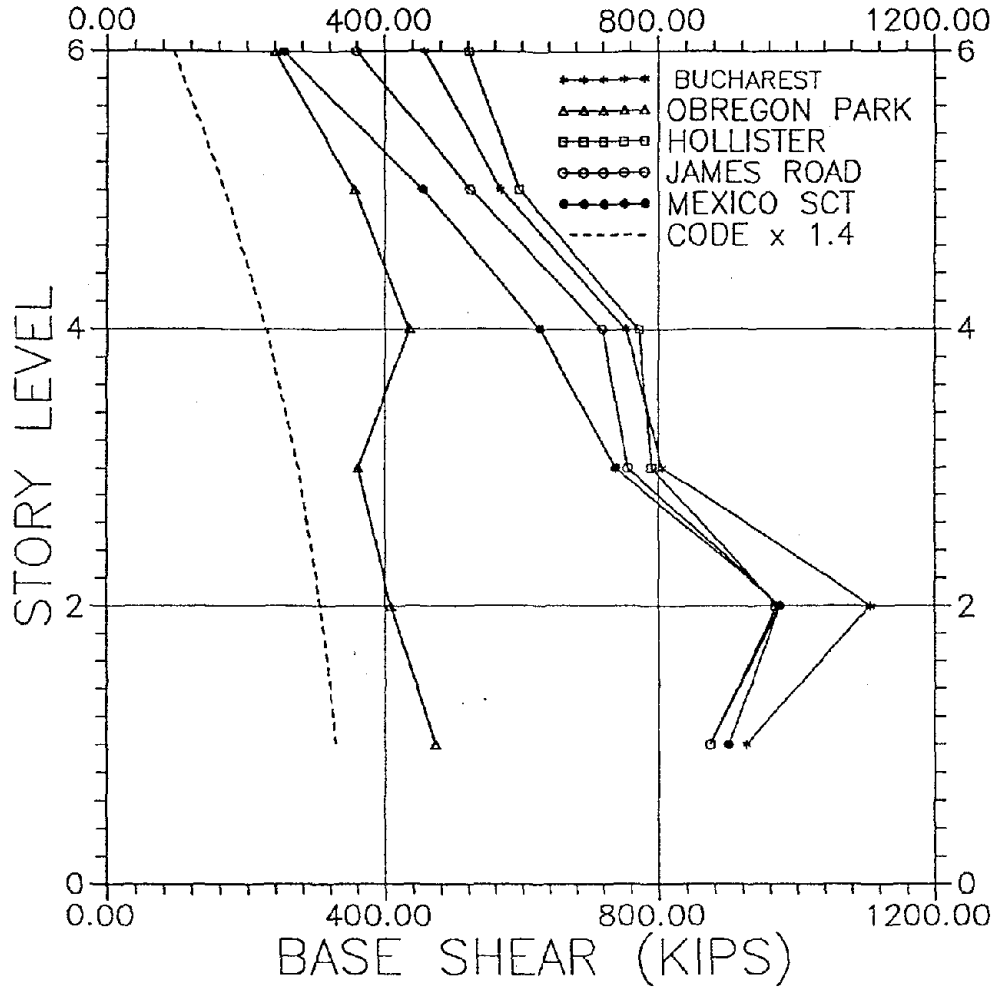
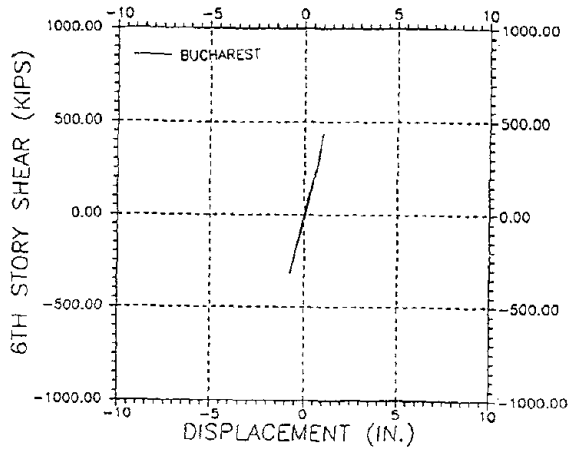
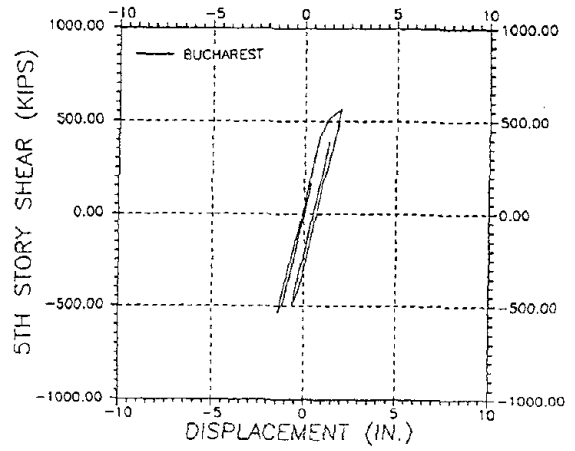


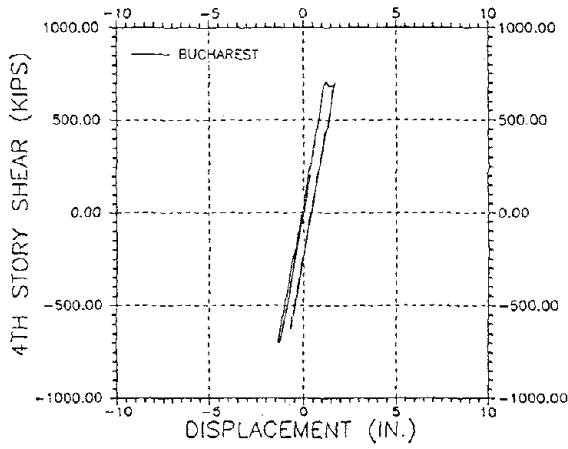
Fig. 70 Maximum Story Shear Envelopes



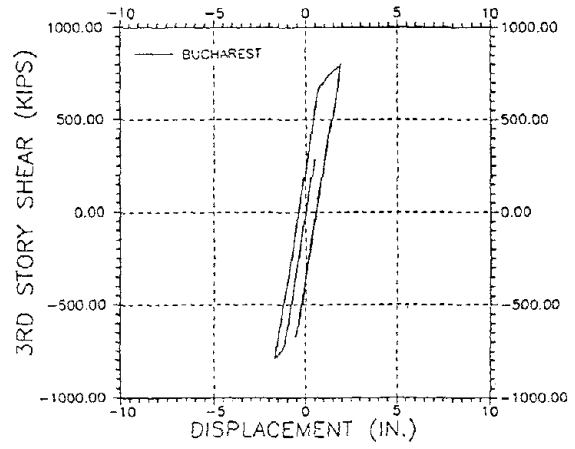
(a) Sixth Story



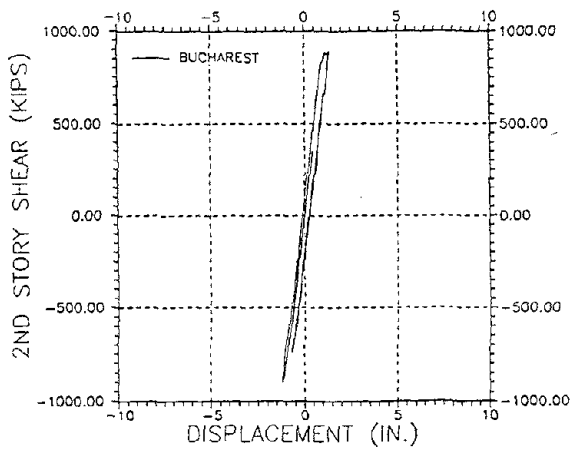
(b) Fifth Story



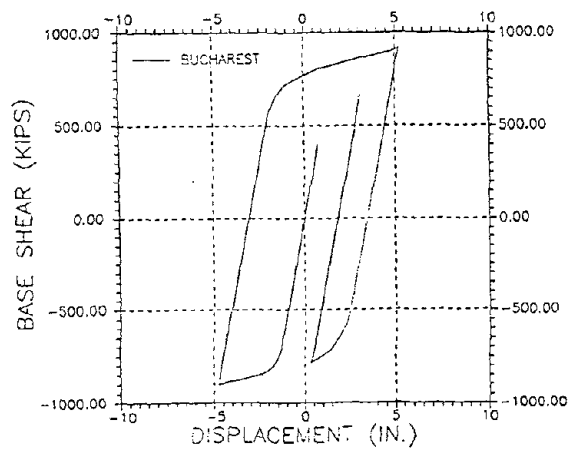
(c) Fourth Story



(d) Third Story

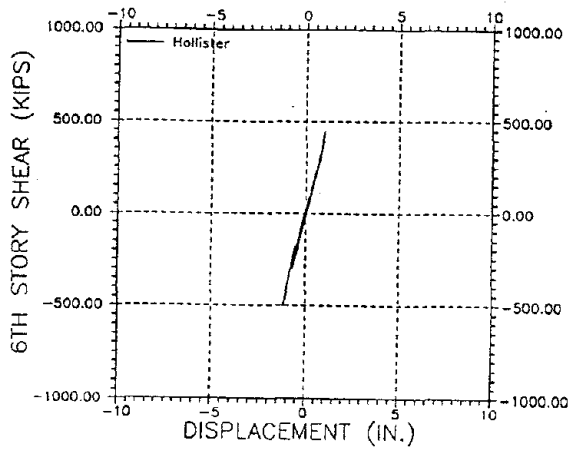


(e) Second Story

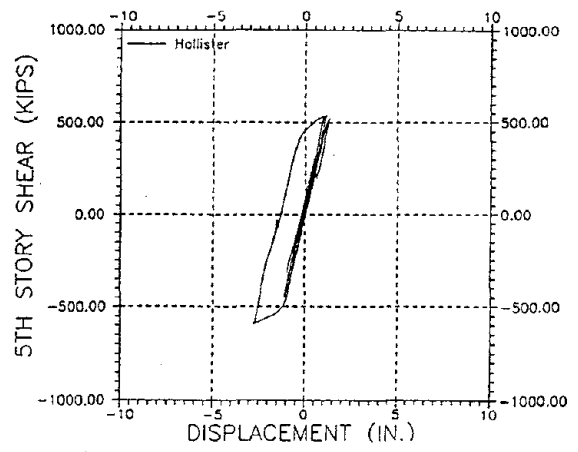


(f) First Story

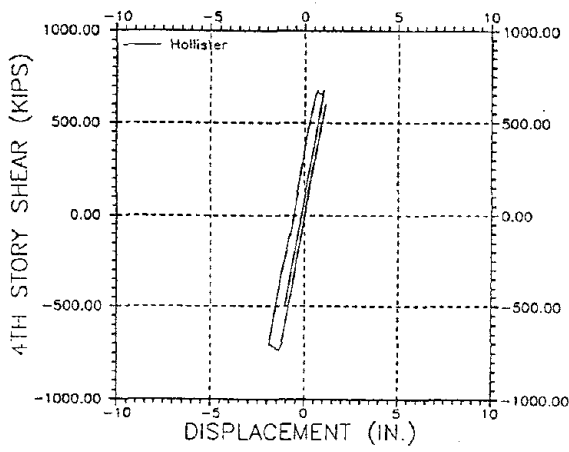
Fig. 71 Story Shear vs. Interstory Displacement, Bucharest



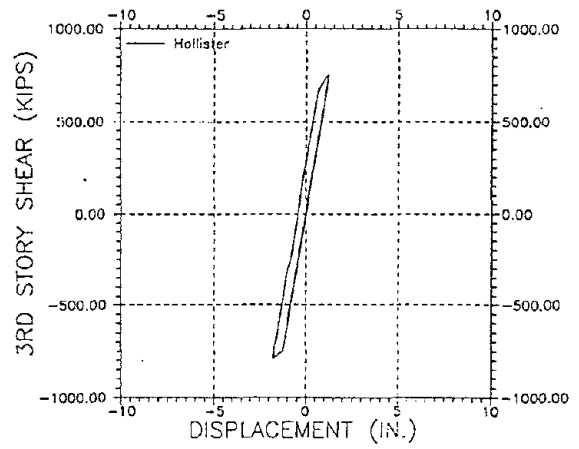
(a) Sixth Story



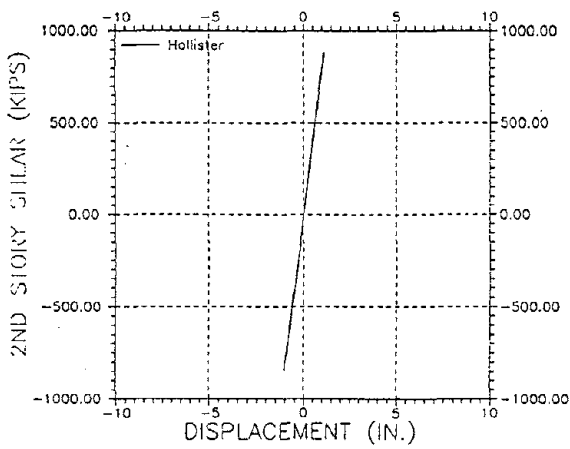
(b) Fifth Story



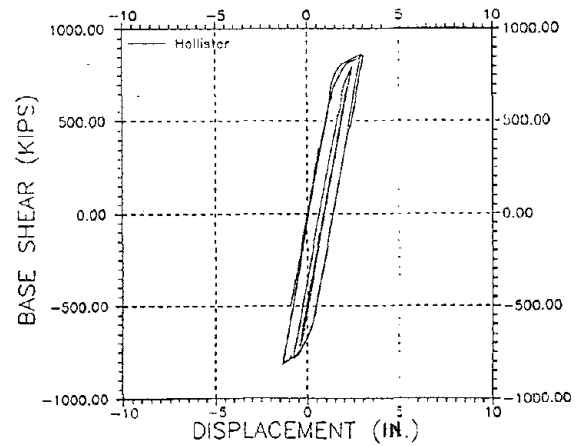
(c) Fourth Story



(d) Third Story



(e) Second Story



(f) First Story

Fig. 72 Story Shear vs. Interstory Displacement, Hollister

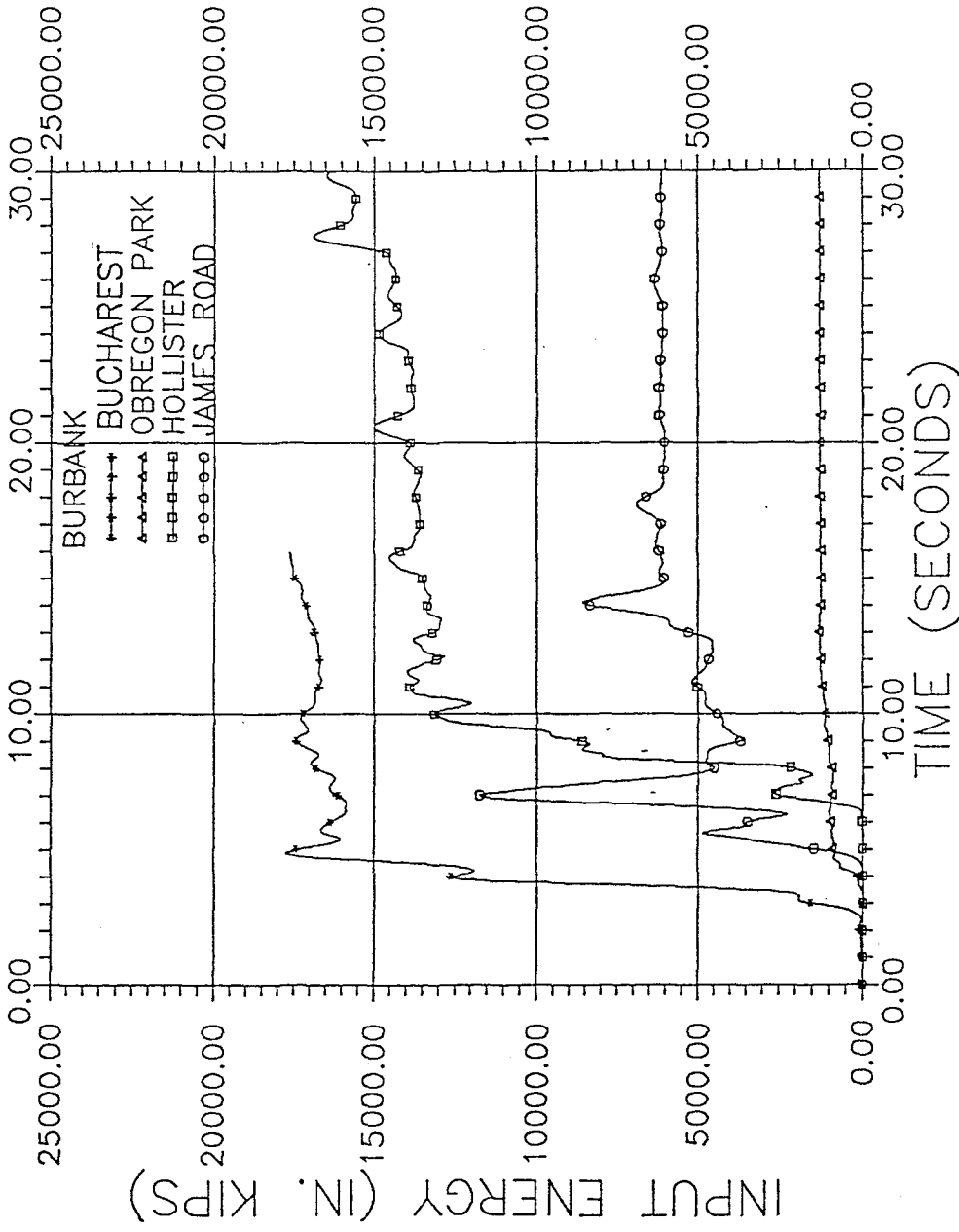
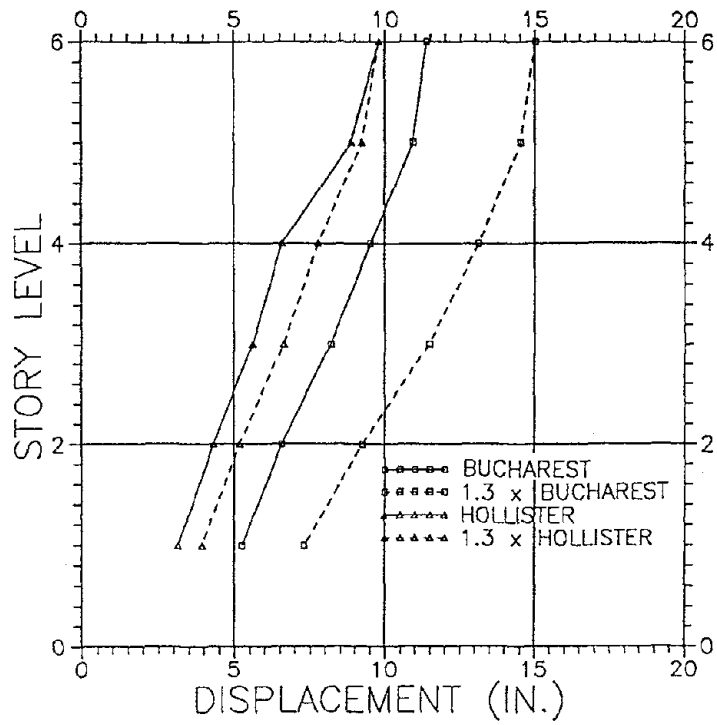
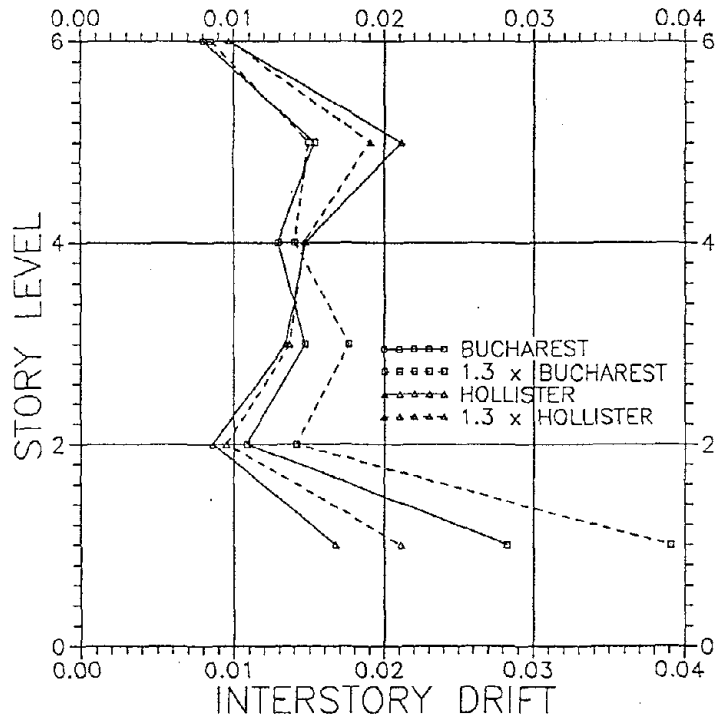


Fig. 73 Input Energy from Recent Earthquakes

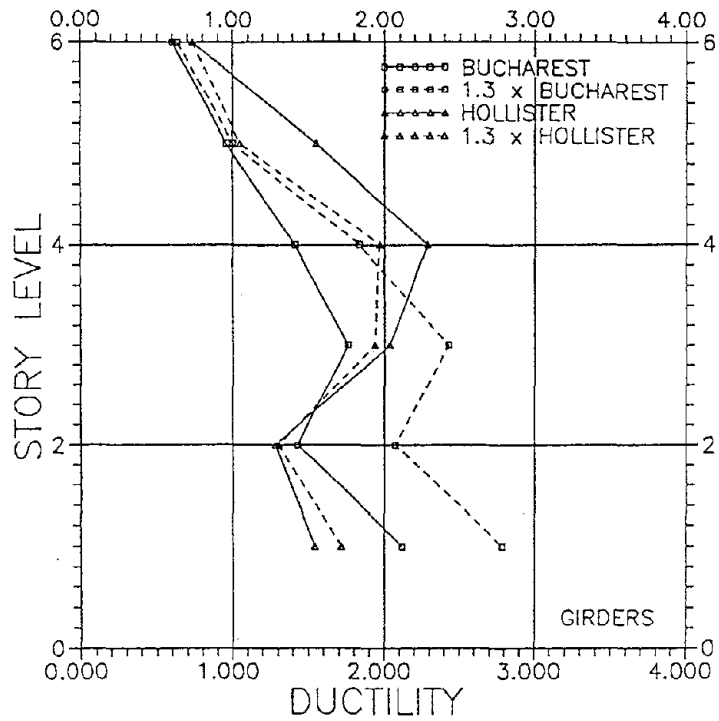


(a) Lateral Displacement

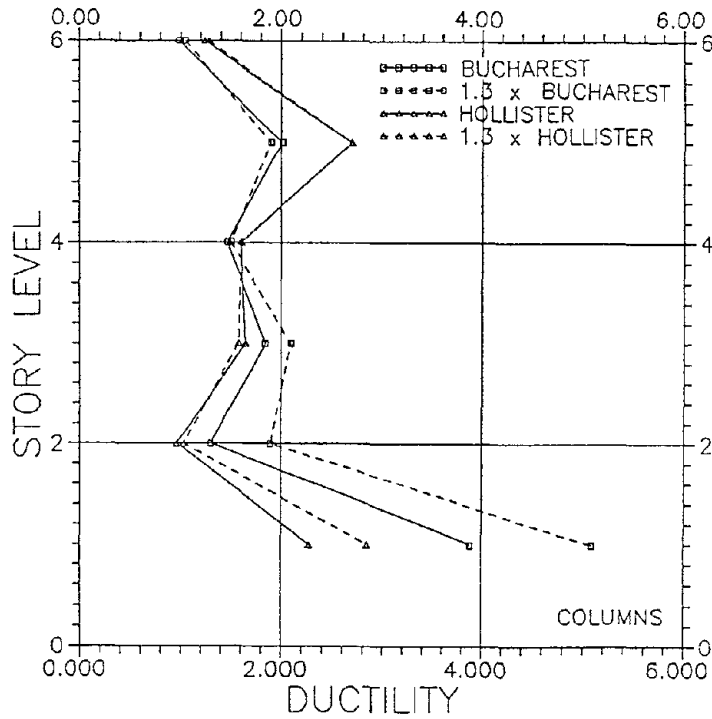


(b) Interstory Drift Index

Fig. 74 Maximum Displacement Response, Increased PGA

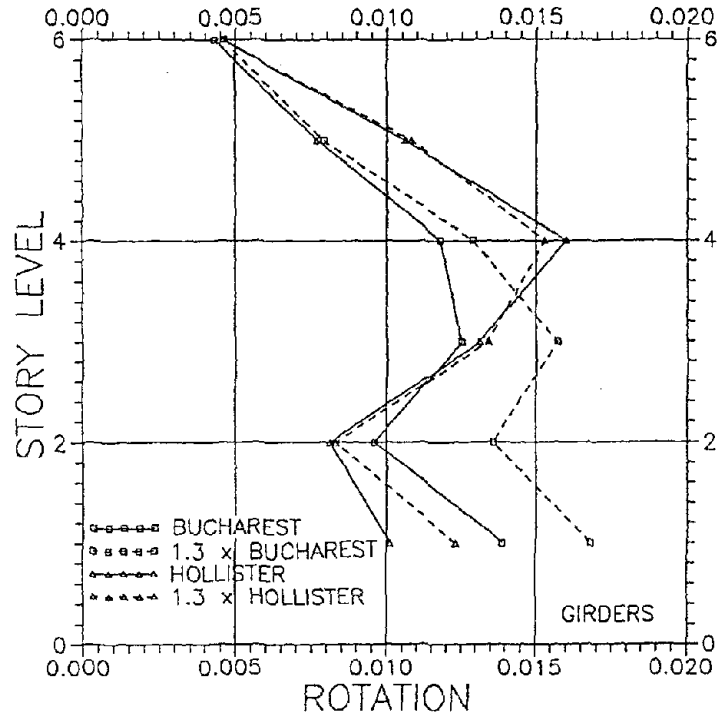


(a) Girders

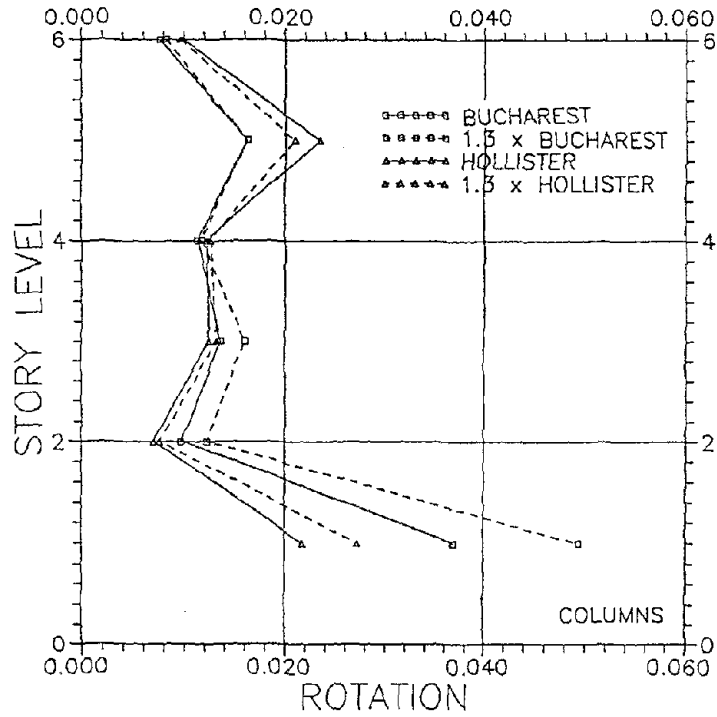


(b) Columns

Fig. 75 Curvature Ductility Demand, Increased PGA

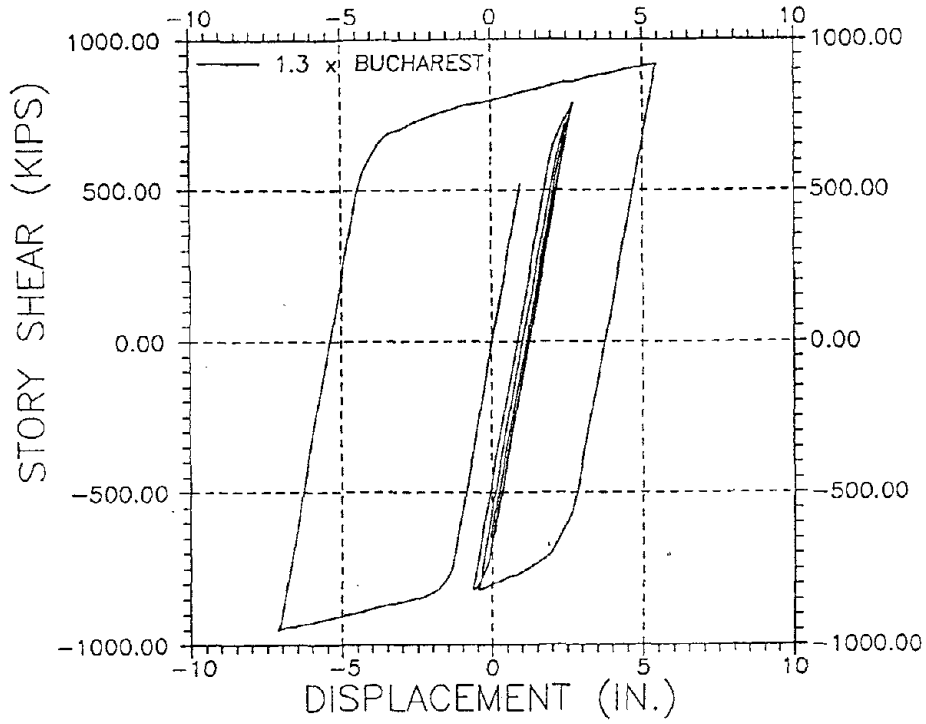


(a) Girders

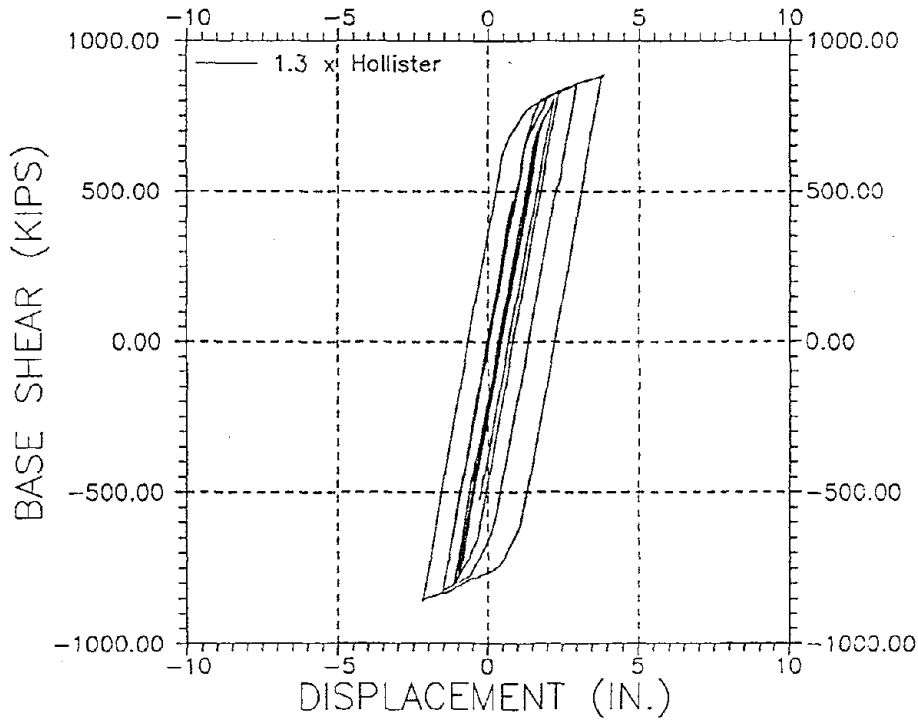


(b) Columns

Fig. 76 Maximum Rotation Demand, Increased PGA



(a) Bucharest



(b) Hollister

Fig. 77 Base Shear vs. Interstory Disp., Increased PGA



## REFERENCES

1. CSMIP, "Strong Motion Records From the Whittier California Earthquake of 1 October 1987," Report OSMS 87-05, Office of Strong Motion Studies, Division of Mines and Geology, California Department of Conservation, 1987.
2. USGS, "Strong-Motion Data From the October 1, 1987, Whittier Narrows Earthquake, Open-File Report 87-616, U.S. Geological Survey, Menlo Park, CA 94025.
3. International Conference of Building Officials, Uniform Building Code, Whittier, CA 1973.
4. Mahin, S. A. and Lin, J., "Construction of Inelastic Response Spectra for Single-Degree-of-Freedom Systems," Report No. UCB/EERC-83/17, Earthquake Engineering Research Center, University of California, Berkeley, CA 1983.
5. Wilson, E. L. and Habibullah, A., "SAP90, A Series of Computer Programs for the Static and Dynamic Finite Element Analysis of Structures," Computers and Structures, Inc., Berkeley, CA 1989.
6. Habibullah, A., "ETABS, Three Dimensional Analysis of Building Systems," Computers and Structures, Inc., Berkeley, CA 1989.
7. Habibullah, A. and Wilson, E. L., "SAPSTL, A Steel Stress Check Postprocessor for SAP90," Computers and Structures, Inc., Berkeley, CA 1989.
8. Manual of Steel Construction, Allowable Stress Design, Ninth Edition, American Institute of Steel Construction, Chicago, IL 1989.
9. Sudhakar, Arun, "ULARC, Computer Program for Small Displacement Elasto Plastic Analysis of Plane Steel and Reinforced Concrete Frames," Report No. CE/299-561, Department of Civil Engineering, University of California, Berkeley, CA 1972.
10. Krawinkler, H. and Popov, E. P., "Seismic Behavior of Moment Connections and Joints," Journal of the Structural Division, ASCE, Vol. 108, No. ST2, February, 1982.
11. Linderman, R. R. and Anderson, J. C., "Steel Beam to Box Column Connections," Proceedings, Structural Engineers Association of California, San Diego, 1989.

Preceding page blank

12. Anderson, J. C. and Bertero, V. V., "Uncertainties in Establishing Design Earthquakes," Journal of the Structural Division, ASCE, Vol. 113, No. 8, August, 1987.
13. Uang, C. M. and Bertero, V. V., "Implications of Recorded Earthquake Ground Motions on Seismic Design of Building Structures," Earthquake Engineering Research Center, Report No. UCB/EERC-88/13, University of California, Berkeley, November, 1988.
14. Bertero, V. V., "Strength and Deformation Capacities of Buildings Made Under Extreme Environments," Structural Engineering and Structural Mechanics, ed. K.S. Pister, Prentice Hall, Inc., 1980.

## EARTHQUAKE ENGINEERING RESEARCH CENTER REPORT SERIES

EERC reports are available from the National Information Service for Earthquake Engineering(NISEE) and from the National Technical Information Service(NTIS). Numbers in parentheses are Accession Numbers assigned by the National Technical Information Service; these are followed by a price code. Contact NTIS, 5285 Port Royal Road, Springfield Virginia, 22161 for more information. Reports without Accession Numbers were not available from NTIS at the time of printing. For a current complete list of EERC reports (from EERC 67-1) and availability information, please contact University of California, EERC, NISEE, 1301 South 46th Street, Richmond, California 94804.

- UCB/EERC-81/01 "Control of Seismic Response of Piping Systems and Other Structures by Base Isolation," by Kelly, J.M., January 1981, (PB81 200 735)A05.
- UCB/EERC-81/02 "OPTNSR- An Interactive Software System for Optimal Design of Statically and Dynamically Loaded Structures with Nonlinear Response," by Bhatti, M.A., Ciampi, V. and Pister, K.S., January 1981, (PB81 218 851)A09.
- UCB/EERC-81/03 "Analysis of Local Variations in Free Field Seismic Ground Motions," by Chen, J.-C., Lysmer, J. and Seed, H.B., January 1981, (AD-A099508)A13.
- UCB/EERC-81/04 "Inelastic Structural Modeling of Braced Offshore Platforms for Seismic Loading," by Zayas, V.A., Shing, P.-S.B., Mahin, S.A. and Popov, E.P., January 1981, INEL4, (PB82 138 777)A07.
- UCB/EERC-81/05 "Dynamic Response of Light Equipment in Structures," by Der Kiureghian, A., Sackman, J.L. and Nour-Omid, B., April 1981, (PB81 218 497)A04.
- UCB/EERC-81/06 "Preliminary Experimental Investigation of a Broad Base Liquid Storage Tank," by Bouwkamp, J.G., Kollegger, J.P. and Stephen, R.M., May 1981, (PB82 140 385)A03.
- UCB/EERC-81/07 "The Seismic Resistant Design of Reinforced Concrete Coupled Structural Walls," by Aktan, A.E. and Bertero, V.V., June 1981, (PB82 113 358)A11.
- UCB/EERC-81/08 "Unassigned," by Unassigned, 1981.
- UCB/EERC-81/09 "Experimental Behavior of a Spatial Piping System with Steel Energy Absorbers Subjected to a Simulated Differential Seismic Input," by Stiemer, S.F., Godden, W.G. and Kelly, J.M., July 1981, (PB82 201 898)A04.
- UCB/EERC-81/10 "Evaluation of Seismic Design Provisions for Masonry in the United States," by Sveinsson, B.I., Mayes, R.L. and McNiven, H.D., August 1981, (PB82 166 075)A08.
- UCB/EERC-81/11 "Two-Dimensional Hybrid Modelling of Soil-Structure Interaction," by Tzong, T.-J., Gupta, S. and Penzien, J., August 1981, (PB82 142 118)A04.
- UCB/EERC-81/12 "Studies on Effects of Infills in Seismic Resistant R/C Construction," by Brokken, S. and Bertero, V.V., October 1981, (PB82 166 190)A09.
- UCB/EERC-81/13 "Linear Models to Predict the Nonlinear Seismic Behavior of a One-Story Steel Frame," by Valdimarsson, H., Shah, A.H. and McNiven, H.D., September 1981, (PB82 138 793)A07.
- UCB/EERC-81/14 "TLUSH: A Computer Program for the Three-Dimensional Dynamic Analysis of Earth Dams," by Kagawa, T., Mejia, L.H., Seed, H.B. and Lysmer, J., September 1981, (PB82 139 940)A06.
- UCB/EERC-81/15 "Three Dimensional Dynamic Response Analysis of Earth Dams," by Mejia, L.H. and Seed, H.B., September 1981, (PB82 137 274)A12.
- UCB/EERC-81/16 "Experimental Study of Lead and Elastomeric Dampers for Base Isolation Systems," by Kelly, J.M. and Hodder, S.B., October 1981, (PB82 166 182)A05.
- UCB/EERC-81/17 "The Influence of Base Isolation on the Seismic Response of Light Secondary Equipment," by Kelly, J.M., April 1981, (PB82 255 266)A04.
- UCB/EERC-81/18 "Studies on Evaluation of Shaking Table Response Analysis Procedures," by Blondet, J. M., November 1981, (PB82 197 278)A10.
- UCB/EERC-81/19 "DELIGHT.STRUCT: A Computer-Aided Design Environment for Structural Engineering," by Balling, R.J., Pister, K.S. and Polak, E., December 1981, (PB82 218 496)A07.
- UCB/EERC-81/20 "Optimal Design of Seismic-Resistant Planar Steel Frames," by Balling, R.J., Ciampi, V. and Pister, K.S., December 1981, (PB82 220 179)A07.
- UCB/EERC-82/01 "Dynamic Behavior of Ground for Seismic Analysis of Lifeline Systems," by Sato, T. and Der Kiureghian, A., January 1982, (PB82 218 926)A05.
- UCB/EERC-82/02 "Shaking Table Tests of a Tubular Steel Frame Model," by Ghanaat, Y. and Clough, R.W., January 1982, (PB82 220 161)A07.
- UCB/EERC-82/03 "Behavior of a Piping System under Seismic Excitation: Experimental Investigations of a Spatial Piping System supported by Mechanical Shock Arrestors," by Schneider, S., Lee, H.-M. and Godden, W. G., May 1982, (PB83 172 544)A09.
- UCB/EERC-82/04 "New Approaches for the Dynamic Analysis of Large Structural Systems," by Wilson, E.L., June 1982, (PB83 148 080)A05.
- UCB/EERC-82/05 "Model Study of Effects of Damage on the Vibration Properties of Steel Offshore Platforms," by Shahrivar, F. and Bouwkamp, J.G., June 1982, (PB83 148 742)A10.
- UCB/EERC-82/06 "States of the Art and Practice in the Optimum Seismic Design and Analytical Response Prediction of R/C Frame Wall Structures," by Aktan, A.E. and Bertero, V.V., July 1982, (PB83 147 736)A05.
- UCB/EERC-82/07 "Further Study of the Earthquake Response of a Broad Cylindrical Liquid-Storage Tank Model," by Manos, G.C. and Clough, R.W., July 1982, (PB83 147 744)A11.
- UCB/EERC-82/08 "An Evaluation of the Design and Analytical Seismic Response of a Seven Story Reinforced Concrete Frame," by Charney, F.A. and Bertero, V.V., July 1982, (PB83 157 628)A09.
- UCB/EERC-82/09 "Fluid-Structure Interactions: Added Mass Computations for Incompressible Fluid," by Kuo, J.S.-H., August 1982, (PB83 156 281)A07.
- UCB/EERC-82/10 "Joint-Opening Nonlinear Mechanism: Interface Smeared Crack Model," by Kuo, J.S.-H., August 1982, (PB83 149 195)A05.

- UCB/EERC-82/11 "Dynamic Response Analysis of Tchi Dam," by Clough, R.W., Stephen, R.M. and Kuo, J.S.-H., August 1982, (PB83 147 496)A06.
- UCB/EERC-82/12 "Prediction of the Seismic Response of R/C Frame-Coupled Wall Structures," by Aktan, A.E., Bertero, V.V. and Piazzo, M., August 1982, (PB83 149 203)A09.
- UCB/EERC-82/13 "Preliminary Report on the Smart 1 Strong Motion Array in Taiwan," by Bolt, B.A., Loh, C.H., Penzien, J. and Tsai, Y.B., August 1982, (PB83 159 400)A10.
- UCB/EERC-82/14 "Seismic Behavior of an Eccentrically X-Braced Steel Structure," by Yang, M.S., September 1982, (PB83 260 778)A12.
- UCB/EERC-82/15 "The Performance of Stairways in Earthquakes," by Roha, C., Axley, J.W. and Bertero, V.V., September 1982, (PB83 157 693)A07.
- UCB/EERC-82/16 "The Behavior of Submerged Multiple Bodies in Earthquakes," by Liao, W.-G., September 1982, (PB83 158 709)A07.
- UCB/EERC-82/17 "Effects of Concrete Types and Loading Conditions on Local Bond-Slip Relationships," by Cowell, A.D., Popov, E.P. and Bertero, V.V., September 1982, (PB83 153 577)A04.
- UCB/EERC-82/18 "Mechanical Behavior of Shear Wall Vertical Boundary Members: An Experimental Investigation," by Wagner, M.T. and Bertero, V.V., October 1982, (PB83 159 764)A05.
- UCB/EERC-82/19 "Experimental Studies of Multi-support Seismic Loading on Piping Systems," by Kelly, J.M. and Cowell, A.D., November 1982, (PB90 262 684)A07.
- UCB/EERC-82/20 "Generalized Plastic Hinge Concepts for 3D Beam-Column Elements," by Chen, P. F.-S. and Powell, G.H., November 1982, (PB83 247 981)A13.
- UCB/EERC-82/21 "ANSR-II: General Computer Program for Nonlinear Structural Analysis," by Oughourlian, C.V. and Powell, G.H., November 1982, (PB83 251 330)A12.
- UCB/EERC-82/22 "Solution Strategies for Statically Loaded Nonlinear Structures," by Simons, J.W. and Powell, G.H., November 1982, (PB83 197 970)A06.
- UCB/EERC-82/23 "Analytical Model of Deformed Bar Anchorages under Generalized Excitations," by Ciampi, V., Eligchausen, R., Bertero, V.V. and Popov, E.P., November 1982, (PB83 169 532)A06.
- UCB/EERC-82/24 "A Mathematical Model for the Response of Masonry Walls to Dynamic Excitations," by Sucuoglu, H., Mengi, Y. and McNiven, H.D., November 1982, (PB83 169 011)A07.
- UCB/EERC-82/25 "Earthquake Response Considerations of Broad Liquid Storage Tanks," by Cambra, F.J., November 1982, (PB83 251 215)A09.
- UCB/EERC-82/26 "Computational Models for Cyclic Plasticity, Rate Dependence and Creep," by Mosaddad, B. and Powell, G.H., November 1982, (PB83 245 829)A08.
- UCB/EERC-82/27 "Inelastic Analysis of Piping and Tubular Structures," by Mahasverachai, M. and Powell, G.H., November 1982, (PB83 249 987)A07.
- UCB/EERC-83/01 "The Economic Feasibility of Seismic Rehabilitation of Buildings by Base Isolation," by Kelly, J.M., January 1983, (PB83 197 988)A05.
- UCB/EERC-83/02 "Seismic Moment Connections for Moment-Resisting Steel Frames," by Popov, E.P., January 1983, (PB83 195 412)A04.
- UCB/EERC-83/03 "Design of Links and Beam-to-Column Connections for Eccentrically Braced Steel Frames," by Popov, E.P. and Malley, J.O., January 1983, (PB83 194 811)A04.
- UCB/EERC-83/04 "Numerical Techniques for the Evaluation of Soil-Structure Interaction Effects in the Time Domain," by Bayo, E. and Wilson, E.L., February 1983, (PB83 245 605)A09.
- UCB/EERC-83/05 "A Transducer for Measuring the Internal Forces in the Columns of a Frame-Wall Reinforced Concrete Structure," by Sause, R. and Bertero, V.V., May 1983, (PB84 119 494)A06.
- UCB/EERC-83/06 "Dynamic Interactions Between Floating Ice and Offshore Structures," by Croteau, P., May 1983, (PB84 119 486)A16.
- UCB/EERC-83/07 "Dynamic Analysis of Multiply Tuned and Arbitrarily Supported Secondary Systems," by Igusa, T. and Der Kiureghian, A., July 1983, (PB84 118 272)A11.
- UCB/EERC-83/08 "A Laboratory Study of Submerged Multi-body Systems in Earthquakes," by Ansari, G.R., June 1983, (PB83 261 842)A17.
- UCB/EERC-83/09 "Effects of Transient Foundation Uplift on Earthquake Response of Structures," by Yim, C.-S. and Chopra, A.K., June 1983, (PB83 261 396)A07.
- UCB/EERC-83/10 "Optimal Design of Friction-Braced Frames under Seismic Loading," by Austin, M.A. and Pister, K.S., June 1983, (PB84 119 288)A06.
- UCB/EERC-83/11 "Shaking Table Study of Single-Story Masonry Houses: Dynamic Performance under Three Component Seismic Input and Recommendations," by Manos, G.C., Clough, R.W. and Mayes, R.L., July 1983, (UCB/EERC-83/11)A08.
- UCB/EERC-83/12 "Experimental Error Propagation in Pseudodynamic Testing," by Shiing, P.B. and Mahin, S.A., June 1983, (PB84 119 270)A09.
- UCB/EERC-83/13 "Experimental and Analytical Predictions of the Mechanical Characteristics of a 1/5-scale Model of a 7-story R/C Frame-Wall Building Structure," by Aktan, A.E., Bertero, V.V., Chowdhury, A.A. and Nagashima, T., June 1983, (PB84 119 213)A07.
- UCB/EERC-83/14 "Shaking Table Tests of Large-Panel Precast Concrete Building System Assemblages," by Oliva, M.G. and Clough, R.W., June 1983, (PB86 110 210/AS)A11.
- UCB/EERC-83/15 "Seismic Behavior of Active Beam Links in Eccentrically Braced Frames," by Hjelmstad, K.D. and Popov, E.P., July 1983, (PB84 119 676)A09.
- UCB/EERC-83/16 "System Identification of Structures with Joint Rotation," by Dimsdale, J.S., July 1983, (PB84 192 210)A06.
- UCB/EERC-83/17 "Construction of Inelastic Response Spectra for Single-Degree-of-Freedom Systems," by Mahin, S. and Lin, J., June 1983, (PB84 208 834)A05.
- UCB/EERC-83/18 "Interactive Computer Analysis Methods for Predicting the Inelastic Cyclic Behaviour of Structural Sections," by Kaba, S. and Mahin, S., July 1983, (PB84 192 012)A06.
- UCB/EERC-83/19 "Effects of Bond Deterioration on Hysteretic Behavior of Reinforced Concrete Joints," by Filippou, F.C., Popov, E.P. and Bertero, V.V., August 1983, (PB84 192 020)A10.

- UCB/EERC-83/20 "Correlation of Analytical and Experimental Responses of Large-Panel Precast Building Systems," by Oliva, M.G., Clough, R.W., Velkov, M. and Gavrilovic, P., May 1988, (PB90 262 692)A06.
- UCB/EERC-83/21 "Mechanical Characteristics of Materials Used in a 1/5 Scale Model of a 7-Story Reinforced Concrete Test Structure," by Bertero, V.V., Aktan, A.E., Harris, H.G. and Chowdhury, A.A., October 1983, (PB84 193 697)A05.
- UCB/EERC-83/22 "Hybrid Modelling of Soil-Structure Interaction in Layered Media," by Tzong, T.-J. and Penzien, J., October 1983, (PB84 192 178)A08.
- UCB/EERC-83/23 "Local Bond Stress-Slip Relationships of Deformed Bars under Generalized Excitations," by Elgehausen, R., Popov, E.P. and Bertero, V.V., October 1983, (PB84 192 848)A09.
- UCB/EERC-83/24 "Design Considerations for Shear Links in Eccentrically Braced Frames," by Malley, J.O. and Popov, E.P., November 1983, (PB84 192 186)A07.
- UCB/EERC-84/01 "Pseudodynamic Test Method for Seismic Performance Evaluation: Theory and Implementation," by Shing, P.-S.B. and Mahin, S.A., January 1984, (PB84 190 644)A08.
- UCB/EERC-84/02 "Dynamic Response Behavior of Kiang Hong Dian Dam," by Clough, R.W., Chang, K.-T., Chen, H.-Q. and Stephen, R.M., April 1984, (PB84 209 402)A08.
- UCB/EERC-84/03 "Refined Modelling of Reinforced Concrete Columns for Seismic Analysis," by Kaba, S.A. and Mahin, S.A., April 1984, (PB84 234 384)A06.
- UCB/EERC-84/04 "A New Floor Response Spectrum Method for Seismic Analysis of Multiply Supported Secondary Systems," by Asfura, A. and Der Kiureghian, A., June 1984, (PB84 239 417)A06.
- UCB/EERC-84/05 "Earthquake Simulation Tests and Associated Studies of a 1/5th-scale Model of a 7-Story R/C Frame-Wall Test Structure," by Bertero, V.V., Aktan, A.E., Charney, F.A. and Sause, R., June 1984, (PB84 239 409)A09.
- UCB/EERC-84/06 "Unassigned," by Unassigned, 1984.
- UCB/EERC-84/07 "Behavior of Interior and Exterior Flat-Plate Connections subjected to Inelastic Load Reversals," by Zee, H.L. and Moehle, J.P., August 1984, (PB86 117 629/AS)A07.
- UCB/EERC-84/08 "Experimental Study of the Seismic Behavior of a Two-Story Flat-Plate Structure," by Moehle, J.P. and Diebold, J.W., August 1984, (PB86 122 553/AS)A12.
- UCB/EERC-84/09 "Phenomenological Modeling of Steel Braces under Cyclic Loading," by Ikeda, K., Mahin, S.A. and Dermitzakis, S.N., May 1984, (PB86 132 198/AS)A08.
- UCB/EERC-84/10 "Earthquake Analysis and Response of Concrete Gravity Dams," by Fenves, G. and Chopra, A.K., August 1984, (PB85 193 902/AS)A11.
- UCB/EERC-84/11 "EAGD-84: A Computer Program for Earthquake Analysis of Concrete Gravity Dams," by Fenves, G. and Chopra, A.K., August 1984, (PB85 193 613/AS)A05.
- UCB/EERC-84/12 "A Refined Physical Theory Model for Predicting the Seismic Behavior of Braced Steel Frames," by Ikeda, K. and Mahin, S.A., July 1984, (PB85 191 450/AS)A09.
- UCB/EERC-84/13 "Earthquake Engineering Research at Berkeley - 1984," by EERC, August 1984, (PB85 197 341/AS)A10.
- UCB/EERC-84/14 "Moduli and Damping Factors for Dynamic Analyses of Cohesionless Soils," by Seed, H.B., Wong, R.T., Idriss, I.M. and Tokimatsu, K., September 1984, (PB85 191 468/AS)A04.
- UCB/EERC-84/15 "The Influence of SPT Procedures in Soil Liquefaction Resistance Evaluations," by Seed, H.B., Tokimatsu, K., Harder, L.F. and Chung, R.M., October 1984, (PB85 191 732/AS)A04.
- UCB/EERC-84/16 "Simplified Procedures for the Evaluation of Settlements in Sands Due to Earthquake Shaking," by Tokimatsu, K. and Seed, H.B., October 1984, (PB85 197 887/AS)A03.
- UCB/EERC-84/17 "Evaluation of Energy Absorption Characteristics of Highway Bridges Under Seismic Conditions - Volume I (PB90 262 627)A16 and Volume II (Appendices) (PB90 262 635)A13," by Imbsen, R.A. and Penzien, J., September 1986.
- UCB/EERC-84/18 "Structure-Foundation Interactions under Dynamic Loads," by Liu, W.D. and Penzien, J., November 1984, (PB87 124 889/AS)A11.
- UCB/EERC-84/19 "Seismic Modelling of Deep Foundations," by Chen, C.-H. and Penzien, J., November 1984, (PB87 124 798/AS)A07.
- UCB/EERC-84/20 "Dynamic Response Behavior of Quan Shui Dam," by Clough, R.W., Chang, K.-T., Chen, H.-Q., Stephen, R.M., Ghanaat, Y. and Qi, J.-H., November 1984, (PB86 115177/AS)A07.
- UCB/EERC-85/01 "Simplified Methods of Analysis for Earthquake Resistant Design of Buildings," by Cruz, E.F. and Chopra, A.K., February 1985, (PB86 112299/AS)A12.
- UCB/EERC-85/02 "Estimation of Seismic Wave Coherency and Rupture Velocity using the SMART 1 Strong-Motion Array Recordings," by Abrahamson, N.A., March 1985, (PB86 214 343)A07.
- UCB/EERC-85/03 "Dynamic Properties of a Thirty Story Condominium Tower Building," by Stephen, R.M., Wilson, E.L. and Stander, N., April 1985, (PB86 118965/AS)A06.
- UCB/EERC-85/04 "Development of Substructuring Techniques for On-Line Computer Controlled Seismic Performance Testing," by Dermitzakis, S. and Mahin, S., February 1985, (PB86 132941/AS)A08.
- UCB/EERC-85/05 "A Simple Model for Reinforcing Bar Anchorages under Cyclic Excitations," by Filippou, F.C., March 1985, (PB86 112 919/AS)A05.
- UCB/EERC-85/06 "Racking Behavior of Wood-framed Gypsum Panels under Dynamic Load," by Oliva, M.G., June 1985, (PB90 262 643)A04.
- UCB/EERC-85/07 "Earthquake Analysis and Response of Concrete Arch Dams," by Fok, K.-L. and Chopra, A.K., June 1985, (PB86 139672/AS)A10.
- UCB/EERC-85/08 "Effect of Inelastic Behavior on the Analysis and Design of Earthquake Resistant Structures," by Lin, J.P. and Mahin, S.A., June 1985, (PB86 135340/AS)A08.
- UCB/EERC-85/09 "Earthquake Simulator Testing of a Base-Isolated Bridge Deck," by Kelly, J.M., Buckle, I.G. and Tsai, H.-C., January 1986, (PB87 124 152/AS)A06.

- UCB/EERC-85/10 "Simplified Analysis for Earthquake Resistant Design of Concrete Gravity Dams," by Fenves, G. and Chopra, A.K., June 1986, (PB87 124 160/AS)A08.
- UCB/EERC-85/11 "Dynamic Interaction Effects in Arch Dams," by Clough, R.W., Chang, K.-T., Chen, H.-Q. and Ghanaat, Y., October 1985, (PB86 135027/AS)A05.
- UCB/EERC-85/12 "Dynamic Response of Long Valley Dam in the Mammoth Lake Earthquake Series of May 25-27, 1980," by Lai, S. and Seed, H.B., November 1985, (PB86 142304/AS)A05.
- UCB/EERC-85/13 "A Methodology for Computer-Aided Design of Earthquake-Resistant Steel Structures," by Austin, M.A., Pister, K.S. and Mahin, S.A., December 1985, (PB86 159480/AS)A10.
- UCB/EERC-85/14 "Response of Tension-Leg Platforms to Vertical Seismic Excitations," by Liou, G.-S., Penzien, J. and Yeung, R.W., December 1985, (PB87 124 871/AS)A08.
- UCB/EERC-85/15 "Cyclic Loading Tests of Masonry Single Piers: Volume 4 - Additional Tests with Height to Width Ratio of 1," by Sveinsson, B., McNiven, H.D. and Sucuoglu, H., December 1985.
- UCB/EERC-85/16 "An Experimental Program for Studying the Dynamic Response of a Steel Frame with a Variety of Infill Partitions," by Yanev, B. and McNiven, H.D., December 1985, (PB90 262 676)A05.
- UCB/EERC-86/01 "A Study of Seismically Resistant Eccentrically Braced Steel Frame Systems," by Kasai, K. and Popov, E.P., January 1986, (PB87 124 178/AS)A14.
- UCB/EERC-86/02 "Design Problems in Soil Liquefaction," by Seed, H.B., February 1986, (PB87 124 186/AS)A03.
- UCB/EERC-86/03 "Implications of Recent Earthquakes and Research on Earthquake-Resistant Design and Construction of Buildings," by Bertero, V.V., March 1986, (PB87 124 194/AS)A05.
- UCB/EERC-86/04 "The Use of Load Dependent Vectors for Dynamic and Earthquake Analyses," by Leger, P., Wilson, E.L. and Clough, R.W., March 1986, (PB87 124 202/AS)A12.
- UCB/EERC-86/05 "Two Beam-To-Column Web Connections," by Tsai, K.-C. and Popov, E.P., April 1986, (PB87 124 301/AS)A04.
- UCB/EERC-86/06 "Determination of Penetration Resistance for Coarse-Grained Soils using the Becker Hammer Drill," by Harder, L.F. and Seed, H.B., May 1986, (PB87 124 210/AS)A07.
- UCB/EERC-86/07 "A Mathematical Model for Predicting the Nonlinear Response of Unreinforced Masonry Walls to In-Plane Earthquake Excitations," by Mengi, Y. and McNiven, H.D., May 1986, (PB87 124 780/AS)A06.
- UCB/EERC-86/08 "The 19 September 1985 Mexico Earthquake: Building Behavior," by Bertero, V.V., July 1986.
- UCB/EERC-86/09 "EACD-3D: A Computer Program for Three-Dimensional Earthquake Analysis of Concrete Dams," by Fok, K.-L., Hall, J.F. and Chopra, A.K., July 1986, (PB87 124 228/AS)A08.
- UCB/EERC-86/10 "Earthquake Simulation Tests and Associated Studies of a 0.3-Scale Model of a Six-Story Concentrically Braced Steel Structure," by Uang, C.-M. and Bertero, V.V., December 1986, (PB87 163 564/AS)A17.
- UCB/EERC-86/11 "Mechanical Characteristics of Base Isolation Bearings for a Bridge Deck Model Test," by Kelly, J.M., Buckle, I.G. and Koh, C.-G., November 1987, (PB90 262 668)A04.
- UCB/EERC-86/12 "Effects of Axial Load on Elastomeric Isolation Bearings," by Koh, C.-G. and Kelly, J.M., November 1987.
- UCB/EERC-87/01 "The FPS Earthquake Resisting System: Experimental Report," by Zayas, V.A., Low, S.S. and Mahin, S.A., June 1987.
- UCB/EERC-87/02 "Earthquake Simulator Tests and Associated Studies of a 0.3-Scale Model of a Six-Story Eccentrically Braced Steel Structure," by Whitaker, A., Uang, C.-M. and Bertero, V.V., July 1987.
- UCB/EERC-87/03 "A Displacement Control and Uplift Restraint Device for Base-Isolated Structures," by Kelly, J.M., Griffith, M.C. and Aiken, I.D., April 1987.
- UCB/EERC-87/04 "Earthquake Simulator Testing of a Combined Sliding Bearing and Rubber Bearing Isolation System," by Kelly, J.M. and Chalhoub, M.S., 1987.
- UCB/EERC-87/05 "Three-Dimensional Inelastic Analysis of Reinforced Concrete Frame-Wall Structures," by Moazzami, S. and Bertero, V.V., May 1987.
- UCB/EERC-87/06 "Experiments on Eccentrically Braced Frames with Composite Floors," by Ricles, J. and Popov, E., June 1987.
- UCB/EERC-87/07 "Dynamic Analysis of Seismically Resistant Eccentrically Braced Frames," by Ricles, J. and Popov, E., June 1987.
- UCB/EERC-87/08 "Undrained Cyclic Triaxial Testing of Gravels-The Effect of Membrane Compliance," by Evans, M.D. and Seed, H.B., July 1987.
- UCB/EERC-87/09 "Hybrid Solution Techniques for Generalized Pseudo-Dynamic Testing," by Thewalt, C. and Mahin, S.A., July 1987.
- UCB/EERC-87/10 "Ultimate Behavior of Butt Welded Splices in Heavy Rolled Steel Sections," by Bruneau, M., Mahin, S.A. and Popov, E.P., September 1987.
- UCB/EERC-87/11 "Residual Strength of Sand from Dam Failures in the Chilean Earthquake of March 3, 1985," by De Alba, P., Seed, H.B., Retamal, E. and Seed, R.B., September 1987.
- UCB/EERC-87/12 "Inelastic Seismic Response of Structures with Mass or Stiffness Eccentricities in Plan," by Bruneau, M. and Mahin, S.A., September 1987, (PB90 262 650)A14.
- UCB/EERC-87/13 "CSTRUCT: An Interactive Computer Environment for the Design and Analysis of Earthquake Resistant Steel Structures," by Austin, M.A., Mahin, S.A. and Pister, K.S., September 1987.
- UCB/EERC-87/14 "Experimental Study of Reinforced Concrete Columns Subjected to Multi-Axial Loading," by Low, S.S. and Moehle, J.P., September 1987.
- UCB/EERC-87/15 "Relationships between Soil Conditions and Earthquake Ground Motions in Mexico City in the Earthquake of Sept. 19, 1985," by Seed, H.B., Romo, M.P., Sun, J., Jaime, A. and Lysmer, J., October 1987.
- UCB/EERC-87/16 "Experimental Study of Seismic Response of R. C. Setback Buildings," by Shahrooz, B.M. and Moehle, J.P., October 1987.

- UCB/EERC-87/17 "The Effect of Slabs on the Flexural Behavior of Beams," by Pantazopoulou, S.J. and Moehle, J.P., October 1987, (PB90 262 700)A07.
- UCB/EERC-87/18 "Design Procedure for R-FBI Bearings," by Mostaghel, N. and Kelly, J.M., November 1987, (PB90 262 718)A04.
- UCB/EERC-87/19 "Analytical Models for Predicting the Lateral Response of R C Shear Walls: Evaluation of their Reliability," by Vulcano, A. and Bertero, V.V., November 1987.
- UCB/EERC-87/20 "Earthquake Response of Torsionally-Coupled Buildings," by Hejal, R. and Chopra, A.K., December 1987.
- UCB/EERC-87/21 "Dynamic Reservoir Interaction with Monticello Dam," by Clough, R.W., Ghanaat, Y. and Qiu, X-F., December 1987.
- UCB/EERC-87/22 "Strength Evaluation of Coarse-Grained Soils," by Siddiqi, F.H., Seed, R.B., Chan, C.K., Seed, H.B. and Pyke, R.M., December 1987.
- UCB/EERC-88/01 "Seismic Behavior of Concentrically Braced Steel Frames," by Khatib, I., Mahin, S.A. and Pister, K.S., January 1988.
- UCB/EERC-88/02 "Experimental Evaluation of Seismic Isolation of Medium-Rise Structures Subject to Uplift," by Griffith, M.C., Kelly, J.M., Coveney, V.A. and Koh, C.G., January 1988.
- UCB/EERC-88/03 "Cyclic Behavior of Steel Double Angle Connections," by Astaneh-Asl, A. and Nader, M.N., January 1988.
- UCB/EERC-88/04 "Re-evaluation of the Slide in the Lower San Fernando Dam in the Earthquake of Feb. 9, 1971," by Seed, H.B., Seed, R.B., Harder, L.F. and Jong, H.-L., April 1988.
- UCB/EERC-88/05 "Experimental Evaluation of Seismic Isolation of a Nine-Story Braced Steel Frame Subject to Uplift," by Griffith, M.C., Kelly, J.M. and Aiken, I.D., May 1988.
- UCB/EERC-88/06 "DRAIN-2DX User Guide," by Allahabadi, R. and Powell, G.H., March 1988.
- UCB/EERC-88/07 "Theoretical and Experimental Studies of Cylindrical Water Tanks in Base-Isolated Structures," by Chalhoub, M.S. and Kelly, J.M., April 1988.
- UCB/EERC-88/08 "Analysis of Near-Source Waves: Separation of Wave Types using Strong Motion Array Recordings," by Darragh, R.B., June 1988.
- UCB/EERC-88/09 "Alternatives to Standard Mode Superposition for Analysis of Non-Classically Damped Systems," by Kusainov, A.A. and Clough, R.W., June 1988.
- UCB/EERC-88/10 "The Landslide at the Port of Nice on October 16, 1979," by Seed, H.B., Seed, R.B., Schlosser, F., Blondeau, F. and Juran, I., June 1988.
- UCB/EERC-88/11 "Liquefaction Potential of Sand Deposits Under Low Levels of Excitation," by Carter, D.P. and Seed, H.B., August 1988.
- UCB/EERC-88/12 "Nonlinear Analysis of Reinforced Concrete Frames Under Cyclic Load Reversals," by Filippou, F.C. and Issa, A., September 1988.
- UCB/EERC-88/13 "Implications of Recorded Earthquake Ground Motions on Seismic Design of Building Structures," by Uang, C.-M. and Bertero, V.V., November 1988.
- UCB/EERC-88/14 "An Experimental Study of the Behavior of Dual Steel Systems," by Whittaker, A.S., Uang, C.-M. and Bertero, V.V., September 1988.
- UCB/EERC-88/15 "Dynamic Moduli and Damping Ratios for Cohesive Soils," by Sun, J.I., Golezorkhi, R. and Seed, H.B., August 1988.
- UCB/EERC-88/16 "Reinforced Concrete Flat Plates Under Lateral Load: An Experimental Study Including Biaxial Effects," by Pan, A. and Moehle, J., October 1988.
- UCB/EERC-88/17 "Earthquake Engineering Research at Berkeley - 1988," by EERC, November 1988.
- UCB/EERC-88/18 "Use of Energy as a Design Criterion in Earthquake-Resistant Design," by Uang, C.-M. and Bertero, V.V., November 1988.
- UCB/EERC-88/19 "Steel Beam-Column Joints in Seismic Moment Resisting Frames," by Tsai, K.-C. and Popov, E.P., November 1988.
- UCB/EERC-88/20 "Base Isolation in Japan, 1988," by Kelly, J.M., December 1988.
- UCB/EERC-89/01 "Behavior of Long Links in Eccentrically Braced Frames," by Engelhardt, M.D. and Popov, E.P., January 1989.
- UCB/EERC-89/02 "Earthquake Simulator Testing of Steel Plate Added Damping and Stiffness Elements," by Whittaker, A., Bertero, V.V., Alonso, J. and Thompson, C., January 1989.
- UCB/EERC-89/03 "Implications of Site Effects in the Mexico City Earthquake of Sept. 19, 1985 for Earthquake-Resistant Design Criteria in the San Francisco Bay Area of California," by Seed, H.B. and Sun, J.I., March 1989.
- UCB/EERC-89/04 "Earthquake Analysis and Response of Intake-Outlet Towers," by Goyal, A. and Chopra, A.K., July 1989.
- UCB/EERC-89/05 "The 1985 Chile Earthquake: An Evaluation of Structural Requirements for Bearing Wall Buildings," by Wallace, J.W. and Moehle, J.P., July 1989.
- UCB/EERC-89/06 "Effects of Spatial Variation of Ground Motions on Large Multiply-Supported Structures," by Hao, H., July 1989.
- UCB/EERC-89/07 "EADAP - Enhanced Arch Dam Analysis Program: Users's Manual," by Ghanaat, Y. and Clough, R.W., August 1989.
- UCB/EERC-89/08 "Seismic Performance of Steel Moment Frames Plastically Designed by Least Squares Stress Fields," by Ohi, K. and Mahin, S.A., August 1989.
- UCB/EERC-89/09 "Feasibility and Performance Studies on Improving the Earthquake Resistance of New and Existing Buildings Using the Friction Pendulum System," by Zayas, V., Low, S., Mahin, S.A. and Bozzo, L., July 1989.
- UCB/EERC-89/10 "Measurement and Elimination of Membrane Compliance Effects in Undrained Triaxial Testing," by Nicholson, P.G., Seed, R.B. and Anwar, H., September 1989.
- UCB/EERC-89/11 "Static Tilt Behavior of Unanchored Cylindrical Tanks," by Lau, D.T. and Clough, R.W., September 1989.
- UCB/EERC-89/12 "ADAP-88: A Computer Program for Nonlinear Earthquake Analysis of Concrete Arch Dams," by Fenves, G.L., Mojtahedi, S. and Reimer, R.B., September 1989.
- UCB/EERC-89/13 "Mechanics of Low Shape Factor Elastomeric Seismic Isolation Bearings," by Aiken, I.D., Kelly, J.M. and Tajirian, F.F., November 1989.
- UCB/EERC-89/14 "Preliminary Report on the Seismological and Engineering Aspects of the October 17, 1989 Santa Cruz (Loma Prieta) Earthquake," by EERC, October 1989.

- UCB/EERC-89/15 "Experimental Studies of a Single Story Steel Structure Tested with Fixed, Semi-Rigid and Flexible Connections," by Nader, M.N. and Astaneh-Asl, A., August 1989, (PB91 229 211/AS)A10.
- UCB/EERC-89/16 "Collapse of the Cypress Street Viaduct as a Result of the Loma Prieta Earthquake," by Nims, D.K., Miranda, E., Aiken, I.D., Whitaker, A.S. and Bertero, V.V., November 1989, (PB91 217 935/AS)A05.
- UCB/EERC-90/01 "Mechanics of High-Shape Factor Elastomeric Seismic Isolation Bearings," by Kelly, J.M., Aiken, I.D. and Tajirian, F.F., March 1990.
- UCB/EERC-90/02 "Javid's Paradox: The Influence of Preform on the Modes of Vibrating Beams," by Kelly, J.M., Sackman, J.L. and Javid, A., May 1990, (PB91 217 943/AS)A03.
- UCB/EERC-90/03 "Earthquake Simulator Testing and Analytical Studies of Two Energy-Absorbing Systems for Multistory Structures," by Aiken, I.D. and Kelly, J.M., October 1990.
- UCB/EERC-90/04 "Damage to the San Francisco-Oakland Bay Bridge During the October 17, 1989 Earthquake," by Astaneh, A., June 1990.
- UCB/EERC-90/05 "Preliminary Report on the Principal Geotechnical Aspects of the October 17, 1989 Loma Prieta Earthquake," by Seed, R.B., Dickenson, S.E., Riemer, M.F., Bray, J.D., Sitar, N., Mitchell, J.K., Idriss, I.M., Kayen, R.E., Kropp, A., Harder, L.F., Jr. and Power, M.S., April 1990.
- UCB/EERC-90/06 "Models of Critical Regions in Reinforced Concrete Frames Under Seismic Excitations," by Zulfikar, N. and Filippou, F., May 1990.
- UCB/EERC-90/07 "A Unified Earthquake-Resistant Design Method for Steel Frames Using ARMA Models," by Takewaki, I., Conte, J.P., Mahin, S.A. and Pister, K.S., June 1990.
- UCB/EERC-90/08 "Soil Conditions and Earthquake Hazard Mitigation in the Marina District of San Francisco," by Mitchell, J.K., Masood, T., Kayen, R.E. and Seed, R.B., May 1990.
- UCB/EERC-90/09 "Influence of the Earthquake Ground Motion Process and Structural Properties on Response Characteristics of Simple Structures," by Conte, J.P., Pister, K.S. and Mahin, S.A., July 1990.
- UCB/EERC-90/10 "Experimental Testing of the Resilient-Friction Base Isolation System," by Clark, P.W. and Kelly, J.M., July 1990.
- UCB/EERC-90/11 "Seismic Hazard Analysis: Improved Models, Uncertainties and Sensitivities," by Araya, R. and Der Kiureghian, A., March 1988.
- UCB/EERC-90/12 "Effects of Torsion on the Linear and Nonlinear Seismic Response of Structures," by Sedarat, H. and Bertero, V.V., September 1989.
- UCB/EERC-90/13 "The Effects of Tectonic Movements on Stresses and Deformations in Earth Embankments," by Bray, J. D., Seed, R. B. and Seed, H. B., September 1989.
- UCB/EERC-90/14 "Inelastic Seismic Response of One-Story, Asymmetric-Plan Systems," by Goel, R.K. and Chopra, A.K., October 1990.
- UCB/EERC-90/15 "Dynamic Crack Propagation: A Model for Near-Field Ground Motion," by Seyyedian, H. and Kelly, J.M., 1990.
- UCB/EERC-90/16 "Sensitivity of Long-Period Response Spectra to System Initial Conditions," by Blasquez, R., Ventura, C. and Kelly, J.M., 1990.
- UCB/EERC-90/17 "Behavior of Peak Values and Spectral Ordinates of Near-Source Strong Ground-Motion over a Dense Array," by Niazi, M., June 1990.
- UCB/EERC-90/18 "Material Characterization of Elastomers used in Earthquake Base Isolation," by Papoulia, K.D. and Kelly, J.M., 1990.
- UCB/EERC-90/19 "Cyclic Behavior of Steel Top-and-Bottom Plate Moment Connections," by Harriott, J.D. and Astaneh, A., August 1990, (PB91 229 260/AS)A05.
- UCB/EERC-90/20 "Seismic Response Evaluation of an Instrumented Six Story Steel Building," by Shen, J.-H. and Astaneh, A., December 1990.
- UCB/EERC-90/21 "Observations and Implications of Tests on the Cypress Street Viaduct Test Structure," by Bollo, M., Mahin, S.A., Mochle, J.P., Stephen, R.M. and Qi, X., December 1990.
- UCB/EERC-91/01 "Experimental Evaluation of Nitinol for Energy Dissipation in Structures," by Nims, D.K., Sasaki, K.K. and Kelly, J.M., 1991.
- UCB/EERC-91/02 "Displacement Design Approach for Reinforced Concrete Structures Subjected to Earthquakes," by Qi, X. and Mochle, J.P., January 1991.
- UCB/EERC-91/03 "Shake Table Tests of Long Period Isolation System for Nuclear Facilities at Soft Soil Sites," by Kelly, J.M., March 1991.
- UCB/EERC-91/04 "Dynamic and Failure Characteristics of Bridgestone Isolation Bearings," by Kelly, J.M., April 1991.
- UCB/EERC-91/05 "Base Sliding Response of Concrete Gravity Dams to Earthquakes," by Chopra, A.K. and Zhang, L., May 1991.
- UCB/EERC-91/06 "Computation of Spatially Varying Ground Motion and Foundation-Rock Impedance Matrices for Seismic Analysis of Arch Dams," by Zhang, L. and Chopra, A.K., May 1991.
- UCB/EERC-91/07 "Estimation of Seismic Source Processes Using Strong Motion Array Data," by Chiou, S.-J., July 1991.
- UCB/EERC-91/08 "A Response Spectrum Method for Multiple-Support Seismic Excitations," by Der Kiureghian, A. and Neuenhofer, A., August 1991.
- UCB/EERC-91/09 "A Preliminary Study on Energy Dissipating Cladding-to-Frame Connection," by Cohen, J.M. and Powell, G.H., September 1991.
- UCB/EERC-91/10 "Evaluation of Seismic Performance of a Ten-Story RC Building During the Whittier Narrows Earthquake," by Miranda, E. and Bertero, V.V., October 1991.
- UCB/EERC-91/11 "Seismic Performance of an Instrumented Six Story Steel Building," by Anderson, J.C. and Bertero, V.V., November 1991.